Defense Threat Reduction Agency
8725 John J. Kingman Road, MS 6201
Fort Belvoir, VA 22060-6201

DTRA-TR-14-43

TECHNICAL REPORT

Investigation of Fundamental Processes and Crystal-Level Defect Structures in Metal-Loaded High-Explosive Materials under Dynamic Thermo-Mechanical Loads and their Relationships to Impact Survivability of Munitions (Thrust 4, Topic J)

Approved for public release; distribution is unlimited.

June 2014

HDTRA1-10-1-0078

Donald L. Thompson and
Thomas D. Sewell

Prepared by:
University of Missouri
316 University Hall
Columbia, MO 65211-3020

DESTRUCTION NOTICE:

Destroy this report when it is no longer needed.
Do not return to sender.

PLEASE NOTIFY THE DEFENSE THREAT REDUCTION AGENCY, ATTN: DTRIAC/ J9STT, 8725 JOHN J. KINGMAN ROAD, MS-6201, FT BELVOIR, VA 22060-6201, IF YOUR ADDRESS IS INCORRECT, IF YOU WISH THAT IT BE DELETED FROM THE DISTRIBUTION LIST, OR IF THE ADDRESSEE IS NO LONGER EMPLOYED BY YOUR ORGANIZATION.

REPORT DOCUMENTATION PAGE

Form Approved
OMB No. 0704-0188

1. REPORT DATE *(DD-MM-YYYY)*	**2. REPORT TYPE**	**3. DATES COVERED** *(From - To)*
00-06-2014	Technical	July 12, 2010 - July 11, 2013

4. TITLE AND SUBTITLE

Investigation of Fundamental Processes and Crystal-Level Defect Structures in Metal-Loaded High-Explosive Materials under Dynamic Thermo-Mechanical Loads and their Relationships to Impact Survivability of Munitions (Thrust 4, Topic J)

5a. CONTRACT NUMBER

5b. GRANT NUMBER
HDTRA1-10-1-0078

5c. PROGRAM ELEMENT NUMBER

6. AUTHOR(S)

Donald L. Thompson and Thomas D. Sewell

5d. PROJECT NUMBER

5e. TASK NUMBER

5f. WORK UNIT NUMBER

7. PERFORMING ORGANIZATION NAME(S) AND ADDRESS(ES)

University of Missouri System DBA Curators of the University of Missouri
316 University Hall
Columbia MO, 65211-3020

8. PERFORMING ORGANIZATION REPORT NUMBER

9. SPONSORING / MONITORING AGENCY NAME(S) AND ADDRESS(ES)

Defense Threat Reduction Agency
8725 John J. Kingman Road, STOP 6201
Fort Belvoir, VA 22060-6201

10. SPONSOR/MONITOR'S ACRONYM(S)

DTRA

11. SPONSOR/MONITOR'S REPORT NUMBER(S)

DTRA-TR-14-43

12. DISTRIBUTION / AVAILABILITY STATEMENT

Approved for public release; distribution is unlimited.

13. SUPPLEMENTARY NOTES

14. ABSTRACT

Theoretical (molecular dynamics) and experimental methods (microscopy and impact measurements) were used to investigate fundamental aspects of the physics and chemistry that determine the behavior of energetic materials in response to weak shock or non-shock insults, with emphasis on stress states relevant to penetrator applications. We considered the composite AFX-757 as a representative formulation. The theoretical studies were focused on RDX and hydroxy-terminated polybutadiene. The experimental focus was AFX-757 composites formulated using three different grades of RDX crystals. Additional theoretical studies were performed for PETN and nitromethane.

15. SUBJECT TERMS

Molecular dynamics, confocal scanning laser microscopy, ballistic impact chamber, shock waves, impact sensitivity

16. SECURITY CLASSIFICATION OF:			**17. LIMITATION OF ABSTRACT**	**18. NUMBER OF PAGES**	**19a. NAME OF RESPONSIBLE PERSON**
a. REPORT	**b. ABSTRACT**	**c. THIS PAGE**	UU	99	Suhithi Peiris
Unclassified	Unclassified	Unclassified			**19b. TELEPHONE NUMBER** *(include area code)* 703-767-4732

CONVERSION TABLE

Conversion Factors for U.S. Customary to metric (SI) units of measurement.

MULTIPLY →	BY →	TO GET
TO GET ←	BY ←	DIVIDE
angstrom	1.000 000 x E -10	meters (m)
atmosphere (normal)	1.013 25 x E +2	kilo pascal (kPa)
bar	1.000 000 x E +2	kilo pascal (kPa)
barn	1.000 000 x E -28	meter^2 (m^2)
British thermal unit (thermochemical)	1.054 350 x E +3	joule (J)
calorie (thermochemical)	4.184 000	joule (J)
cal (thermochemical/cm^2)	4.184 000 x E -2	mega joule/m^2 (MJ/m^2)
curie	3.700 000 x E +1	*giga bacquerel (GBq)
degree (angle)	1.745 329 x E -2	radian (rad)
degree Fahrenheit	$t_k = (t^\circ f + 459.67)/1.8$	degree kelvin (K)
electron volt	1.602 19 x E -19	joule (J)
erg	1.000 000 x E -7	joule (J)
erg/second	1.000 000 x E -7	watt (W)
foot	3.048 000 x E -1	meter (m)
foot-pound-force	1.355 818	joule (J)
gallon (U.S. liquid)	3.785 412 x E -3	meter^3 (m^3)
inch	2.540 000 x E -2	meter (m)
jerk	1.000 000 x E +9	joule (J)
joule/kilogram (J/kg) radiation dose absorbed	1.000 000	Gray (Gy)
kilotons	4.183	terajoules
kip (1000 lbf)	4.448 222 x E +3	newton (N)
kip/$inch^2$ (ksi)	6.894 757 x E +3	kilo pascal (kPa)
ktap	1.000 000 x E +2	newton-second/m^2 ($N-s/m^2$)
micron	1.000 000 x E -6	meter (m)
mil	2.540 000 x E -5	meter (m)
mile (international)	1.609 344 x E +3	meter (m)
ounce	2.834 952 x E -2	kilogram (kg)
pound-force (lbs avoirdupois)	4.448 222	newton (N)
pound-force inch	1.129 848 x E -1	newton-meter (N-m)
pound-force/inch	1.751 268 x E +2	newton/meter (N/m)
pound-force/$foot^2$	4.788 026 x E -2	kilo pascal (kPa)
pound-force/$inch^2$ (psi)	6.894 757	kilo pascal (kPa)
pound-mass (lbm avoirdupois)	4.535 924 x E -1	kilogram (kg)
pound-mass-$foot^2$ (moment of inertia)	4.214 011 x E -2	kilogram-meter^2 ($kg-m^2$)
pound-mass/$foot^3$	1.601 846 x E +1	kilogram-meter^3 (kg/m^3)
rad (radiation dose absorbed)	1.000 000 x E -2	**Gray (Gy)
roentgen	2.579 760 x E -4	coulomb/kilogram (C/kg)
shake	1.000 000 x E -8	second (s)
slug	1.459 390 x E +1	kilogram (kg)
torr (mm Hg, 0^0 C)	1.333 22 x E -1	kilo pascal (kPa)

*The bacquerel (Bq) is the SI unit of radioactivity; 1 Bq = 1 event/s.

**The Gray (GY) is the SI unit of absorbed radiation.

Final Report

Investigation of Fundamental Processes and Crystal-Level Defect Structures in Metal-Loaded High-Explosive Materials under Dynamic Thermo-Mechanical Loads and their Relationships to Impact Survivability of Munitions (Thrust 4, Topic J)

Grant Number: HDTRA-1-10-1-0078

PI: Prof. Donald L. Thompson (Chemistry, University of Missouri-Columbia)
Co-PI: Prof. Thomas D. Sewell (Chemistry, University of Missouri-Columbia)

Subcontractor: The Netherlands Organization Defence and Security (TNO)
PI: Dr. R. H. B. Bouma
Co-PI: Dr. A. E. D. M. van der Heijden

Period of Performance: 07/12/2010 - 07/11/2013

Theoretical (molecular dynamics) and experimental methods (microscopy and impact measurements) were used to investigate fundamental aspects of the physics and chemistry that determine the behavior of energetic materials in response to weak shock or non-shock insults, with emphasis on stress states and strain rates relevant to penetrator applications. We considered the RDX/Al/HTPB composite AFX-757 as a representative formulation. The theoretical studies were focused shock wave processes in RDX, PETN, nitromethane, and hydroxy-terminated polybutadiene. The experimental focus was AFX-757 composites formulated using three different grades of RDX crystals designated K1, K6, and K7 in the international RDX Round Robin collaboration.

Keywords: Molecular dynamics, confocal scanning laser microscopy, ballistic impact chamber, explosive, impact sensitivity, AFX-757, RDX, HTPB, shock waves

The **objective** of the research is to investigate fundamental physical and chemical processes that determine responses of EMs to shock and non-shock excitation: stress states, strain rates, energy localization, chemical initiation. The **relevance** is to contribute to understanding basic properties that determine metal-loaded composite materials survivability in penetrator applications, in particular understanding the relation between crystal defect structure and impact resistance and thereby improving requirements for the quality of EM ingredients. Among the fundamental physical issues of relevance are:

- Intrinsic material anisotropy, morphology, and complexity
- Mechanisms and energetics for inelastic deformation (plasticity) in low-symmetry polyatomic crystals, in polymers, and at interphases
- Fundamental intra-crystalline processes: Energy transfer mechanisms and rates, effects of hydrogen bonding, effects of defects
- Phase transitions: Shock-induced melting, and stress- and strain-induced polymorphism
- Interfaces: Stored energy and stress at interfaces or defects; transport properties at interfaces; polymer wetting properties

The **approaches taken** are (1) MD simulations performed using realistic force fields and (2) experimental characterization & validation of theoretical methods using systematic variation of RDX structure/morphology.

One Ph.D. in Chemistry will be granted for research performed as part of this project. (Reilly Eason, University of Missouri-Columbia)

Titles, authors, journal citations, and abstracts of all *published* manuscripts supported by this project are included below. Submitted manuscripts or ones in preparation, approximately five in total, are not included in the listing.

Molecular dynamics simulations of shock waves in hydroxyl-terminated polybutadiene melts: Mechanical and structural responses
Markus G. Fröhlich, Thomas D. Sewell, and Donald L. Thompson
Journal of Chemical Physics **140**, 024902 (2014)

The mechanical and structural responses of hydroxyl-terminated cis -1,4-polybutadiene melts to shock waves were investigated by means of all-atom non-reactive molecular dynamics simulations. The simulations were performed using the OPLS-AA force field but with the standard 12-6 Lennard-Jones potential replaced by the Buckingham exponential-6 potential to better represent the interactions at high compression. Monodisperse systems containing 64, 128, and 256 backbone carbon atoms were studied. Supported shock waves were generated by impacting the samples onto stationary pistons at impact velocities of 1.0, 1.5, 2.0, and 2.5 km s^{-1}, yielding shock pressures between approximately 2.8 GPa and 12.5 GPa. Single-molecule structural properties (squared radii of gyration, asphericity parameters, and orientational order parameters) and mechanical properties (density, shock pressure, shock temperature, and shear stress) were analyzed using a geometric binning scheme to obtain spatio-temporal resolution in the reference frame centered on the shock front. Our results indicate that while shear stress behind the shock front is relieved on a ~0.5 ps time scale, a shock-induced transition to a glass-like state occurs with a concomitant increase of structural relaxation times by several orders of magnitude.

Molecular dynamics simulations of shock waves in cis-1,4-polybutadiene melts
Lan He, Thomas D. Sewell, and Donald L. Thompson
Journal of Applied Physics **114**, 163517 (2013)

Molecular dynamics simulations of supported shock waves in monodisperse melts of cis-1,4-polybutadiene initially at atmospheric pressure and T = 413K were performed to study the shock-induced structural changes and post-shock relaxation. Simulations were performed for Rankine-Hugoniot shock pressures between 7.22 GPa and 8.26 GPa using the united-atom force field due to Smith and Paul [G. D. Smith and W. Paul, J. Phys. Chem. A **102**, 1200 (1998)] for systems composed of chains containing 32, 64, or 128 united atoms. The sensitivity of the results to the non-bonded interaction potential was studied by comparing results obtained using the Lennard-Jones 12–6 potential from the original Smith and Paul force field to ones obtained when the 12–6 potential was replaced by the Buckingham exponential–6 potential. Several structural and mechanical properties were studied as functions of distance (time) behind the shock front.

Bulk relaxation was characterized by calculating profiles of temperature, density, and principal and shear stress. Microscopic shock-induced structural rearrangement and relaxation were studied by calculating the ratio of Cartesian components of the mean-squared radius of gyration to corresponding values for the equilibrated material; dihedral angle distributions; and the distribution of, and second Legendre polynomial order parameter for, the angle formed by covalent bond vectors and the shock propagation direction.

Pivot algorithm and push-off method for efficient system generation of all-atom polymer melts: Application to hydroxyl-terminated polybutadiene
Markus G. Fröhlich and Thomas D. Sewell
Macromolecular Theory and Simulations **22**, 344 (2013)

Procedures used to generate initial conditions for all-atom molecular dynamics (MD) simulations of amorphous polymer systems are described. The pivot algorithm is applied directly to produce unbranched hydroxyl-terminated cis-1,4-polybutadiene molecules with chain lengths ranging from 8 to 64 monomeric units (32 to 256 carbon atoms), based on the OPLS all-atom force field. The generated molecular configurations are characteristic of (pseudo-) ideal conditions and therefore exhibit the same properties as polymer chains in a melt. We analyze both the mean squared chain dimensions and their distributions in order to validate the correctness of this approach. The chains are efficiently packed into 3d-periodic simulation cells using the push-off method and subsequently equilibrated by standard MD. Together, the pivot algorithm and push-off method provide the means for efficient generation of equilibrated dense polymer melts for multi-million-atom systems.

Microscopic characterization of defect structure in RDX crystals
R. H. B. Bouma, W. Duvalois, and A. E. D. M. van der Heijden
Journal of Microscopy **252**, 263 (2013)

Three batches of the commercial energetic material RDX, as received from various production locations and differing in sensitivity towards shock initiation, have been characterized with different microscopic techniques in order to visualize the defect content in these crystals. The RDX crystals are embedded in an epoxy matrix and cross-sectioned. By a treatment of grinding and polishing of the crystals, the internal defect structure of a multitude of energetic crystals can be visualized using optical microscopy, scanning electron microscopy and confocal scanning laser microscopy. Earlier optical micrographs of the same crystals immersed in a refractive index matched liquid could visualize internal defects, only not in the required detail. The combination of different microscopic techniques allows for a better characterization of the internal defects, down to inclusions of approximately 0.5μm in size. The defect structure can be correlated to the sensitivity towards a high-amplitude shock wave of the RDX crystals embedded in a polymer bonded explosive. The obtained experimental results comprise details on the size, type and quantity of the defects. These details should provide modellers with relevant and realistic information for modeling defects in energetic materials and their effect on the initiation and propagation of shock waves in PBX formulations.

Post-shock relaxation in crystalline nitromethane
Luis A. Rivera-Rivera, Thomas D. Sewell, and Donald L. Thompson
Journal of Chemical Physics **138**, 084512 (2013)

Molecular dynamics simulations of shocked (100)-oriented crystalline nitromethane were carried out to determine the rates of relaxation behind the shock wave. The forces were described by the fully flexible non-reactive Sorescu-Rice-Thompson force field [D. C. Sorescu, B. M. Rice, and D. L. Thompson, J. Phys. Chem. B **104**, 8406 (2000)]. The time scales for local and overall thermal equilibration in the shocked crystal were determined. The molecular center-of-mass and atomic kinetic energy distributions rapidly reach substantially different local temperatures. Several picoseconds are required for the two distributions to converge, corresponding to establishment of thermal equilibrium in the shocked crystal. The decrease of the molecular center-of-mass temperature and the increase of the atomic temperature behind the shock front exhibit essentially exponential dependence on time. Analysis of covalent bond distance distributions ahead of, immediately behind, and well behind the shock front showed that the effective bond stretching potentials are essentially harmonic. Effective force constants for the C–N, C–H, and N–O bonds immediately behind the shock front are larger by factors of 1.6, 2.5, and 2.0, respectively, than in the unshocked crystal; and by factors of 1.2, 2.2, and 1.7, respectively, compared to material sufficiently far behind the shock front to be essentially at thermal equilibrium.

Molecular dynamics simulations of shock waves in oriented nitromethane single crystals: Plane-specific effects
Lan He, Thomas D. Sewell, and Donald L. Thompson
Journal of Chemical Physics **136**, 034501 (2012)

Molecular dynamics simulations of supported shock waves (shock pressure $P_s \sim 15$ GPa) propagating along the [110], [011], [101], and [111] directions in crystalline nitromethane initially at T = 200 K were performed using the nonreactive Sorescu-Rice-Thompson force field [D. C. Sorescu, B. M. Rice, and D. L. Thompson, J. Phys. Chem. B **104**, 8406 (2000)]. These simulations, combined with those from a preceding study of shocks propagating along [100], [010], and [001] directions in nitromethane for similar conditions of temperature and shock pressure [L. He, T. D. Sewell, and D. L. Thompson, J. Chem. Phys. **134**, 124506 (2011)], have been used to study the post-shock relaxation phenomena. Shocks along [010] and [101] lead to a crystal-crystal structure transformation. Shocks propagating along [011], [110], [111], [100], and [001] exhibit plane-specific disordering, which was characterized by calculating as functions of time the 1D mean square displacement (MSD), 2D radial distribution function (RDF), and 2D orientation order parameter $P_2(\theta)$ in orthogonal planes mutually perpendicular to the shock plane; and by calculating as functions of distance behind the shock front the Cartesian components of intermolecular, intramolecular, and total kinetic energies. The 2D RDF results show that the structural disordering for shocks along [100], [110], and [111] is strongly plane-specific; whereas for shocks along [001] and [011], the loss of crystal structural order is almost equivalent in the orthogonal planes perpendicular to the shock plane. Based on the entire set of simulations, there is a trend for the most extensive disordering to occur in the (010) and (110) planes, less extensive disordering to occur in the (100) plane, and essentially no disordering to occur in the (001) plane. The 2D $P_2(\theta)$ and 1D MSD profiles show, respectively, that the orientational and translational disordering is plane-specific, which results in the plane-specific structural disordering observed

in the 2D RDF. By contrast, the kinetic energy partitioning and redistribution do not exhibit plane specificity, as shown by the similarity of spatial profiles of the Cartesian components of the intermolecular, intramolecular, and total kinetic energies in orthogonal planes perpendicular to the shock plane.

Shock-Induced Inelastic deformation in oriented Pentaerythritol Tetranitrate (Invited article)
Reilly M. Eason and Thomas D. Sewell
Journal of Physical Chemistry C **116**, 2226 (2012)

Molecular dynamics simulations were used to study the mechanisms of shock-induced inelastic deformation in oriented single crystals of the energetic material pentaerythritol tetranitrate (PETN). Supported planar shock waves with Rankine-Hugoniot shock pressures $\mathbf{P}_{\text{R-H}} \sim 9$ GPa were propagated along two different crystal directions: one that is sensitive to initiation ([001]) and another that is relatively insensitive to initiation ([100]). Qualitatively, it was observed that for the sensitive orientation only elastic compression occurred, leading to the propagation of a single wave through the material, whereas for the insensitive direction elastic compression at and immediately behind the shock front was followed by inelastic deformation, leading to a two-wave structure in which the sharp elastic front moves through the crystal at a higher speed than the broader plastic wave. The detailed responses were characterized by calculating several structural and thermal properties including: relative center-of-mass molecular displacements (RMDs), classification of molecules behind the shock front as either elastically compressed or inelastically displaced, spatially resolved intermolecular and intramolecular temperatures (kinetic energies), and pre- and postshock intramolecular dihedral angle distributions. A quasi-2D system was studied for the [100] shock to further characterize the inelastic deformation mechanisms. Subregions exhibiting differing types of deformation were identified and examined in greater detail; specifically, time histories of the total kinetic energy (expressed in temperature units) and the rotational order parameter were calculated separately for elastically compressed and inelastically displaced molecules in a given subregion. The times required for re-establishment of the Maxwell-Boltzmann distribution of atomic kinetic energies and molecular center-of-mass kinetic energies in the shocked material were determined.

Simulations of deformation processes in energetic materials (Invited book chapter)
Richard H. B. Bouma, Antoine E. D. M. van der Heijden, Thomas D. Sewell, and Donald L. Thompson
In "Numerical Simulations of Physical and Engineering Processes", J. Awrejcewicz Ed. (InTech Open Access, Rijeka, Croatia, 2011). pp. 17-58.

[Summary paragraph from Introduction] This chapter gives an overview of simulations of deformation processes in energetic materials at the macro-, meso-, and molecular scales. Both non-reactive and reactive processes are considered. Macroscale simulations are usually developed to mimic real life situations (for example, munitions performance under intended conditions or response under accident scenarios) or are used in the development of small-scale experiments designed to elucidate fundamental properties and behaviors. Because macroscale simulations lack detailed information concerning microscopic physics and chemistry, their use for predicting energetic materials initiation is generally limited to engineering applications of the types mentioned above. For many applications, however, the macroscopic treatment is sufficient

to characterize and explain the deformation behavior of PBXs. At the other extreme of space and time scales, MD can be used to simulate the fine scale details of deformation, including detailed mechanisms of phase changes, chemistry, and processes that occur at material interfaces or other spatial heterogeneities. Mesoscale simulation and theory is required to bridge the gap between these limiting cases.

Molecular dynamics simulations of shock waves in oriented nitromethane single crystals
Lan He, Thomas D. Sewell, and Donald L. Thompson
Journal of Chemical Physics **134**, 124506 (2011)

The structural relaxation of crystalline nitromethane initially at $T = 200$ K subjected to moderate (∼15 GPa) supported shocks on the (100), (010), and (001) crystal planes has been studied using microcanonical molecular dynamics with the nonreactive Sorescu–Rice–Thompson force field [D. C. Sorescu, B. M. Rice, and D. L. Thompson, J. Phys. Chem. B **104**, 8406 (2000)]. The responses to the shocks were determined by monitoring the mass density, the intermolecular, intramolecular, and total temperatures (average kinetic energies), the partitioning of total kinetic energy among Cartesian directions, the radial distribution functions for directions perpendicular to those of shock propagation, the mean-square displacements in directions perpendicular to those of shock propagation, and the time dependence of molecular rotational relaxation as a function of time. The results show that the mechanical response of crystalline nitromethane strongly depends on the orientation of the shock wave. Shocks propagating along [100] and [001] result in translational disordering in some crystal planes but not in others, a phenomenon that we refer to as *plane-specific disordering*; whereas for [010] the shock-induced stresses are relieved by a complicated structural rearrangement that leads to a paracrystalline structure. The plane-specific translational disordering is more complete by the end of the simulations (∼6 ps) for shock propagation along [001] than along [100]. Transient excitation of the intermolecular degrees of freedom occurs in the immediate vicinity of the shock front for all three orientations; the effect is most pronounced for the [010] shock. In all three cases excitation of molecular vibrations occurs more slowly than the intermolecular excitation. The intermolecular and intramolecular temperatures are nearly equal by the end of the simulations, with 400–500 K of net shock heating. Results for two-dimensional mean-square molecular center-of-mass displacements, calculated as a function of time since shock wave passage in planes perpendicular to the direction of shock propagation, show that the molecular translational mobility in the picoseconds following shock wave passage is greatest for [001] and least for the [010] case. In all cases the root-mean-square center-of-mass displacement is small compared to the molecular diameter of nitromethane on the time scale of the simulations. The calculated time scales for the approach to thermal equilibrium are generally consistent with the predictions of a recent theoretical analysis due to Hooper [J. Chem. Phys. **132**, 014507 (2010)].

First Year Report

Investigations of Fundamental Processes and Crystal-Level Defect Structures in Metal-Loaded High-Explosive Materials under Dynamic Thermo-Mechanical Loads and their Relationships to Impact Survivability of Munitions

HDTRA1-10-1-0078

Report Period: September 1, 2010 – August 31, 2011

PI: Donald L. Thompson

Department of Chemistry

University of Missouri-Columbia (MU)

Columbia, MO 65211-7600

Telephone: 573.882.0051

E-mail: thompsondon@missouri.edu

Co-PI: Thomas D. Sewell

MU Department of Chemistry

Subcontractor: TNO Defence, Safety, and Security

The Netherlands

PI: Dr. R. H. B. Bouma

Co-PI: Dr. A. E. D. M. van der Heijden

30 September 2011

This report summarizes the progress made during the first year of a combined theoretical and experimental study of factors controlling sensitivity and violence of reaction in metal-loaded RDX-based high explosive formulations under dynamic thermo-mechanical loads and their relationships to impact survivability of munitions. The theoretical work is being performed at the University of Missouri while the experimental work is being performed at TNO Defence, Safety, and Security (The Netherlands). Research performed in this report period consists of experiments and molecular dynamics (MD) simulations designed to investigate fundamental aspects of the physics and chemistry that determine the behavior of energetic materials in response to weak shocks or ramp-wave loading. One goal of the research is to identify, characterize, and quantify the underlying unit processes that, collectively, underpin the practical global behaviors of energetic composites that emerge on continuum length scales. Another objective is to characterize and demonstrate experimentally in small-scale laboratory tests the influence of energetic crystal defect structures on the sensitivity under strain rate conditions relevant to penetrator applications for actual explosive formulations.

Molecular Dynamics Simulations of Inelastic Deformation in Oriented Crystalline PETN (to appear in *J. Phys. Chem. C*)

Molecular dynamics simulations were used to study the mechanisms of shock-induced inelastic deformation in oriented single crystals of the energetic material pentaerythritol tetranitrate (PETN, see Fig. 1). Supported planar shock waves with Rankine-Hugoniot shock pressures $P_{R\text{-}H} \sim 9$ GPa were propagated along two different crystal directions; one that is sensitive to initiation ([001]) and another that is relatively insensitive to initiation ([100]).[1-3] Qualitatively it was observed that for the sensitive orientation only elastic compression occurred, leading to the propagation of a single wave through the material; whereas for the insensitive direction elastic compression at and immediately behind the shock front was followed by inelastic deformation, leading to a two-wave structure in which the sharp elastic front moves through the crystal at a higher speed than the broader plastic wave. The detailed responses were characterized by calculating several structural and thermal properties including: relative center-of-mass molecular displacements (RMDs), classification of molecules behind the shock front as either elastically compressed or inelastically displaced, spatially-resolved intermolecular and intramolecular temperatures (kinetic energies), and pre- and post-shock intramolecular dihedral angle distributions. A quasi-2D system was studied for the [100] shock to further characterize the inelastic deformation mechanisms. Subregions exhibiting differing types of deformation were identified and examined in greater detail; specifically, time histories of the total kinetic energy (expressed in temperature units) and the rotational order parameter were calculated separately for elastically-compressed and inelastically-displaced molecules in a given subregion. The times required for re-establishment of the Maxwell-Boltzmann distribution of atomic kinetic energies and molecular center-of-mass kinetic energies in the shocked material were determined. All simulations were performed using the LAMMPS[4] code in conjunction with the nonpolarizable, nonreactive, flexible-molecule force field for alkyl nitrates developed by Borodin *et al*.[5]

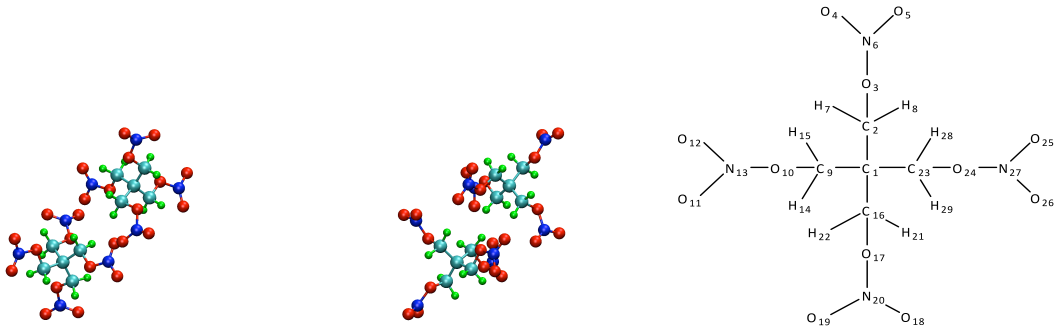

FIG. 1. *Depictions of PETN crystal. (Left) Unit cell viewed down the [001] axis; (Center) unit cell viewed down the [100] axis. Atoms colors are: carbon, cyan; nitrogen, blue, oxygen, red; hydrogen, green. (Right) Covalent atomic connectivity and numbering scheme used in the simulations.*

Inelastic deformation at the molecular scale was characterized by calculating relative molecular displacements (RMDs) of nearest-neighbor molecular centers of mass using the method described by Jaramillo *et al*.[6] Components of the RMDs calculated at the times of maximum compression for the [001] and [100] shocks are shown in Figures 2(a)-(b) and 2(c)-(d), respectively. In all cases the abscissa corresponds to the shock direction. The two ordinates for a given shock correspond to the transverse directions; that is, the RMDs are projected into (010) and (100) planes for shocks propagating along [001], and (001) and (010) planes for shocks propagating along [100]. For shock propagation along [001] (Figures 2(a)-(b)) the RMDs in both planes cluster around zero, suggesting that only elastic compression has occurred in the material. By contrast, while [001] components of RMDs for the [100] shock are clustered relatively close to zero (Figure 2d), significant displacements are observed for [100] and [010] components (Figures 2(c)-(d)), meaning that relatively large translational displacements have occurred.

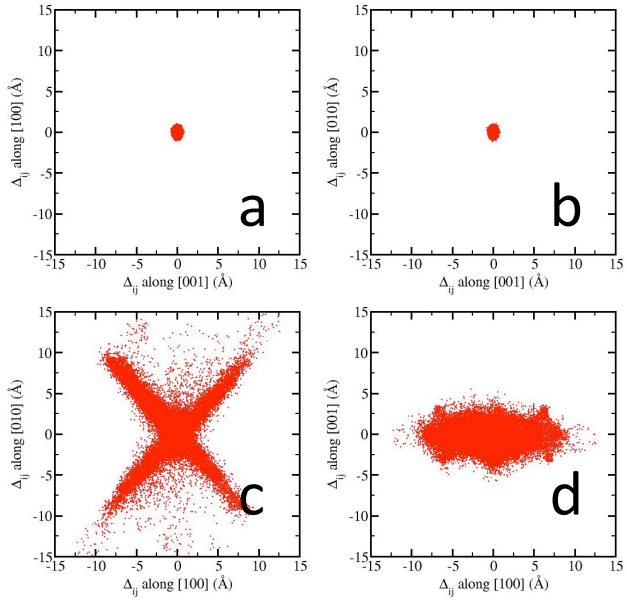

FIG. 2. *Relative molecular displacements at times of maximum compression. Panels (a) and (b): Projections into the (010) and (100) planes, respectively, for the [001] shock. Panels (c) and (d): Projections into the (001) and (010) planes, respectively, for the [100] shock.*

The results in Figure 2 are consistent with expectations from the steric hindrance model.[64] For the impact strength considered, shocks along the sensitive [001] direction do not activate any slip systems that would relieve the shear stress imparted by the shock (at least, not on the time scale and space scale of the present simulations, which were performed for crystals with no pre-existing defects). Therefore, little or no inelastic deformation should occur, consistent with the results in Figures 2(a)-(b). By contrast, shocks along the insensitive [100] direction do activate a slip system that relieves the shock-induced shear stresses, leading to the inelastic deformation that is evident in Figures 2(c)-(d).

Figure 3 contains snapshots of the 3D systems for [001] and [100] shocks (panels (a) and (b), respectively) at the times of maximum compression. Only molecular centers of mass are shown. Elastically-compressed molecules are shown in blue while those deemed to have undergone inelastic displacements are colored red. Note that whereas for the [001] shock (Figure 3a) only elastic compression has occurred, for the [100] shock (Figure 3b) there are two distinct regions in the shocked material; a region of elastic compression immediately behind the shock front and a region further to the left in which plasticity is developing. Therefore, for the shock strength considered the (100)-oriented crystal is clearly in the two-wave elastic-plastic region of the shock Hugoniot locus. Because the two waves propagate at different speeds, it is not appropriate to regard as stationary a spatiotemporal reference frame centered on the shock front.

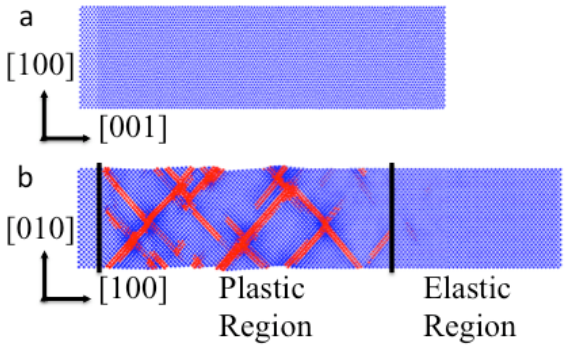

FIG. 3. *Orthographic projections of the pistons and flexible slabs at the times of maximum compression in the 3D systems. (a) [001] shock; (b) [100] shock. Only molecular centers of mass are shown. Elastically-compressed and inelastically-displaced molecules are colored blue and red, respectively.*

Spatially-resolved kinetic energies, expressed in temperature units for ease of presentation and henceforth referred to as temperatures, were partitioned into translational and ro-vibrational components using the method due to Strachan and Holian.[7] Instantaneous spatial profiles of the intermolecular and intramolecular temperatures are shown in Figure 4 at 5.0 ps intervals starting from $t = 0$. Results for the intermolecular and intramolecular temperatures for the [001] shock are shown in panels (a) and (b), respectively; corresponding quantities for the [100] shock are shown in panels (c) and (d). The rapid initial rise and subsequent decrease in intermolecular temperature (panels (a) and (c)) confirms expectations that energy from the shock wave is initially distributed principally among the lattice modes of the crystal. The intramolecular temperatures increase monotonically for both shock orientations; no transient excitation is observed. Note that complete equilibration between the intermolecular and intramolecular temperatures has not been established for either shock orientation by the respective times of maximum compression; in both cases the two temperature measures differ by 20-30 K. Overall, the qualitative features of the temperature profiles for the two shocks are consistent with the steric hindrance model, for which a split wave is anticipated in the [100] shock (insensitive orientation) but not in the [001] shock (sensitive orientation).

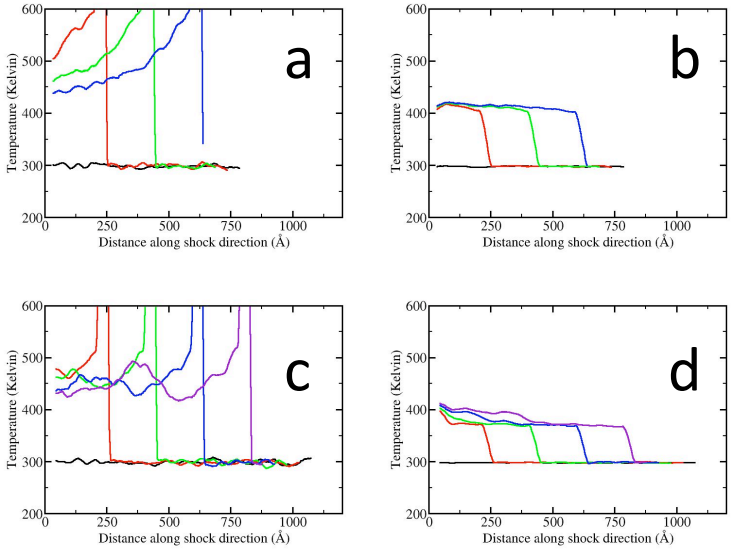

FIG. 4. *Instantaneous spatial profiles for intermolecular (panels (a) and (c)) and intramolecular (panels (b) and (d)) temperature at 5.0 ps intervals starting from the time of shock initiation in the flexible slabs (t = 0). Panels (a) and (b): [001] shock; panels (c) and (d): [100] shock.*

Distributions of CCON and CONO dihedral angles were calculated to assess the differences in intramolecular distortion caused by the shock waves; these internal coordinates are of particular interest due to the floppy nature of the PETN molecule (see Figure 1). There are four CCON and eight CONO dihedral angles per molecule. Results for the CCON and CONO dihedrals are presented in Figures 5 and 6, respectively. In both figures panel (a) corresponds to unshocked material and panel (b) to material in the [001] shock; panels (c) and (d) are for the [100] shock and correspond, respectively, to elastically-compressed and inelastically-displaced molecules. Results in panels (b)-(d) were obtained at the times of maximum compression for the respective shocks.

The CCON dihedral angles are essentially *trans* in the unshocked crystal (peaks at ±180° in Figure 5a). Comparing panels (a) and (b), shock loading along [001] leads to modest splitting of the *trans* peak into two peaks with unequal amplitudes and shifted toward smaller angles by about 20°; no new peaks emerge. Shocking along [100] leads to greater changes in the CCON dihedral distributions (panels (c) and

(d)). The main peak still corresponds to the *trans* CCON dihedral both for the elastically-compressed and inelastically-displaced molecules (panels (c) and (d), respectively). In both cases new broad peaks emerge, centered about ±90°; the amplitudes of these peaks for the inelastically-displaced molecules are much larger than for the elastically-compressed ones. Based on these results we conclude that the CCON dihedrals in [100]-shocked PETN crystal rotate with less hindrance than those in [001]-shocked crystal. The less hindered dihedral rotation about C-O bonds for shocks along the [100] direction compared to the [001] direction could play a role in facilitating slip in shocked (100)-oriented PETN as part of the mechanism for relieving the shock-induced shear stresses.

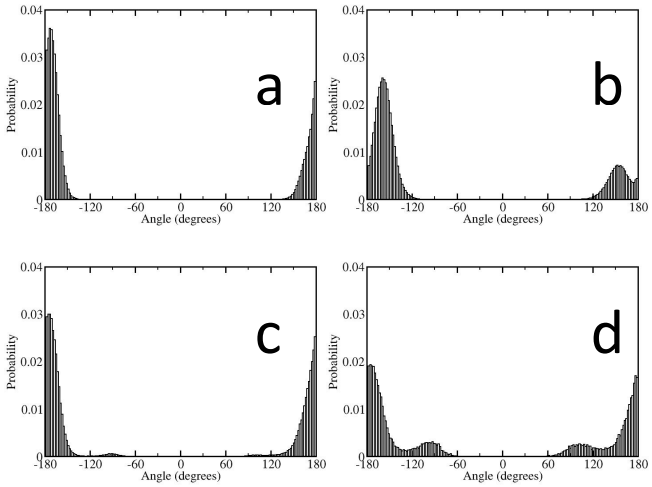

FIG. 5. *Distributions of CCON dihedral angles. (a) Unshocked material (equivalent for both shock orientations); (b) [001] shock; (c) and (d) [100] shock: molecules determined to have undergone (c) elastic compression and (d) inelastic displacement. Results in (b)-(d) correspond to instants of maximum compression in the respective simulations.*

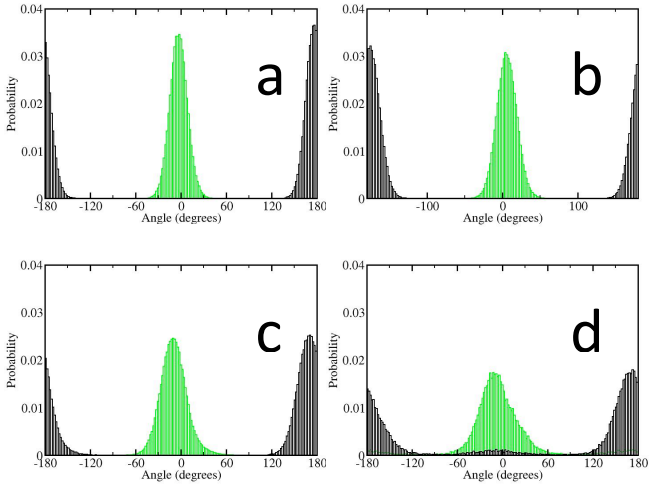

FIG. 6. *As in Figure 5 except results for CONO dihedral angles are shown. Green and black histograms correspond to molecules initially in* cis *and* trans *conformations, respectively.*

Each H_2C-O-NO_2 moiety in PETN has one *cis* and one *trans* CONO dihedral in the equilibrium crystal structure. Shock loading along [001] has very little effect on the CONO dihedral distributions at the instant of maximum compression (Figure 6b); the distributions are noticeably broadened, but all CONO dihedrals remain essentially *cis* or *trans* and there is no evidence for rotation of the NO_2 group. That is, there are no initially *cis* dihedrals that have become *trans* at the end of the simulation or *vice versa*. The situation is different for the [100] shock; while most CONO dihedrals at the time of maximum compression are either *cis* or *trans*, the distribution exhibits nonzero probability for all angles in the domain. Moreover, a number of initially *trans* CONO dihedrals have become *cis* by the time of maximum compression and *vice versa*, indicating that NO_2 rotation does occur for molecules involved in inelastic deformation events.

A [100] shock simulation was performed using a large quasi-2D slab to eliminate any possible finite-size effects in the (001) plane and allow for more thorough characterization of the shock-induced inelastic deformation. The results revealed several types of deformation processes in the plastic zone including full dislocations, stacking faults, intersecting slip zones, and regions of more generalized plastic flow. Subregions of material containing these defects were identified for additional study. The same approach used to construct Figure 3 based on classification of individual molecules as either elastically compressed or inelastically displaced at the instant of maximum compression was used to generate Figure 7, in which it is evident that finite-size effects in the (001) plane have been essentially, if not completely, eliminated.

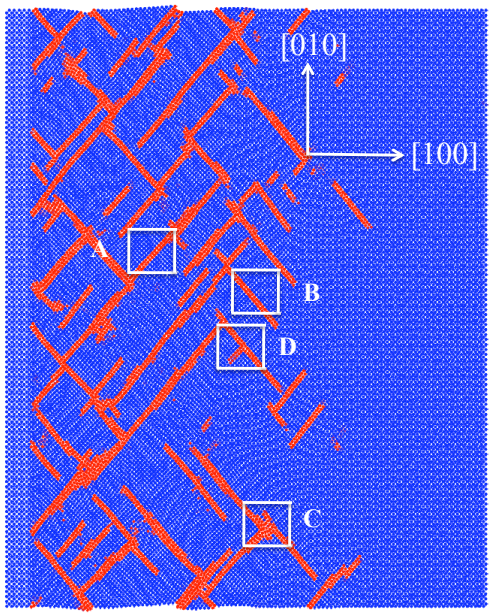

FIG. 7. *Orthographic projection of the piston and flexible slab for the quasi-2D shock at the time of maximum compression. Elastically-compressed and inelastically-displaced molecules are colored blue and red, respectively. Regions A, B, C, and D are discussed in Figure 8.*

Time histories of total kinetic energies, expressed in temperature units using the equipartition theorem $T = 2E_k/(3Nk)$, were calculated separately for elastically-compressed and inelastically-displaced molecules in each region (see Figure 8). Passage of the elastic precursor wave leads to an initial shock heating to about 375 K in all cases, followed by increases in temperature due to passage of the plastic wave through the material. The temperature of the inelastically-displaced molecules in regions A and B

rises from 375 K to about 460 K in a time span of 4 ps followed by a slower cooling to a final temperature of about 425 K. The increase is due to the conversion of potential energy to kinetic energy during the localized slip process and the cooling is due to the subsequent energy equilibration with the surroundings. Region C exhibits a slower rate of heating than the other regions but settles at a higher final temperature (~450 K). The slower rate in region C is a result of the less-localized deformation, while the higher temperature overall arises due to the greater net plastic deformation in that region. Region D exhibits an initial rise in temperature as the process of slip begins. The increase ceases at a temperature of about 420 K when the intersection of the planes of deformation halts the growth of both slip zones.

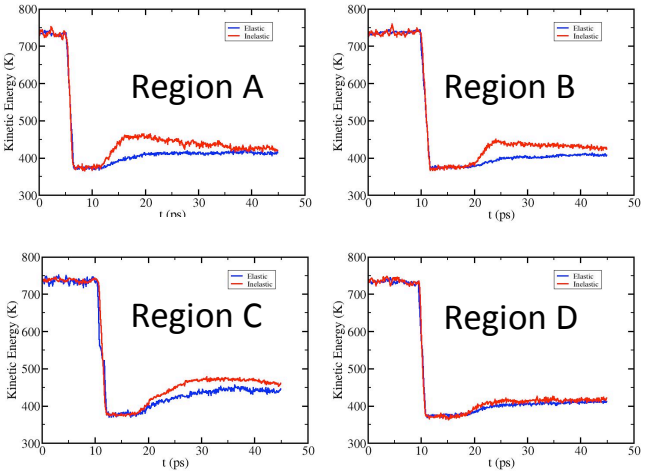

FIG. 8. *Time histories of total kinetic energies, expressed in temperature units, for molecules determined to be elastically (blue) and inelastically (red) displaced at the time of maximum compression in the quasi-2D [100] shock. Regions A, B, C, and D are defined in Fig. 7.*

For the [100] shock strength considered, $P_{R\text{-}H}^{[100]}$ = 8.7 GPa, distributions of molecular center-of-mass kinetic energies do not remain in local thermal equilibrium during the shock rise. Distribution functions for that quantity calculated in the shock front exhibit pronounced deviations from the Maxwell-Boltzmann distribution[8] that persist for a few to several molecular layers (*i.e.*, a few hundred to several hundred fs) behind the shock front (Fig. 9).

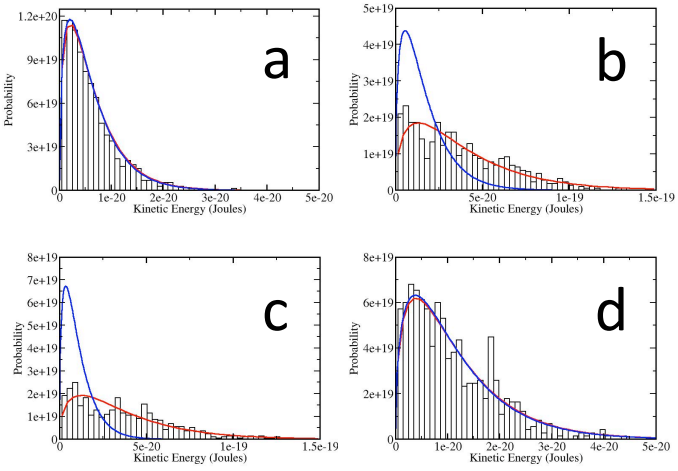

FIG 9. *Normalized histograms of molecular center-of-mass kinetic energies for [100]-shocked material: (a) five molecular layers in front of the shock front, (b) in the layer containing the shock front, (c) one molecular layer behind the shock front, and (d) two layers behind the shock front. Blue curves are Maxwell-Boltzmann distributions with the temperature defined in terms of the average kinetic energy in a given layer. Red curves are fits of the Maxwell-Boltzmann distribution to the histogram data, with temperature as the only fitting parameter. Note that abscissa and ordinate scales vary from one panel to the next.*

Molecular Dynamics Simulations of Shock Waves in Oriented Nitromethane Single Crystals: Plane-Specific Effects (submitted to *J. Chem. Phys.*)

Most theoretical studies of shock-induced deformation in molecular materials have been performed for energetic (high explosive) materials. Molecular dynamics (MD) studies have shown that shock-induced plastic deformation is governed by dislocations in PETN[2,9,10] and α-HMX[6] for weak shocks (4.7 GPa < shock pressure P_s < 7.2 GPa) propagating along [100]. In α-HMX the deformation mechanism changes to one dominated by nanoscale shear bands as the shock strength increases (7.2 GPa ≤ P_s < 23.2 GPa). Dislocation-mediated plasticity (homogeneously nucleated metastable stacking faults) has been predicted for weak shocks (1.3 GPa < P_s < 2.0 GPa) on (111)[11] and (021)[12] planes in α-RDX; for that same material, nanoscale shear bands were predicted for shocks (P_s ~ 10.0 GPa) propagating along [100][13,14] and the polymorphic α-γ solid-solid phase transition was reported for shocks propagating along [001].[14-16]

These kinds of well-defined plastic deformation processes observed for PETN, α-HMX, and α-RDX are less pronounced in shocked crystalline nitromethane. The MD simulation results of Siavosh-Haghighi *et al*.[17] show that shocks along [100] with P_s > 17.0 GPa induce melting within 4 ps in nitromethane. Our previous study[18] showed that the post-shock structural relaxation is strongly dependent on the shock orientation. Shocks propagating along [100] and [001] induced extensive disordering in some crystal planes but not others, a phenomenon that we referred to as *plane-specific disordering*; whereas the stresses induced by a shock of similar strength propagating along [010] were relieved through a solid-solid phase (crystal-paracrystal) transition. Insight into the nature and extent of plane-specific disordering is of fundamental relevance to understanding plasticity in energetic materials as well as other kinds of molecular crystals; for instance, pharmaceutical substances often have mechanical and structural properties quite similar to those of energetic materials. Our initial study[18] only qualitatively characterized plane-specific shock-induced disordering. We now have performed MD simulations with the non-reactive Sorescu-Rice-Thompson (SRT) force field,[19,20] which was used in our previous study, for shock waves propagating along [110], [011], [101], and [111] to quantitatively determine whether plane-specific disordering exists for translational as well as orientational motions. The new simulations were carried out for the same initial temperature (200 K) and impact velocity (2.0 km/s) studied previously[18] to allow direct comparisons with the results for the [100], [010], and [001] shocks.

The results, which are not detailed here due to the space that would be required, show that for the [010] and [101] shocks the post-shock material remains crystalline whereas for the other five cases plane-specific disordering occurs. To characterize the detailed mechanism of the plane-specific disordering phenomena, 2-D radial distribution functions (RDFs), 2-D orientation order parameters $P_2(\theta)$, and 1-D mean squared displacements (MSDs) were evaluated for orthogonal pairs of planes perpendicular to the shock planes for the [100], [001], [011], [110] and [111] shocks. The 2-D RDFs show that the structural disordering for the [100], [110], and [111] shocks is strongly dependent on which plane among those including the shock propagation direction is chosen, whereas for [001] and [011] shocks the loss of the structural order is less dependent on the particular plane chosen. Furthermore, some ordering of the post-shock material in the (001) plane occurs for both the [100] and [110] shocks, which implies that the structures in the family of (001) planes tend to retain some order. For both the [100] and [001] shocks the greatest disordering of the post-shock material appears in the (010) plane and for the [110] and [111] shocks the greatest disordering occurs in the $(\bar{1}10)$ plane. Together, these results imply that the post-shock structures in the (010) and $(\bar{1}10)$ planes have a greater tendency toward disordering. The most disordering for the [011] shock occurs in the $(0\bar{1}1)$ plane, whereas the least for this shock orientation (and also for the [001] shock) occurs in the (100) plane.

The plane-specific structural disordering follows from the plane-resolved rotational and translational motions. The 2-D $P_2(\theta)$ and 1-D MSD show that the loss of orientational and translational order is also

plane-specific. For the [100], [110], and [111] shocks, for which the plane-specific structural disordering is significant, the corresponding plane-specific orientational and translational disordering are readily apparent. The results, lower values of $P_2(\theta)$ and higher values of MSD, for those cases suggest that the loss of orientational and translational order is faster and more extensive in the structurally disordered planes. For the [001] and [011] shocks, for which most of the structural order is lost in both planes perpendicular to the shock plane, the pathways by which this occurs differ for the two planes studied. Specifically, for the [001] shock the post-shock material in the (100) plane approaches a disordered state *via* faster rotational motion coupled with slower translational motion whereas in the (010) plane it tends to take the opposite pathway. For the [011] shock, the lower rotational and translational mobility in the $(0\bar{1}1)$ plane still leads to more disordering, due to the lower ordered state for the pre-shock material in this plane.

The analysis, for the [111] shock, of Cartesian components of intermolecular, intramolecular, and total kinetic energies as functions of position along the shock propagation direction reveal that the partitioning and redistribution of the kinetic energies in the planes perpendicular to the shock plane does not vary from one plane to the next, which implies that plane-specific rotational and translational motions cannot be attributed to the localization of kinetic energy partitioning. Equilibration among Cartesian components of intermolecular kinetic energy parallel and perpendicular to the shock direction occurs almost instantly whereas for the intramolecular kinetic energy the perpendicular components remain distinct from the parallel component for distances greater than 150 Å behind the shock front. However, the overall equilibration time is orientation-dependent. Therefore, the predicted overall plane-specific disordering (including structural, rotational and translational disordering), intrinsically results from the structural anisotropy of the nitromethane crystal.

Molecular Dynamics Simulations of Void Collapse in (100)-Oriented RDX

Following appropriate checks on force field implementation in the LAMMPS code, we have recently undertaken simulations of void collapse in (100)-oriented RDX using the Smith-Bharadwaj[21] force field developed originally for HMX. These simulations are at a preliminary stage. Figure 10 contains three snapshots depicting the molecular center-of-mass positions during shock-induced collapse of a cylindrical void with initial diameter 20 nm in a quasi-two-dimensional simulation cell. The shock was generating by impacting the sample from the right with speed u_p = 1.0 km·s^{-1} onto a stationary piston, leading to a shock propagating from left to right through the sample with shock velocity u_s = 5.5 km·s^{-1} and associated Rankine-Hugoniot shock pressure P_s = 9.8 GPa. The initial temperature was T = 300 K. Molecules on the surface of the void prior to shock arrival are colored red. The observation of the nucleation and growth of nanoscale shear bands in the material to the left of the void, and symmetric collapse of the void with small jets meeting near the stagnation plane at angles approximately ±45° relative to the direction of shock propagation (blue incursions into the red region in the right-hand panel), are both consistent with expectations[13,22] based on previous simulation results for this shock orientation and impact strength. In the coming year we will perform detailed studies of void collapse for multiple impact speeds, void configurations, and crystal diameters. We are also planning simulations of shock waves propagating normal and perpendicular to crystal grain boundaries and at crystal/polymer interfaces between RDX and polybutadiene.

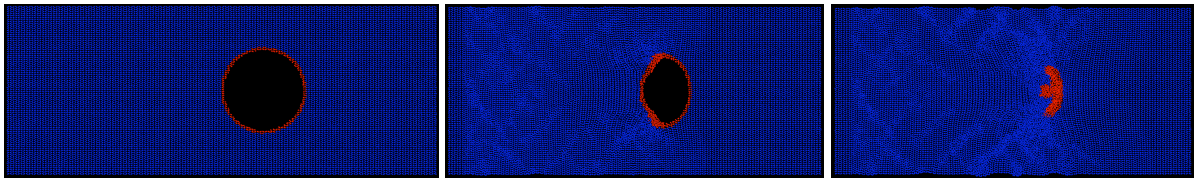

FIG. 10. *Snapshots from a simulation of void collapse in (100)-oriented RDX.*

Generation of Molecular Dynamics Simulation Cells for Amorphous of Poly(Butadiene)

We have developed a code, and are currently validating it, for generating molecular dynamics simulation cells for amorphous polymers. The code, which is based on the algorithm due to Theodorou and Suter,[23] can accommodate multi-chain systems using both coarse-grained (*e.g.*, united atom models in which a —CH_2— group is treated as a single particle) and fully atomic models. It is currently being adapted to treat two-dimensionally periodic simulation cells suitable for use in simulations of shocks in pure polymer or at a polymer/substrate interface. Our initial testing is being performed for all-*cis* poly(butadiene) (PBD) using the united atom model developed by Smith and Paul[24] and using the fully-atomic Generalized AMBER Force Field (GAFF[25]). Figure 11 contains snapshots of a representative energy-minimized three-dimensionally periodic simulation cell containing 40 PBD chains each of which is 96 monomer unit long. The two snapshots correspond to the same system; the left panel depicts unwrapped coordinates in which polymer chains extend beyond the boundaries of the periodic simulation cell whereas the right panel contains the same chains folded into the cell. In the coming year we will perform simulations of shock waves propagating through PBD. We will also study shock waves propagating normal and perpendicular to RDX/PBD interfaces.

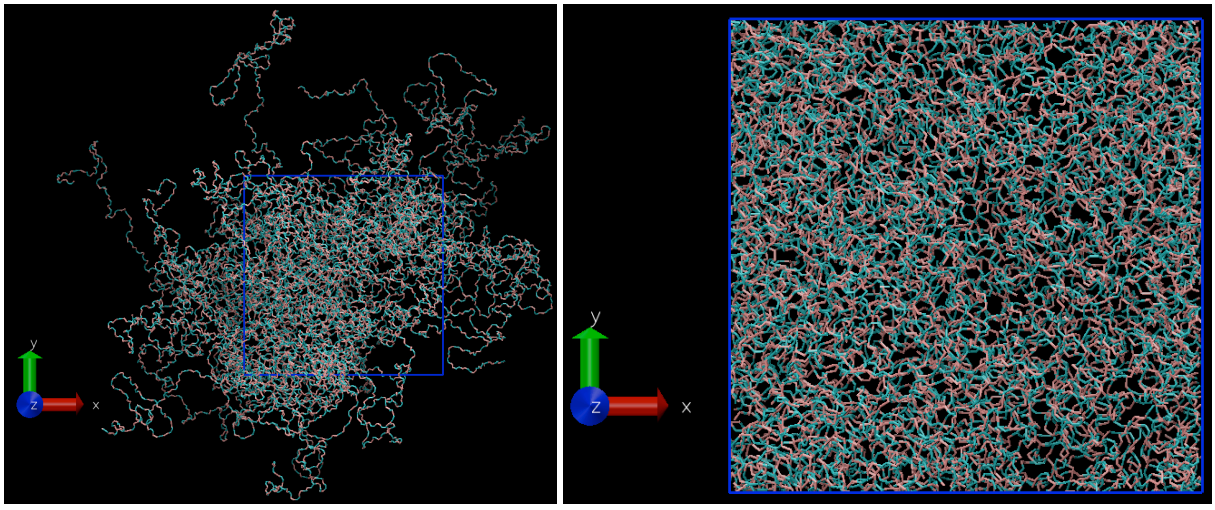

FIG 11. *Snapshots from a simulation cell for amorphous all-*cis *poly(butadiene). Left: unwrapped coordinates; right: wrapped coordinates. The blue square has the same dimensions in both cases.*

REFERENCES

[1] J. J. Dick, *Applied Physics Letters* **1984**, *44*, 859.
[2] J. J. Dick, R. N. Mulford, W. J. Spencer, D. R. Pettit, E. Garcia, D. C. Shaw, *Journal of Applied Physics* **1991**, *70*, 3572.
[3] J. J. Dick, *Journal of Applied Physics* **1997**, *81*, 601.
[4] S. Plimpton, *Journal of Computational Physics* **1995**, *117*, 1; http://lammps.sandia.gov.
[5] O. Borodin, G. D. Smith, T. D. Sewell, D. Bedrov, *The Journal of Physical Chemistry B* **2007**, *112*, 734.
[6] E. Jaramillo, T. D. Sewell, A. Strachan, *Physical Review B* **2007**, *76*, 064112.
[7] A. Strachan. B. L. Holian, *Physical Review Letters* **2005**, *94*, 014301.
[8] D. A. McQuarrie, *Statistical Mechanics*; University Science Books: Sausalito, California, 2000.
[9] J. Halfpenny, K. J. Roberts, J. N. Sherwood, *Journal of Applied Crystallography* **1984**, *17,* 320.
[10] J. J. Dick, J. P. Ritchie, *Journal of Applied Physics* **1994,** *76*, 2726.
[11] M. J. Cawkwell, K. J. Ramos, D. E. Hooks, T. D. Sewell, *Journal of Applied Physics* **2010**, *107*, 063512.

[12] K. J. Ramos, D. E. Hooks, T. D. Sewell, M. J. Cawkwell, *Journal of Applied Physics* **2010**, *108*, 066105.
[13] M. J. Cawkwell, T. D. Sewell, L. Zheng, D. L. Thompson, *Physical Review B* **2008**, *78*, 014107.
[14] D. Bedrov, J. B. Hooper, G. D. Smith, T. D. Sewell, *Journal of Chemical Physics* **2009**, *131*, 034712.
[15] J. E. Patterson, Z. A. Dreger, Y. M. Gupta, *Journal of Physical Chemistry B* **2007**, *111*, 10897.
[16] L. B. Munday, P. W. Chung, B. M. Rice, S. D. Solares, *Journal of Physical Chemistry B* **2011**, *115*, 4378.
[17] A. Siavosh-Haghighi, R. Dawes, T. D. Sewell, D. L. Thompson, *Journal of Chemical Physics* **2009**, *131*, 064503.
[18] L. He, T. D. Sewell, D. L. Thompson, *Journal of Chemical Physics* **2011**, *134*, 124506.
[19] D. C. Sorescu, B. M. Rice, D. L. Thompson, *Journal of Physical Chemistry B* **2000**, *104*, 8406.
[20] P. M. Agrawal, B. M. Rice, D. L. Thompson, *Journal of Chemical Physics* **2003**, ***119***, 9617.
[21] G. D. Smith, R. K. Bharadwaj, *Journal of Physical Chemistry B* **1999**, *103*, 3570.
[22] M. J. Cawkwell, T. D. Sewell (unpublished).
[23] D. N. Theodorou, U. W. Suter, *Macromolecules* **1985**, *18*, 1467.
[24] G. D. Smith, W. Paul, *Journal of Physical Chemistry A* **1998**, *102*, 1200.
[25] J. Wang, R. M. Wolf, J. W. Caldwell, P. A. Kollman, D. A. Case, *Journal of Computational Chemistry* **2004**, *25*, 1157 http://ambermd.org/antechamber/gaff.html .

Memorandum

Earth, Environmental and Life Sciences
Lange Kleiweg 137
2288 GJ Rijswijk
Postbus 45
2280 AA Rijswijk

www.tno.nl

T +31 88 866 80 00
F +31 88 866 69 49
infodesk@tno.nl

Aan

Van
Dr. ir. R.H.B. Bouma

Onderwerp
Annual report

Datum
13 september 2011

Onze referentie
<vnr-ext>

Doorkiesnummer
+31 88 866 14 20

The Statement of Work has been discussed by DTRA, University of Missouri and TNO at the Gordon Conference 2010. The SOW for the first two years is given below. The tasks for the first year are discussed in the annual report.

Year #1

- Y1T1: Implementation of atomic potentials relevant to AFX-757
- Y1T2: Atomic-scale studies of single-component materials (input from TNO regarding RDX orientations of principal interest, output to TNO regarding fundamental material equation of state and thermal properties)
- Y1T3: Anisotropic static and dynamic atomic-scale studies of uniaxial loading (output to TNO regarding dominant orientation-dependent deformation mechanisms in RDX)
- Y1T4: Preparation of three plastic-bonded explosives using different grades of RDX
- Y1T5: Experimental characterization of RDX batches
- Y1T6: Experimental determination of deformation initiation threshold in a homogeneous deformation experiment
- Y4T3: Confocal scanning laser microscopy (CSLM) on crystal/PBX level using the PBXs containing the original RDX batches (different grades, see Y1T4)

Year #2

- Y2T1: Atomic-scale studies of anisotropic response of constituent materials under multi-axial loading
- Y2T2: Atomic-scale studies of effects of voids and other defect structures (input from TNO regarding dominant defect types and geometries, including differences between “bulk” and “surface” defects)
- Y2T3: Atomic-scale studies of interfaces and grain boundaries (with input from TNO regarding particle habit and morphology)
- Y4T3 (Continued): Confocal scanning laser microscopy (CSLM) on crystal/PBX level using the PBXs containing the original RDX batches (different grades, see Y1T4)
- Y2T4: Experimental determination of deformation initiation threshold with the Ballistic Impact Chamber
- Y4T4: Experimental determination of deformation initiation threshold with the Ballistic Impact Chamber set-up using unreacted samples taken from **Y1T6** that were subjected to homogeneous deformation below their initiation threshold in order to assess whether the initiation threshold has changed
- Y5T3: CSLM on crystal/PBX level using deformed unreacted samples from the BIC characterization (see Y2T4) and samples shocked below their deformation initiation threshold (see Y1T6)

Accomplishments

Three RDX grades with different internal quality, from RS-RDX Round Robin program, are chosen and set aside for this project. These RDX grades will be referred to as K1, K6 and K7, have a varying degree of crystal quality and originate from BAe Royal Ordnance, Dyno (Type II), and ADI, respectively. Samples are prepared by embedding the RDX crystals in an epoxy matrix in order to observe the internal defects in the RDX crystals. The surface of the epoxy matrix containing the RDX crystals is polished and a microscope is used to monitor the surface in between polishing steps and adjust the polishing procedure, i.e. co-rotational velocity of sample and polishing plate, pressure, duration. Several microscopic techniques are applied to demonstrate features of the RDX crystal defects. With an optical microscope in incident light mode, voids in the crystals are clearly demonstrated. Differential interference contrast shows small surface features at the cross-sections. More details at the surface of the cross-section are obtained by a FEI NovaNanoSEM 650 Scanning Electron Microscope. The microscope is operated in low vacuum mode to avoid electrical charging and sublimation in high vacuum.

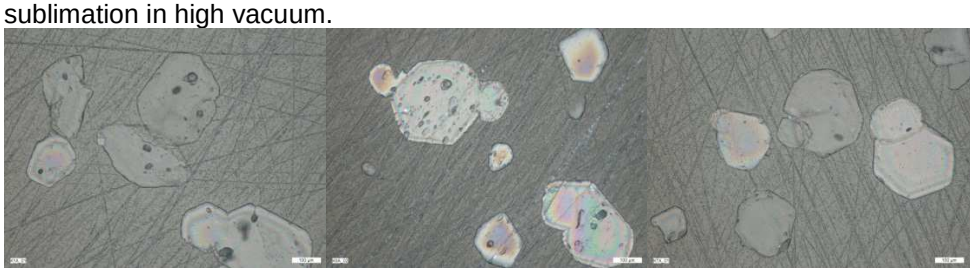

Optical micrographs of K1, K6 and K7 RDX crystals in incident light mode.

Optical micrographs of K1, K6 and K7 RDX crystals in differential interference contrast mode.

During the growth of a crystal the growth conditions like supersaturation, impurity concentration and boundary layer thickness, may vary locally. These variations are reflected in the single crystal in the form of growth banding, growth sectors and sector boundaries. Growth bands and growth sectors have been observed e.g. in K6 and K7, but not in K1, when observing dissections of these crystals by means of differential interference contrast microscopy, see figures above. Typical scanning electron micrographs for the crystals are shown in the figures below. Large epoxy filled cavities can be present in K1 crystals. One may argue if such cavities would have been observed by SEM looking at the crystals themselves. In K6 crystals many submicron voids are observed throughout a crystal cross-section and in many crystals and even “pearl chains” of these submicron voids are now identified. Typical for the K7 crystals are sharp-edged surfaces where one can distinguish individual grains, that are separated even up to a few µm distance.

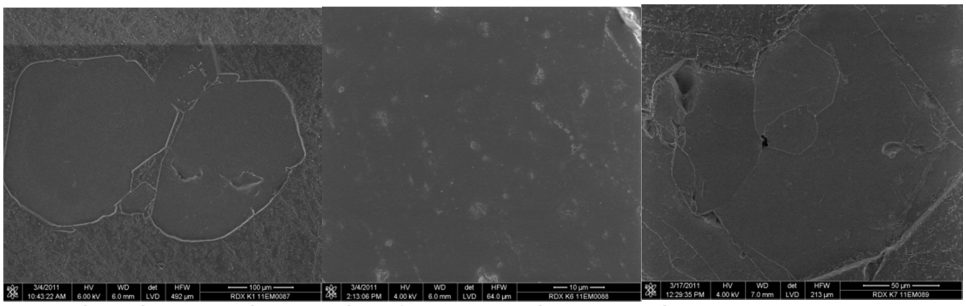

Scanning electron micrographs of K1, K6 and K7 crystals.

At the moment a publication is being prepared. The results of optical microscopy and SEM will be complemented with the results of confocal scanning laser microscopy, to finish this paper.
Samples for CSLM have been prepared and first images are made. 2D CSLM pictures are obtained at various depth in the same crystal. This task is on schedule and will continue according to the project proposal into the second year. One of the issues in the second year is to check the software on the possibility to create 3D defect information based on 2D CSLM pictures.

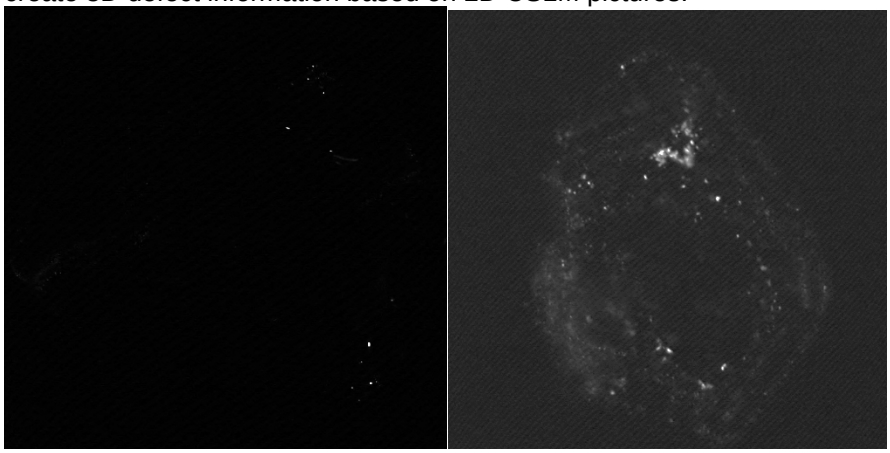

Confocal scanning laser micrograph of K1 and K6 RDX crystal.

Three Polymer Bonded eXplosives have been made with a similar composition. The Class I RDX has been varied using K1, K6 and K7 RDX crystals. The composition contains 25 % Class I RDX (K1, K6 or K7 grade), 33 % aluminium AS081, 30 % AP (200 micron diameter) and an HTPB based binder system: 4.40 % HTPB R-45HT, 6.61 % DOA, 0.45 % IPDI, 0.05 % TPB, 0.05 % Flexzone 6H and 0.40 % lecithine.

Explosion driven deformation tests have been performed in two configurations and with the three PBXs. The left hand picture below shows the standard geometry. The thickness of the plastic explosive layer is varied, and the rubber layer has a fixed thickness. From left to right: a 5 cm steel tube filled sand, a 10 cm steel tube filled with the PBX, and a 5 cm steel tube filled with sand. At the far left is a small amount of plastic explosive in which a detonator is put. As the detonation propagates from left to right, it will deform the three steel tubes and the explosive main charge will react to certain extent.

The right hand picture shows the geometry that is used when in the standard geometry an increasing reaction is noticed. In this geometry there are two 10 cm steel cylinders filled with AFX757.

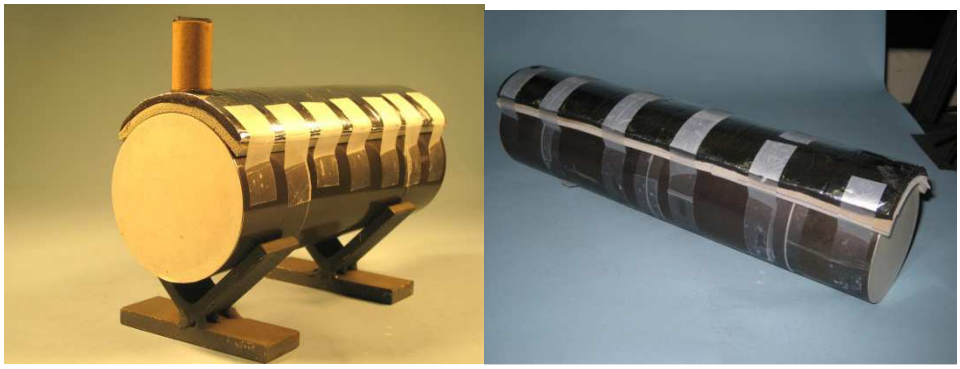

Homogeneous deformation experiment, standard (left) and elongated (right) geometry.

The experimental results with a 5 mm plastic explosive layer are shown here, for both standard and elongated geometry and for all three PBXs.
Results using the PBX with K7 RDX are shown below. At the left is the standard geometry. There is no fracturing of the casing at all. The diameter of the casing increases from left to right and decreases again, because of venting a non-sustained reaction. At the right is the elongated geometry. The reaction can propagate in comparison to the standard geometry, the first explosive filled cylinder has a continuous increasing diameter and the second cylinder has fractured in four parts.

PBX with K7 RDX

In the standard geometry an additional crack is noticed in the casing of the cylinder filled with PBX containing K6 RDX crystals. The reaction is more severe compared to the PBX with K7 RDX. Also in the elongated geometry a more severe reaction is noticed.

PBX with K6 RDX

The behavior of the deformed PBX with K1 RDX is different. In the standard geometry an initial reaction has started with a large crack/opening over the full length of the PBX casing. In the elongated geometry, a reaction builds up in the first 10 cm long steel cylinder. The reaction however is quenched in the second 10 cm long cylinder.

PBX with K1 RDX

The behavior of PBXs in the above explosive deformation test still needs an adequate explanation.

Presentations / publications

- Characterization of RDX from RS-RDX Round Robin by optical, scanning electron, and confocal scanning laser microscopy, R.H.B. Bouma, powerpoint presentation prepared for AC/326 SG1 on Energetic Materials, 26-27 October 2011, NATO, Brussels.
- A few micrographs of the RDX characterization have been incorporated into the chapter “Simulations of deformation processes in energetic materials”, R.H.B. Bouma, A.E.D.M. van der Heijden, T.D. Sewell, D.L. Thompson, in Numerical Simulations of Physical and Engineering Processes, ISBN 978-953-307-620-1, 2011.

Annual Report – Year Two

Investigations of Fundamental Processes and Crystal-Level Defect Structures in Metal-Loaded High-Explosive Materials under Dynamic Thermo-Mechanical Loads and their Relationships to Impact Survivability of Munitions

HDTRA1-10-1-0078

Report Period: September 1, 2011 – August 31, 2012

PI: Donald L. Thompson
Department of Chemistry
University of Missouri-Columbia (MU)
Columbia, MO 65211-7600
Telephone: 573.882.0051
E-mail: thompsondon@missouri.edu

Co-PI: Thomas D. Sewell
MU Department of Chemistry

Subcontractor: TNO Defence, Safety, and Security
The Netherlands
PI: Dr. R. H. B. Bouma
Co-PI: Dr. A. E. D. M. van der Heijden

22 October 2012

This report summarizes the progress made during the second year of a combined theoretical and experimental study of factors controlling sensitivity and violence of reaction in metal-loaded RDX-based high explosive formulations under dynamic thermo-mechanical loads and their relationships to impact survivability of munitions. The theoretical work is being performed at the University of Missouri while the experimental work is being performed at TNO Defence, Safety, and Security (The Netherlands, hereafter TNO). Research performed in this report period consists of experiments and molecular dynamics (MD) simulations designed to investigate fundamental aspects of the physics and chemistry that determine the behavior of energetic materials in response to weak shocks or impact-wave loading.

Mandatory Reporting Category 1: Accomplishments

1. What are the major goals of the project?

The objective of the project is to investigate fundamental physical and chemical processes that determine responses of EMs to shock and non-shock excitation: stress states, strain rates, energy localization, and chemical reaction initiation. The major goals of the research are to:

- Identify, characterize, and quantify the underlying unit processes that, collectively, underpin the practical global behaviors of energetic composites that emerge on continuum length scales.

- Characterize and demonstrate experimentally in small-scale laboratory tests the influence of energetic crystal defect structures on the sensitivity under strain rate conditions relevant to penetrator applications for actual explosive formulations.

2. What was accomplished under these goals?

The major activities are divided into theoretical research performed at the University of Missouri-Columbia and experimental research performed at TNO (The Netherlands). The materials studied were an earth-penetrating plastic-bonded explosives containing RDX, Al, HTPB, and AP, and the constituent materials RDX and HTPB.

Among the theoretical research performed under the auspices of this project during the second year was the development and application of methods for simulating shock waves in polymer materials, spall in molecular crystals and polymers, and shock waves in defective molecular crystals. Experimentally crystal characterization for three grades of RDX was performed using optical and electron microscopy and confocal scanning laser microscopy. Studies of sensitivity and violence of reaction in PBX materials formulated using the three grades of RDX were performed using a non-shock deformation protocol and the Ballistic Impact Chamber (BIC).

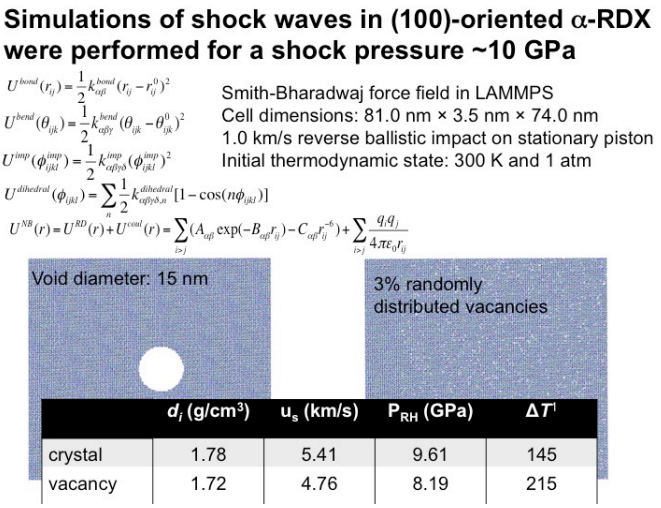

	d_i (g/cm^3)	u_s (km/s)	P_{RH} (GPa)	ΔT^t
crystal	1.78	5.41	9.61	145
vacancy	1.72	4.76	8.19	215

Figure 2. Summary of MD force field and overall physical dimensions and distribution of voids for simulations of shock waves in defective RDX crystals.

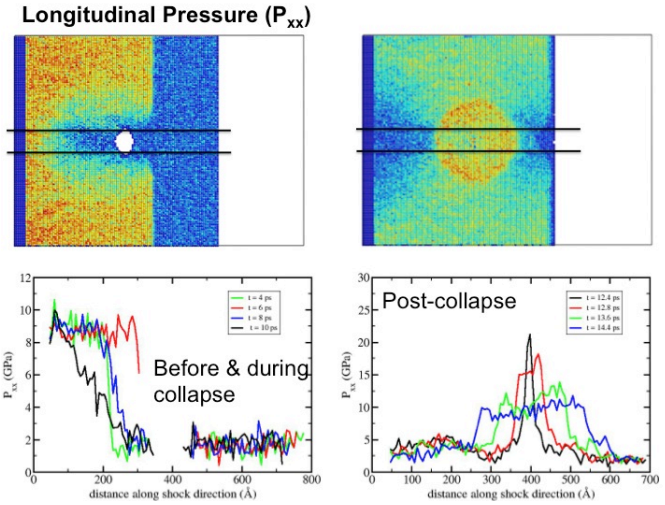

Figure 1. Top: spatial maps of longitudinal stress during (left) and immediately following (right) void collapse in (100)-oriented RDX. Bottom: Longitudinal stress vs. position along centerline for times prior to and during (left) and after (right) void collapse.

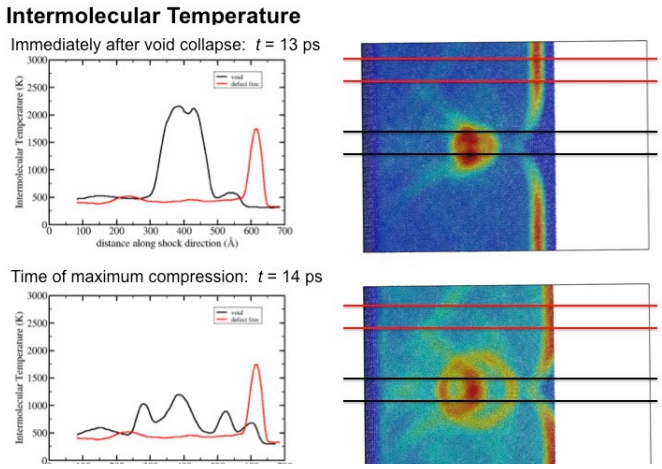

Figure 3. Top: Intermolecular temperature immediately after void collapse in shocked RDX. Pairs of horizontal red and black lines in the spatial maps

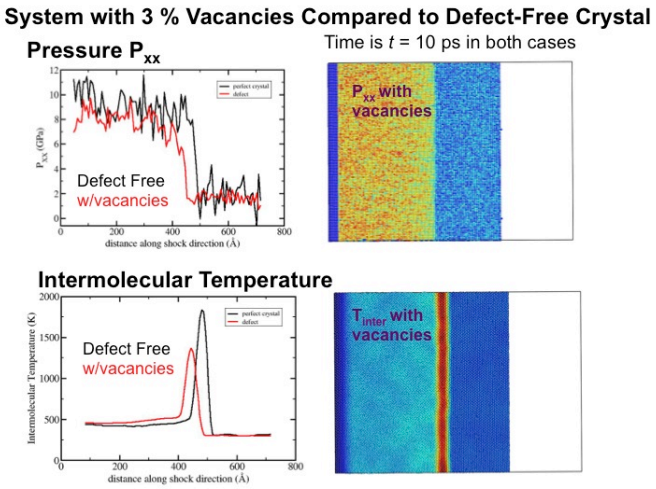

Figure 4. Comparison of longitudinal pressure (top) and intermolecular

MD simulations of shock waves in 1,4-*cis*-polybutadiene multi-chain systems in the amorphous state

cis-polybutadiene: [-CH_2-CH=CH-CH_2-]

➢ **Generation of initial amorphous microstructure**: equivalent Markov process[1] based on the RIS model[2, 3]

➢ **Force field: united-atom potential[4, 5]**

• **two types of non-bonded interaction**:

$$U_{LJ} = 4\varepsilon\left((\sigma/r)^{12} - (\sigma/r)^{6}\right), r < r_c$$
$$U_{\exp-6} = Ae^{-r/\rho} - C/r^{6}, r < r_c$$

• bond-stretching interaction: $U_{str}=K_{str}/2\ (l-l_0)^2$

• angle-bending interaction: $U_{str}=K_\theta/2\ (\theta-\theta_0)^2$

• torsional potential: $U_{tor} = \frac{1}{2}\sum_{n=1}^{6} K_n(1-\cos(n\phi))$

➢ **Relaxation of the initial microstructure**

• minimization + 3-D isothermal-isobaric (NPT) MD simulations

➢ **Shock simulations**

• generation of free surfaces running 2-D canonical (NVT) MD simulations

• shock loading in microcanonical (NVE) ensemble

[1] D. N. Theodorou, and U. W. Suter, Macromolecules **18**, 1467 (1985).
[2] Y. Abe, and P. J. Flory, Macromolecules **4**, 219 (1971). [3] J. E. Mark, J. Am. Chem. Soc. **89** (26), 6829 (1967).
[4] R. H. Gee, and R. H. Boyd, J. Chem. Phys. **101**, 8028 (1994). [5] G. D. Smith, and W. Paul, J. Phys. Chem. **102**, 1200 (1998).

Figure 5. Force field summary and simulation overview for MD simulations of shock waves in *cis*-poly(butadiene) (PBD) represented by coarse-grained (united atom) particles.

Coarse-Grained Force field: Validation

Near perfect agreement with published results for the same FF

▪ **United-atom potential with Lennard-Jones form**

system	C32 (168)~ 20 ns	C64 (64) ~ 40 ns	C96 (40) ~ 120 ns	C128 (32) ~ 150 ns	source
$\langle R^2\rangle$	*283±3*	618±11	*954±28*	1312±36	our results
$\langle R^2\rangle$	*270±10*	600±15	*950±20*	1335±30	Theodorou's[1]
$\langle R_g^2\rangle$	41±1	*96±1*	151±4	*212±6*	our results
$\langle R_g^2\rangle$	45±5	*95±10*	152±16	*215±18*	Theodorou's[1]
$\langle\rho\rangle$	*0.785*	0.826	*0.841*	0.844	our results
$\langle\rho\rangle$	*0.789*	0.827	*0.840*	0.846	Theodorou's[1]

$\langle R^2\rangle$: mean-square end-to-end distance; $\langle R_g^2\rangle$: mean-square radius of gyration; $\langle\rho\rangle$: the bulk mass density; all the results have been obtained from the equilibrated bulk systems after the nano-second NPT MD simulations.

The results also show that torsional angle distributions are in excellent agreement with the theoretical[2] and simulation[1] results.

▪ **the united-atom potential with the fitted exp-6 form**

Using the fitting approach due to Stephen L. Mayo et.al [3], here, ξ=13.772, leading to exp-6 having the same description near r_0 as the LJ form

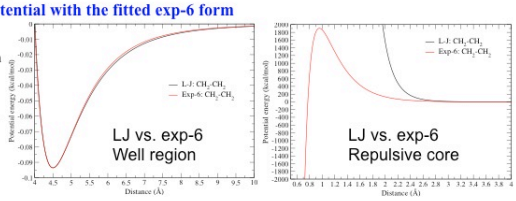

[1] G. Tsolou, V. G. Mavrantzas, and D. N. Theodorou, Macromolecules, **38**, 1478 (2005). [2] Y. Abe, and P. J. Flory, Macromolecules **4**, 219 (1971).
[3] Stephen L. Mayo, Barry D. Olafson, and William A. Goddard III, J. Phys. Chem. **94**, 8897 (1990).

Figure 6. Top: Table containing validation data for coarse-grained force field implemented by us compared to literature results. Bottom: comparison of non-bonded potentials represented by Lennard-Jones (LJ) and exponential-six (exp-6) functions for interatomic separations corresponding to the well region (left) and on the repulsive core (right).

Shock simulation results

▪ **Normal stress profiles**

• For a given chain type, longer chains yield higher principal stresses.
• Principal stresses are slightly higher for the shocked material with LJ interaction than the corresponding exp-6 system.
• The principal stresses equilibrate in a short time after the shock (next slide).

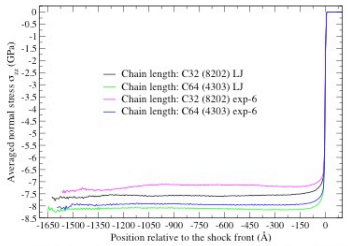

▪ **Shear stress τ_a profiles**

• The shear stress has a dramatic rise at the shock front followed by a fast relaxation.
•Systems with longer chains have higher shock-induced shear stress than those with shorter ones.

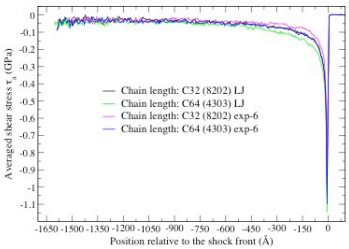

Figure 7. Top: Plots of principal stress components in shocked coarse-grained PBD for two molecular weights (32 and 64 carbon chains) with intermolecular potential represented by LJ and exp-6 functions. Bottom: As for top, except shear stress is shown.

Shock simulation results

▪ **Orientation order parameter P_2 (θ)**

▪ **The distribution of angle θ**

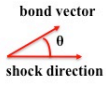

$P_2 = 1/2(3\cos\theta\times\cos\theta-1.0)$

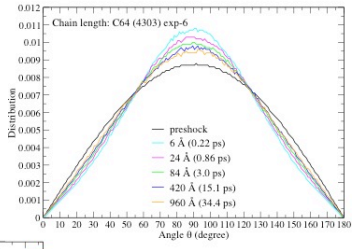

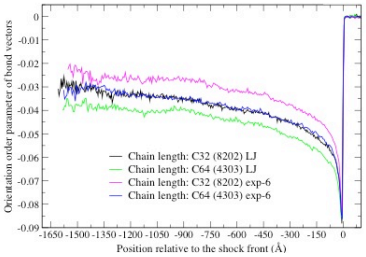

• Tendency for covalent bonds to orient perpendicular to the shock at short post-shock times.

•The bond deformation is reversible; the relaxation of the deformation is faster for the polymer systems in exp-6 interaction.

Figure 8. Top: Distributions of angles between covalent bonds and shock direction for C_{64} PBD for times prior to and following shock passage. Bottom: 2nd Legendre polynomial order parameter for C_{32} and C_{64} chains with LJ and exp-6 nonbonded interactions, showing dynamics of post-shock structural relaxation.

Overview and forcefield:

aim: large-scale MD shock simulations of Hydroxyl-terminated polybutadiene in full atomistic representation to study the behavior of the polymer chains

(n_C = 64,128 and 256 backbone carbons)

OPLS-AA: "Optimized Potentials for Liquid Simulations – all atom"

W.L. Jorgensen, D.S. Maxwell, J. Tirado-Rives, *J. Am. Chem. Soc.*, **118**, 11225 (1996)
G.A. Kaminski, R.A. Friesner, J. Tirado-Rives, W.L. Jorgensen, *J. Phys. Chem. B*, **105**, 6474 (2001)

atom types: H_O … hydroxyl H; H_C … alkane H; H_M … alkene H; C_O … alcoholic C; C_T … alkane C; C_M … alkene C; O_H … hydroxyl O

bonded terms:

$$E_{bond} = \sum_{bonds} K_r (r - r_{eq})^2 \qquad E_{angle} = \sum_{angles} K_\theta (\theta - \theta_{eq})^2$$

$$E_{torsion} = \sum_{dihedrals\ i} \frac{K_1^i}{2}(1+\cos\phi_i) + \frac{K_2^i}{2}(1-\cos 2\phi_i) + \frac{K_3^i}{2}(1+\cos 3\phi_i)$$

Figure 9. Force field summary and simulation overview for MD simulations of shock waves in *cis*-hydroxy-terminated poly(butadiene) (HTPB) represented using the all-atom OPLS force field.

overview and forcefield:

non-bonded terms: 12-6 for MC chain generation, exp-6 for MD!

$$E_{Coulomb} = \sum_{i<j}\left[k\frac{q_i q_j}{r_{ij}}\right]\cdot f_{ij} \qquad E_{LJ} = \sum_{i<j}\left[4\varepsilon_{ij}\left(\frac{\sigma_{ij}^{12}}{r_{ij}^{12}} - \frac{\sigma_{ij}^{6}}{r_{ij}^{6}}\right)\right]\cdot f_{ij} \qquad E_{EXP-6} = \sum_{i<j}\left[A\cdot e^{(1-r_{ij}/\rho)} - \frac{C}{r_{ij}^6}\right]\cdot f_{ij}$$

with $\begin{cases} f_{ij} = 0.0 & 1,2 \text{ and } 1,3 \ldots \\ f_{ij} = 0.5 & 1,4 \text{ interactions} \\ f_{ij} = 1.0 & \text{in all other cases} \end{cases}$

$$A = \varepsilon\cdot\left(\frac{6}{\zeta-6}\right)\cdot e^{\zeta} \quad \rho = \frac{r_0}{\zeta} \quad C = \varepsilon\cdot\left(\frac{\zeta}{\zeta-6}\right)\cdot r_0^6 \quad r_0 = \sqrt[6]{2}\cdot\sigma \quad \zeta = 13.772$$

S.L. Mayo, B.D. Olafson, W.A. Goddard, *J. Phys. Chem.*, **94**, 8897 (1990)

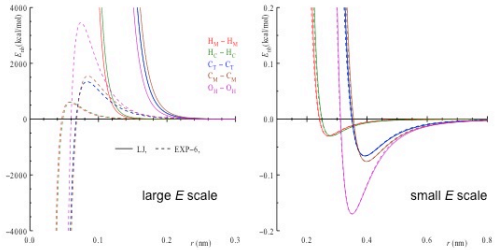

Figure 10. Comparison of non-bonded interatomic potentials represented using Lennard-Jones (LJ) and exponential-six (exp-6) functions. Left: repulsive core region; right: well region.

setup: **general procedure**

generate an ensemble of phantom chains with correct size and shape for a given C_∞ ← dynamic Monte Carlo process, PIVOT – algorithm: change random dihedral angle, accept new configuration according to its Boltzmann factor

pack chains randomly into simulation box

R. Auhl, R. Everaers, G.S. Grest, K. Kremer, S. Plimpton, *J. Chem. Phys.*, **119**,12718 (2003)

minimize $E = \langle n^2 \rangle - \langle n \rangle^2$, the atomic number density fluctuation in each subcell to achieve uniform density distribution ← linked-cell list: divide simulation box into subcells, randomly transform or rotate entire chains and accept only moves which minimize E

final density equilibration, thermalisation, build free polymer surface ← LAMMPS: *soft-* & *exp-6* potential 'Push-off', short NPT run, '2d' – NVT run

Figure 11. Scheme for generating equilibrated all-atom HTPB simulation cell.

Results: **investigated properties**

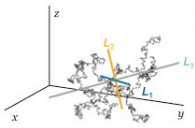

The size and the shape of single chains may be described by the **squared radius of gyration** and its **components along the principle axis of inertia** of an equivalent ellipsoid:

$$s^2 = \frac{1}{N}\sum_{i=1}^{n}\left[(x_i - x_c)^2 + (y_i - y_c)^2 + (z_i - z_c)^2\right] = s_x^2 + s_y^2 + s_z^2 \xrightarrow{\text{transformation}} L_1^2 + L_2^2 + L_3^2$$

The chain stiffness is defined via the **persistence length l_p**, which in turn may be extracted from the exponential decay of the bond-bond autocorrelation function:

$$\langle \mathbf{b}_i \cdot \mathbf{b}_{i+k} \rangle = \exp\left[-k\cdot l_b / l_p\right]$$

In order to analyze the orientation of the chains towards the shock direction (x) the **2nd-order Legendre polynomial $P_2(\theta)$** and the **average angle $\langle\alpha\rangle$ between L_3 and the z-direction** is used, respectively:

$$P_2(\theta) = \frac{1}{2}\left(3\cdot\langle\cos^2(\theta)\rangle - 1\right)$$

For the elucidation of the energy dissipation the **spectral density $S(\nu)$** is calculated from **Fourier transform of the mass-weighted velocity autocorrelation function** $C(\tau)$, given by:

$$C(\tau) = \sum_{i=1}^{n}\sum_{\alpha=1}^{3} m_i \cdot \frac{\langle v_{i\alpha}(0)\cdot v_{i\alpha}(\tau)\rangle}{\langle v_{i\alpha}(0)\cdot v_{i\alpha}(0)\rangle} \quad \rightarrow \quad S(\nu) \propto \int_{-\infty}^{\infty} C(\tau)\exp\left[-i2\pi\nu\tau\right]d\tau$$

Figure 12. Summary of structural and dynamical properties calculated for analysis of shock waves in all-atom HTPB.

Chain lengths: 64, 128, 256

Chain size is decreased by about 20% in the shocked state

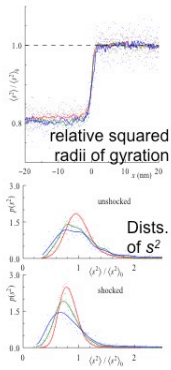

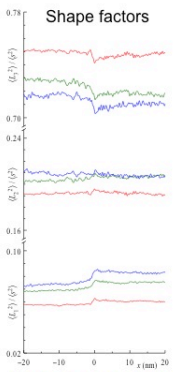

Chains become slightly more prolate under shock; the effect is larger for the longer chains.

Must be careful about transverse finite-size effects! For the longest chain systems, self-interactions may affect the rigid-body orientation of chains in unshocked material.

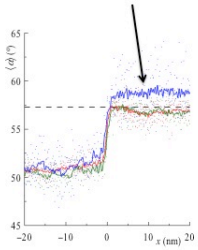

Relaxation of the coarse-grained chains is slower than for all-atom chains.

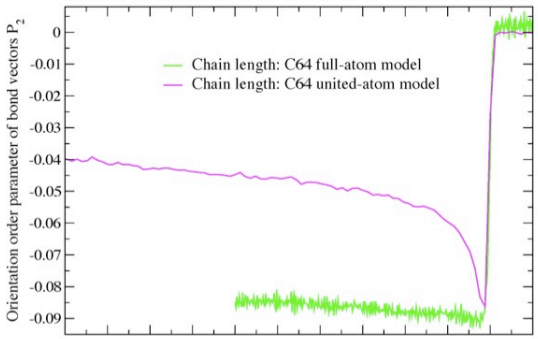

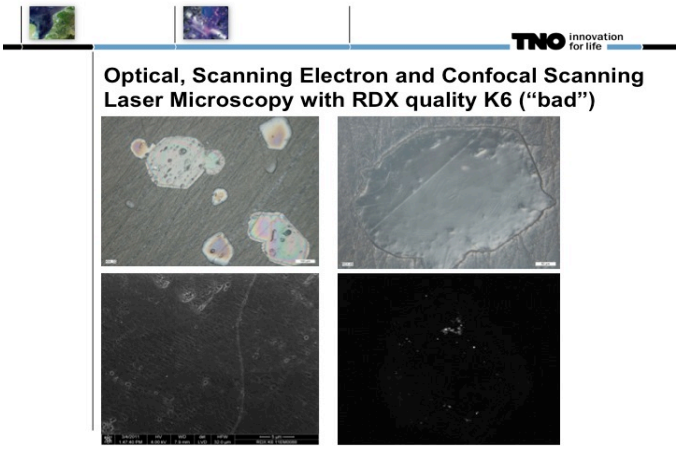

Figure 19. Images of “bad” RDX crystals showing voids/inclusions, growth bands, and “pearl necklace” defect lines.

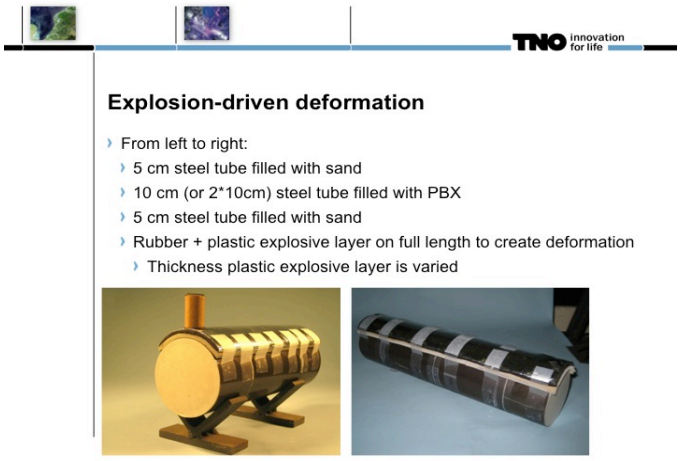

Figure 20. Overview of non-shock explosively-driven deformation experiment.

Figure 21. Results of explosively-driven deformation tests for PBX composites formulated using the “good”, “bad”, and “intermediate” grades of RDX crystals.

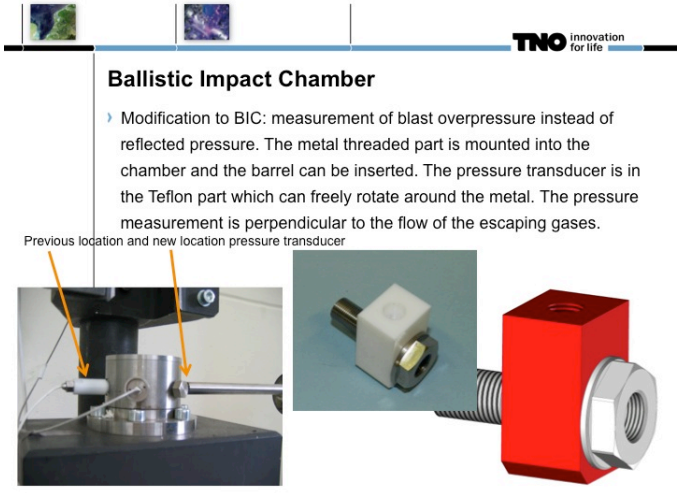

Figure 22. Summary slide describing modifications to BIC apparatus.

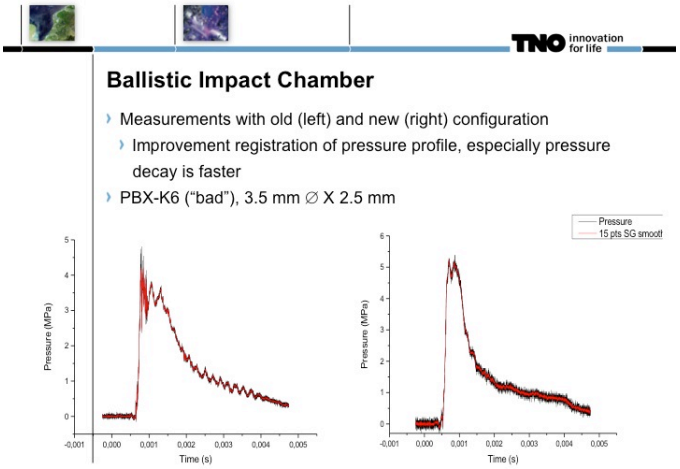

Figure 23. Effect of pressure sensor location in BIC apparatus on measured pressure time histories.

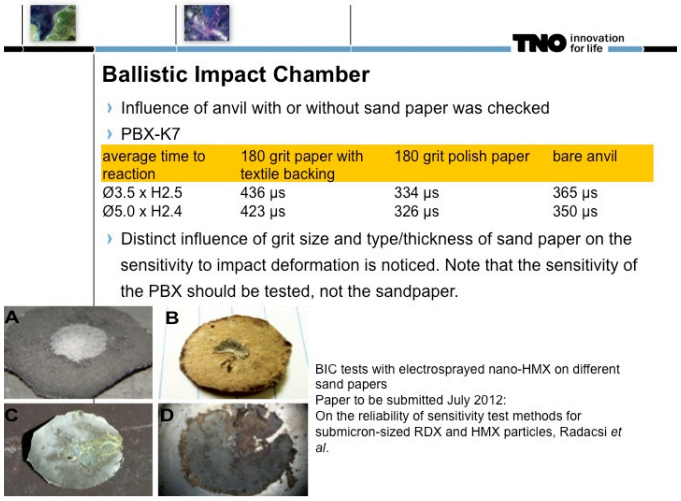

Figure 24. Effect of choice of anvil surface on BIC results.

. What opportunities for training and professional development has the project provided?

At the university of Missouri four postdoctoral research fellows and one Ph.D. graduate student were partially supported by this project during the second year. In addition to poster presentations by Mr. Reilly Eason and Dr. Markus Froehlich at the DTRA annual program review, Dr. Lan He gave a presentations at a LAMMPS (MD code) Users' Workshop as detailed below in Mandatory Reporting Category 2: Products: *Other publications, conference papers and presentations.*

4. How have the results been disseminated to communities of interest?

The research is being published in research journals and presented at scientific conferences and workshops, as detailed below in Mandatory Reporting Category 2.

5. What do you plan to do during the next reporting period to accomplish the goals?

Nothing to report.

Mandatory Reporting Category 2: Products

1. Publications, conference papers, and presentations:

- **Journal publications and invited book chapter**

1. Invited book chapter: Bouma, van der Heijden, Sewell, and Thompson, *Simulations of deformation processes in energetic materials,* in "Numerical Simulations of Physical and Engineering Processes", J. Awrejcewicz Ed. (InTech Open Access, Rijeka, Croatia, 2011). pp. 17-58.
2. Invited journal article: Eason and Sewell, *Shock-Induced Inelastic Deformation in Oriented Crystalline Pentaerythritol Tetranitrate (PETN)*, J. Phys. Chem. C **116**, 2226 (2012)
3. He, Sewell, and Thompson, *Post- Oriented-Shock Plane-Specific Relaxation of Crystalline Nitromethane*, J. Chem. Phys. **136**, 034501 (2012)

4. Bouma, Duvalois, and van der Heijden, *Characterization of defect structure in RDX crystals*, to be submitted to CrystEngComm

- **Other publications, conference papers and presentations**

1. Poster presentation by Dr. Lan He, Chemistry in Dynamic Extremes Workshop (Santa Fe, January 2012)
2. Presentation by Bouma at NATO AC/326 SG1 on Energetic Materials, NATO HQ (Brussels, 26-27/10/2011)
3. Invited presentation by Sewell at APS March Meeting, Focus Session: Simulation of Matter at Extreme Conditions - Energetic Materials (Boston, February 2012)
4. Invited lecture by Sewell at Institute of Shock Physics (Imperial College London) – Symposium on Energetic Materials (London, February 2012)
5. Presentation by Bouma at New Models and Hydrocodes (London, April 2012)
6. Invited presentation by Sewell at New Models and Hydrocodes (London, April 2012)
7. Invited presentation by Sewell at International Center for Applied Computational Mechanics (ICACM), ICACM-2012, Structured Materials: The role of structure on emerging material properties (New York City, June 2012)
8. Invited talk by Thompson at 2012 GRC on Energetic Materials (Snow Mountain, VT, June 2012)
9. Invited Colloquium by Sewell at Naval Postgraduate School (August 2012)

2. Website(s) or other Internet site(s)

Nothing to report.

3. Technologies or techniques

Nothing to report.

4. Inventions, patent applications, and/or licenses

Nothing to report.

5. Other products

Nothing to report.

Mandatory Reporting Category 3: Participants & Other Collaborating Organizations

1. What individuals have worked on the project?

- Donald L. Thompson, PI: 3 weeks summer month salary
  - All aspects of theoretical and computational research performed at the University of Missouri
- Thomas D. Sewell, Co-PI: 3 weeks summer month salary
  - All aspects of theoretical and computational research performed at the University of Missouri
- Lan He, Post-doctoral Fellow: 5 months @ 100% 1.0FTE
  - MD methods development for and simulations of shocks in coarse-grained poly(butadiene)
- Luis A. Rivera-Rivera, Post-doctoral Fellow: 3 months @ 50% 1.0FTE
  - MD simulations of shocks in oriented crystalline nitromethane
- Markus G. Froehlich, Post-doctoral Fellow: 8 months @ 50% 1.0FTE

- Reilly M. Eason, Ph.D. student: 6 months @ 100% 1.0FTE
    - Simulations and analysis of shock waves in oriented RDX crystals containing void defects
- Richard H. B. Bouma, Subcontractor PI
    - Crystal characterization and non-shock impact testing
- Antoine E. D. M. van der Heijden, Subcontractor Co-PI
    - Crystal characterization and non-shock impact testing

2. What other organizations have been involved as partners?

None.

3. Have other collaborators or contacts been involved?

None.

Mandatory Reporting Category 4: Impact

1. What is the impact on the development of the principal discipline(s) of the project?

New methods for simulating the fundamental behaviors of complicated materials with atomic and near-atomic spatial resolution under extreme thermodynamic conditions (shock compression and tension waves) were developed and applied to materials of interest to DTRA. While the methods and analysis tools were developed specifically for PBX constituents, their scope of application is general. For example, the methods developed for generating large samples of equilibrated polymer melts, or for monitoring energy transfer and inelastic deformation in energetic materials, could equally well apply to other application domains in physics, materials science, and the study of pharmaceutical materials. The work of the PI over the last 40 years has led to a Hirsch index of 38, indicating that his research is well-recognized in the scientific community.

2. What is the impact on other disciplines?

The research methods developed are fundamental and general in scope. Because they are directed toward gaining understanding of fundamental properties and processes in materials, they are applicable to a wide variety of materials in disciplines ranging from physics to pharmaceuticals.

3. What is the impact on the development of human resources?

In addition to the senior personnel on the project, four postdoctoral researchers and one graduate student were supported and therefore exposed/educated in areas of relevant to future DTRA needs (and U.S. STEM capabilities more generally). During the second year of the project, Co-PI Sewell was promoted from Associate Professor to Full Professor of Chemistry due, in part, to work performed under the auspices of this project.

4. What is the impact on physical, institutional, and information resources that form infrastructure?

Productivity under this project has increased the visibility of the theoretical chemistry/materials effort at the University of Missouri. This enhanced profile will allow us to attract additional graduate students and postdoctoral researchers, and compete more effectively for future research and equipment funding.

5. What is the impact on technology transfer?

6. What is the impact on society beyond science and technology?

Nothing to report.

7. What dollar amount of the award's budget is being spent in foreign country(ies)?

$153,000 (45%) of the annual $350,000 award was subcontracted to TNO (The Netherlands).

Mandatory Reporting Category 5: Changes/Problems

1. Changes in approach and reasons for change.

Nothing to report.

2. Actual or anticipated problems or delays and actions or plans to resolve them.

Due to our conclusions concerning the accuracy of the ReaxFF MD force field, we have decided the best course of action is to restrict our studies in the third year of the effort to non-reactive models. This does not strongly impact the third-year research plans, but would require some modifications to the proposed work for the optional 4^{th} and 5^{th} year extensions.

3. Changes that have a significant impact on expenditures.

Nothing to report.

Annual Report – Year Three

Investigations of Fundamental Processes and Crystal-Level Defect Structures in Metal-Loaded High-Explosive Materials under Dynamic Thermo-Mechanical Loads and their Relationships to Impact Survivability of Munitions

HDTRA1-10-1-0078

Report Period: September 1, 2012 – July 11, 2013

PI: Donald L. Thompson
Department of Chemistry
University of Missouri-Columbia (MU)
Columbia, MO 65211-7600
Telephone: 573.882.0051
E-mail: thompsondon@missouri.edu

Co-PI: Thomas D. Sewell
MU Department of Chemistry

Subcontractor: TNO Defence, Safety, and Security
The Netherlands
PI: Dr. R. H. B. Bouma
Co-PI: Dr. A. E. D. M. van der Heijden

July 23, 2013

This report summarizes the progress made during the third and final year of a combined theoretical and experimental study of factors controlling sensitivity and violence of reaction in metal-loaded RDX-based high explosive formulations under dynamic thermo-mechanical loads and their relationships to impact survivability of munitions. The theoretical work is being performed at the University of Missouri while the experimental work is being performed at TNO Defence, Safety, and Security (The Netherlands, hereafter TNO). Research performed in this report period consists of experiments and molecular dynamics (MD) simulations designed to investigate fundamental aspects of the physics and chemistry that determine the behavior of energetic materials in response to weak shocks or impact-wave loading.

Investigations of Fundamental Processes in Metal-Loaded High-Explosive Materials under Thermo-Mechanical Loads and Their Relationships to Survivability of Munitions

Theoretical Work:
University of Missouri
Donald L. Thompson
Thomas D. Sewell

Experimental Work:
TNO Defence, Security, and Safety (The Netherlands)
Richard H. B. Bouma
Antoine E. D. M. van der Heijden

Award Number: HDTRA1-10-1-0078

UNCLASSIFIED

Investigations of Fundamental Processes and Crystal-Level Defect Structures in Metal-Loaded High-Explosive Materials Under Thermo-Mechanical Loads and their Relationships to Survivability of Munitions

PI: D. L. Thompson U. of Missouri-Columbia (MU); Co-PI: T. D. Sewell (MU)
Subcontractor: TNO Defence, Security, and Safety (TNO, The Netherlands); PI: R. H. B. Bouma (TNO); Co-PI: A. E. D. M. van der Heijden (TNO)

Award Number: BRBAA08-Per3-J-2-0138

Objective: Investigate fundamental physical & chemical processes that influence responses of EMs to dynamic deformation: effects of crystal-level & inter-material defects on stress states, strain rates, energy localization, chemical initiation.

Relevance: Understanding basic properties that determine metal-loaded composite materials survivability in penetrator applications. Understanding the relation between crystal defect structure and impact resistance. Improving requirements for the quality of EM ingredients.

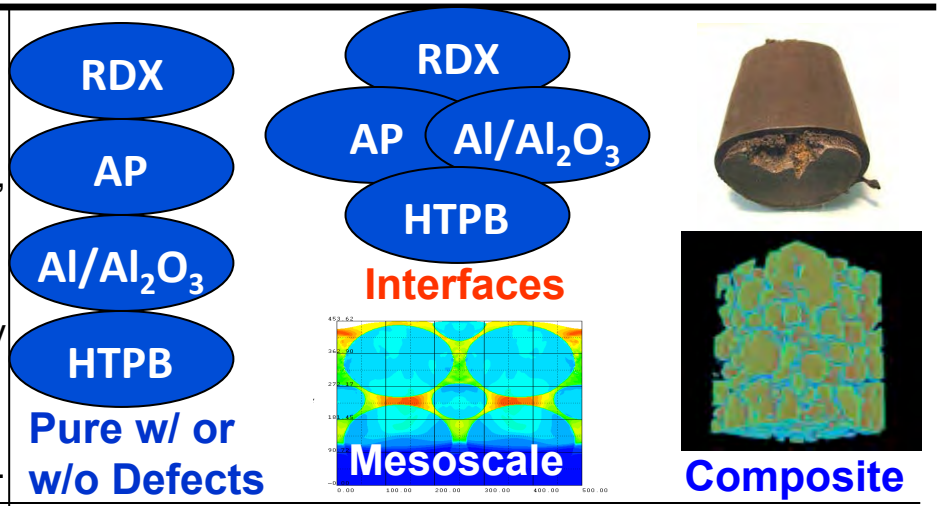

Approach: Target material: AFX-757. Molecular dynamics (MD) simulations using realistic force fields. Mesoscopic dislocation mechanics simulations informed by MD results and experiment. Experimental characterization/validation of theoretical methods using systematic variation of RDX structure/morphology.

Personnel Support:
MU: PI: 1.0 Summer Month; Co-PI: 1.0 Summer Month; Postdoctoral Fellow: 100%, 12 mos./yr; Graduate Student: 50%, 12 mos./yr. **TNO:** 4 (Senior) Scientists, Analytical Chemist, 2 Explosives Technicians

Tasks: ***Y1:*** Fundamental processes, pure components, simple loading; PBX/RDX prep. and characterization. ***Y2:*** Shocks in materials with voids, grain boundaries & inter-component interfaces; non-reactive mesoscale simulations; determination of initiation threshold in composites. ***Y3:*** Multiple shocks & ramp loading in complex materials; reactive mesoscale simulations.

Funding: Year 1: FY10 $347.4K Year 2: FY11 $341.8K Year 3: FY12 $349.3K

PI Contact: Dept. Chemistry, MU-Columbia, Columbia, MO 65211; Voice: 573-882-0051; FAX: 573-882-2754; Email: thompsondon@missouri.edu

Overview

Objective: Investigate fundamental physical and chemical processes that determine responses of EMs to shock and non-shock excitation: stress states, strain rates, energy localization, chemical initiation.

Relevance: Understanding basic properties that determine metal-loaded composite materials survivability in penetrator applications. Understanding the relation between crystal defect structure and impact resistance. Improving requirements for the quality of EM ingredients.

Approach: MD simulations using realistic force fields. Experimental characterization & validation of theoretical methods using systematic variation of RDX structure/ morphology.

Materials Being Studied

We are considering as a representative target formulation a composite containing:

- RDX, ammonium perchlorate (AP), Al, hydroxy-terminated polybutadiene (HTPB) binder.

The focus will be on these components and the interfaces between them. Other materials are also being studied to improve fundamental understanding.

Currently we are limiting the molecular dynamics scope to unreactive simulations due to doubts about the reliability of reactive FFs.

Experimentally single crystals as well as PBX composites formulated using three different grades of RDX are being studied.

Tasks

Year 1: Fundamental processes, pure components, simple loading; PBX/RDX preparation & characterization.

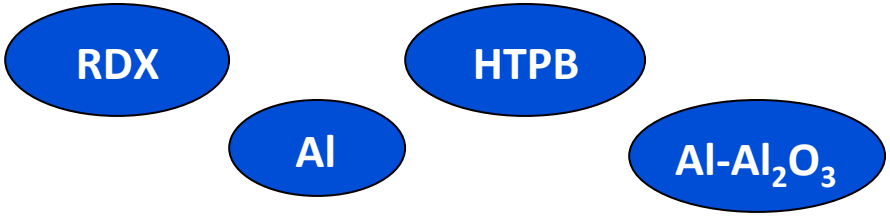

Year 2: Shocks in materials with voids, grain boundaries & inter-component interfaces; determination of initiation threshold in composites.

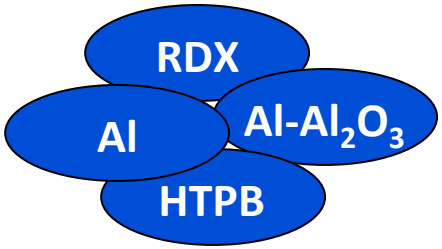

Year 3: Multiple shocks & ramp loading in complex materials.

souri

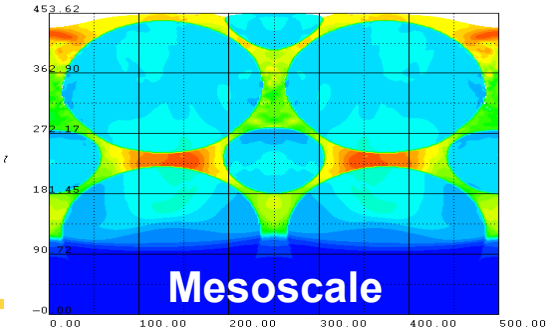

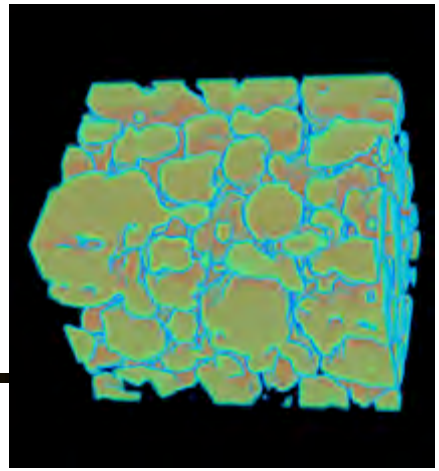

Fundamental physical issues

- Intrinsic material anisotropy, morphology, and complexity
- Mechanisms and energetics for inelastic deformation (plasticity) in low-symmetry polyatomic crystals, in polymers, and at interphases
- Fundamental intra-crystalline processes: Energy transfer mechanisms and rates, effects of hydrogen bonding, effects of defects
- Phase transitions: Shock-induced melting, and stress- and strain-induced polymorphism
- Interfaces: Stored energy and stress at interfaces or defects; transport properties at interfaces; polymer wetting properties

Experimental Work: TNO

Richard H. Bouma
Antoine E. D. M. van der Heijden

Memorandum

Lange Kleiweg 137
2288 GJ Rijswijk
P.O. Box 45
2280 AA Rijswijk
The Netherlands

www.tno.nl

T +31 88 866 80 00
F +31 88 866 69 49
infodesk@tno.nl

To

From
A.E.D.M. van der Heijden

Subject
Annual report third year

Date
3 December 2013

Our reference
<vnr-ext>

Direct dialling
+31 88 866 14 52

The Statement of Work has been discussed by DTRA, University of Missouri and TNO at the Gordon Conference 2010. The SOW for the three years is given below. The tasks for the third year are discussed in this annual report.

Year #1
- Y1T1: Implementation of atomic potentials relevant to AFX-757
- Y1T2: Atomic-scale studies of single-component materials (input from TNO regarding RDX orientations of principal interest, output to TNO regarding fundamental material equation of state and thermal properties)
- Y1T3: Anisotropic static and dynamic atomic-scale studies of uniaxial loading (output to TNO regarding dominant orientation-dependent deformation mechanisms in RDX)
- Y1T4: Preparation of three plastic-bonded explosives using different grades of RDX
- Y1T5: Experimental characterization of RDX batches
- Y1T6: Experimental determination of deformation initiation threshold in a homogeneous deformation experiment
- Y4T3: Confocal scanning laser microscopy (CSLM) on crystal/PBX level using the PBXs containing the original RDX batches (different grades, see Y1T4)

Year #2
- Y2T1: Atomic-scale studies of anisotropic response of constituent materials under multi-axial loading
- Y2T2: Atomic-scale studies of effects of voids and other defect structures (input from TNO regarding dominant defect types and geometries, including differences between “bulk” and “surface” defects)
- Y2T3: Atomic-scale studies of interfaces and grain boundaries (with input from TNO regarding particle habit and morphology)
- Y4T3 (Continued): Confocal scanning laser microscopy (CSLM) on crystal/PBX level using the PBXs containing the original RDX batches (different grades, see Y1T4)
- Y2T4: Experimental determination of deformation initiation threshold with the Ballistic Impact Chamber
- Y4T4: Experimental determination of deformation initiation threshold with the Ballistic Impact Chamber set-up using unreacted samples taken from **Y1T6** that were subjected to homogeneous deformation below their initiation threshold in order to assess whether the initiation threshold has changed
- Y5T3: CSLM on crystal/PBX level using deformed unreacted samples from the BIC characterization (see Y2T4) and samples shocked below their deformation initiation threshold (see Y1T6)

Year #3
- Y3T1: Atomic-scale simulation of shocks on normal, parallel, and oblique

binary interfaces (input from TNO regarding dominant defect types and geometries, including differences between “bulk” and “surface” defects)
- Y3T2: Atomic-scale simulation of shocks in laminate composite structures and at material triple points
- Y3T3: Isentropic compression studies using atomic-scale simulations
- Y5T3 (Continued): CSLM on crystal/PBX level using deformed unreacted samples from the BIC characterization (see Y2T4) and samples shocked below their deformation initiation threshold (see Y1T6)
- Y5T4: Experimental determination of deformation initiation threshold with the Ballistic Impact Chamber set-up using unreacted samples from Y2T4 that were subjected to deformation below their initiation threshold in order to assess whether the initiation threshold has changed

Accomplishments in 3rd year

Y4T3 (Continued): Confocal scanning laser microscopy (CSLM) on crystal/PBX level using the PBXs containing the original RDX batches (different grades, see Y1T4)

CSLM pictures of the last RDX quality batch (K7) have been prepared (K1 and K6 had been examined already earlier). It appears that the inclusions/voids in the K7 batch RDX crystals are mainly concentrated in the periphery of the crystals, whereas the centre of the crystals are relatively “clean”.

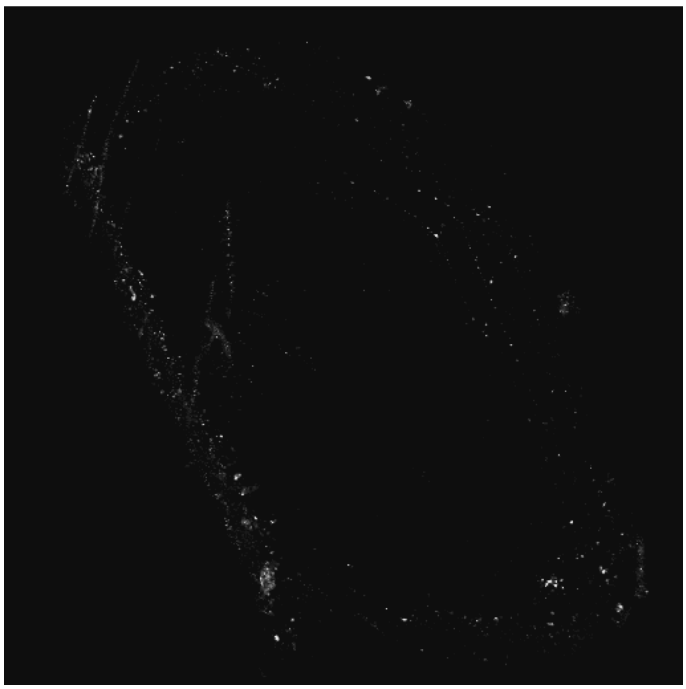

Typical CSLM image of a K7 RDX particle, lying “diagonally” from top left to bottom right (file: RDX K7_Series009_z001_ch00.tif).

The paper *“Characterization of defect structure in RDX crystals”* describing the CSLM results obtained within Y4T3, has been published in *Journal of Microscopy* [4].

Y2T4: Experimental determination of deformation initiation threshold with the Ballistic Impact Chamber

The original RDX batches K1, K6 and K7 have been tested in the BIC as loose powders. The results are shown in the table below, giving the measured time to reaction (in μs) and peak pressure (in MPa). Two different volumes of sample (i.e. 40 and 80 μL) were tested. For all measurements, the pressure transducer was positioned in the barrel.

The time-to-reaction for all RDX batches (both 40 and 80 μL) is in the same order of magnitude (400-500 μs); the peak pressure is in the range of ~8-9 MPa for the 40 μL sample and approximately twice as high (~19-20 MPa) for the 80 μL sample. The measured parameters (time-to-reaction and peak pressure) do not show a trend pointing at differences that might correlate with differences in the product qualities of the three RDX batches K1, K6 and K7.

No correlation between shock sensitivity and sensitivity towards mechanical deformation has been found from the BIC and explosion-driven deformation tests. This means that the current commercially available Reduced Sensitivity RDX grades that help in reducing munition vulnerability in shock/impact scenarios, do not necessarily contribute to vulnerability reduction in low velocity impact or low pressure deformation scenarios.

Measured time to reaction (in μs) and peak pressure (in MPa) of the 3 RDX batches K1, K6 and K7.

Test	Amount [μL]	Reaction [μs]	Pressure (peak) [MPa]
RDX-K1			
K1-01	40	475	8.88
K1-02	40	471	7.98
K1-03	80	412	20.16
K1-04	80	425	20.86
RDX-K6			
K6-01	40	439	8.59
K6-02	40	463	8.87
K6-03	80	472	19.59
K6-04	80	457	19.75
RDX-K7			
K7-01	40	466	9.44
K7-02	40	443	8.34
K7-03	80	439	23.29 [a]
K7-04	80	449	20.81
K7-05	80	452	19.20

[a] Pressure overload.

In addition to the DTRA project award, the 3 non-deformed PBXs have been examined in a Floret test. In the Floret test a sufficiently strong shock is imposed to deliberately cause a Shock-to-Detonation transition (SDT) in the central part of the sample. The purpose of these tests is to investigate the lateral growth of the reaction, which is considered to be a combination of the sensitivity towards

mechanical deformation and the speed of the SDT in the central part of the sample.

The (modified) Floret test set-up, as used at TNO, is shown in the figure below (pictures and schematic drawing). A copper flyer plate is accelerated by initiating a small Semtex initiator using a detonator (not shown in the pictures). The flyer impacts with the explosive sample, leading to a reaction of the sample. After the reaction, the dent profile is measured (depth as a function of radius, volume of the dent), providing a measure for the growth of the reaction of the explosive sample.

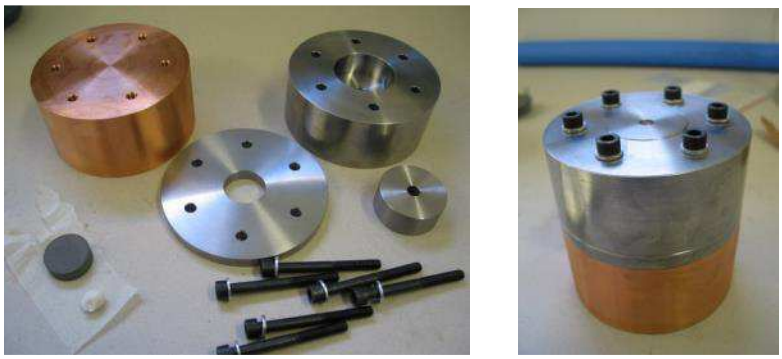

Pictures of disassembled (left) and assembled (right) Floret test set-up. The left picture also shows a PBX sample.

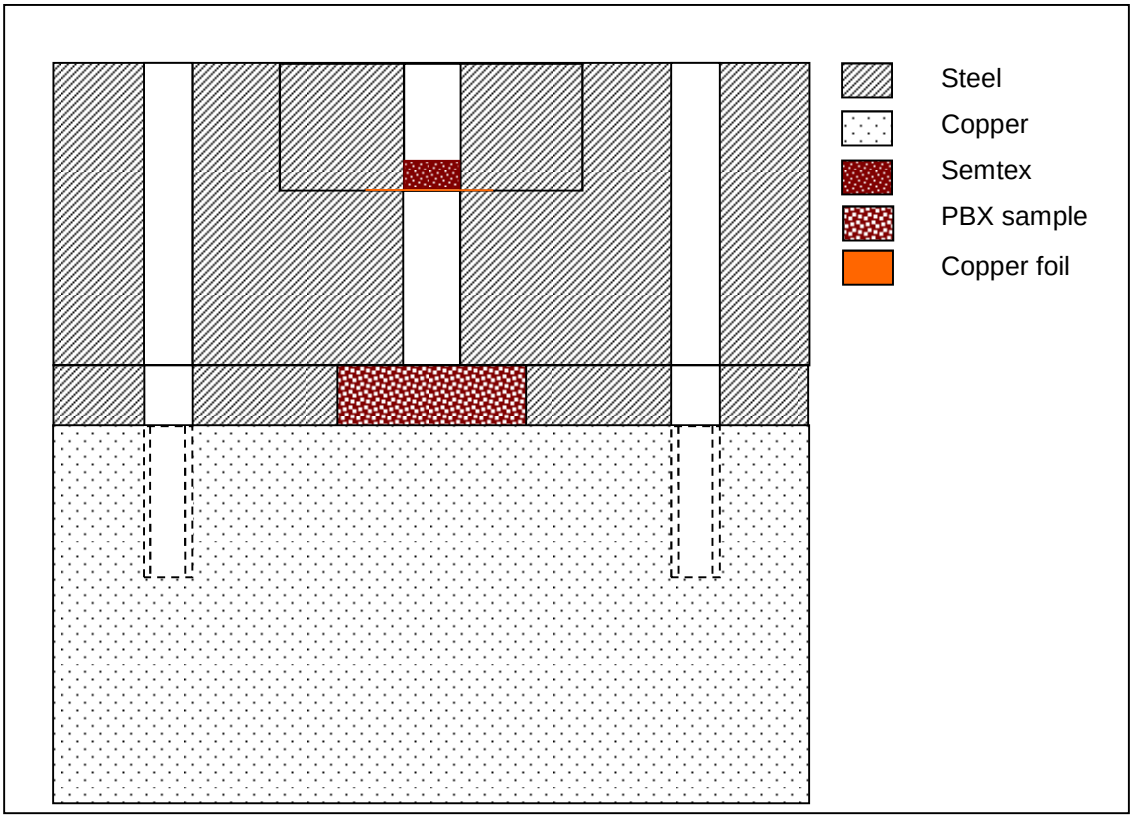

Schematics of the (modified) Floret test as used at TNO.

The images below show the indentations of the copper blocks as a result of the initiation of the PBX formulations and those of the RDX powders.

From left to right: dent profiles of RU185 (containing RDX from batch K7), RU186 (K6) and RU187 (K1).

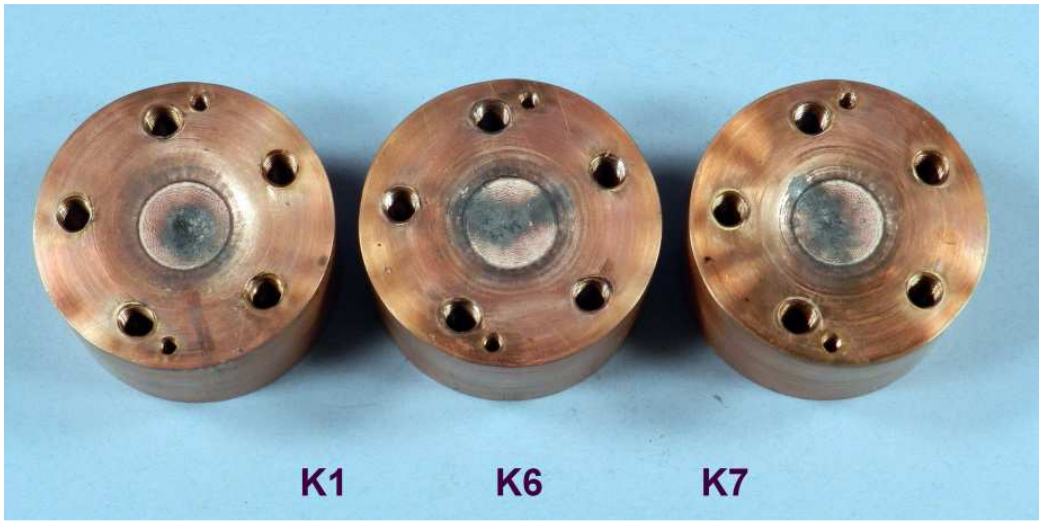

From left to right: dent profiles of RDX batches K1, K6 and K7.

The indentations have been profiled in two perpendicular directions across the copper block. The results are shown in the graphs below. The PBX RU186 has been tested in duplicate. The profiles of the PBXs are very smooth, in contrast to the profiles measured for the RDX powders showing a stepwise profile. The dent profiles are generally rather symmetric, as can be concluded from comparison of the measured profiles in 2 perpendicular directions across the copper block surface. Some deviation from this symmetry can be observed for RDX K1. At the moment no clear explanation is available why the dent profiles of the RDX powders show a stepwise profile and the PBXs a smooth curve.

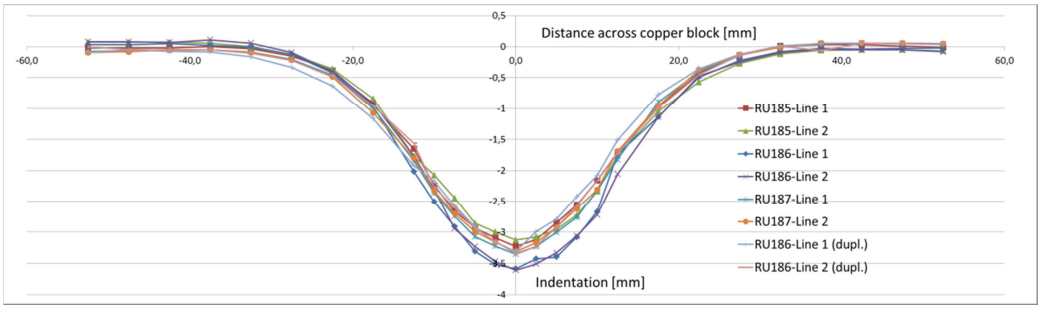

Indentation profiles of the PBXs RU185-186-187. RU186 has been tested in duplicate.

The dent profiles of the PBXs have been analyzed in more detail: the volume of the dent profiles has been determined by splitting up each of the dent curves in 2 half ones. This results in 4 half curves for the profiles measured in 2 perpendicular directions across the copper block. Since these curves are rather smooth, a trend line can be fitted using a third-degree polynomial fit. From this curve a solid of revolution can be made from which the volume can be determined by a straightforward, mathematical integration. In this way 4 volumes can be calculated based on each of the solids of revolution that can be generated from the 4 half curves; these values are then averaged to reach a mean value of the dent volume. The results of these calculations are shown in the table below.

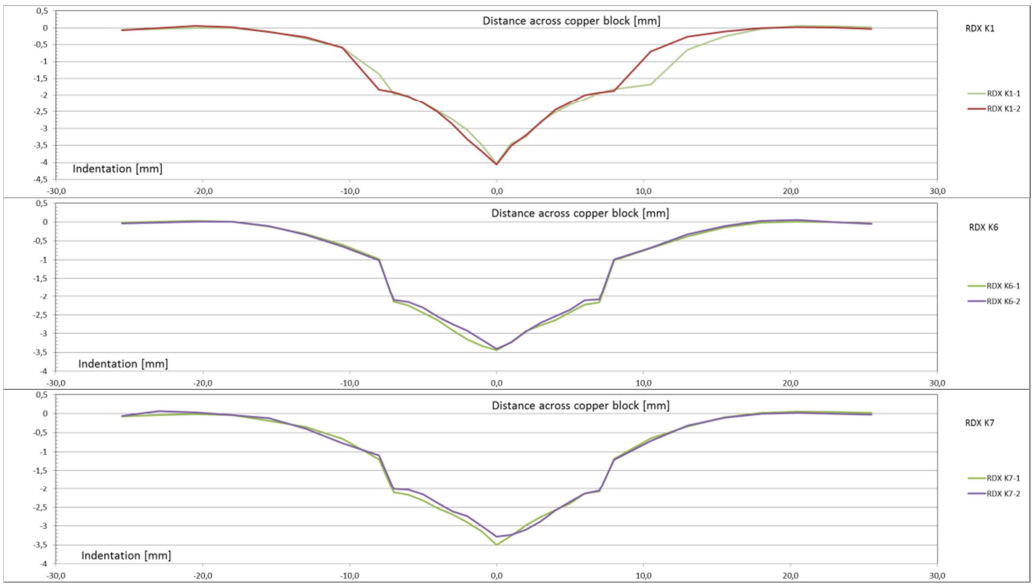

Indentation profiles of the RDX batches K1 (top), K6 (middle) and K7 (bottom).

These results show that the dent volume of PBX RU186, containing RDX K6, has the largest value. The volumes of the other two PBXs are rather close. These data correlate quite well with the shock initiation pressures that have been measured in the Round Robin Program, using PBXN109 formulations: the PBXN109 containing K6 is relatively sensitive (shock initiation pressure of 38.6 kbar) compared to the ones containing K1 (50.6 kbar) and K7 (53.3 kbar), which have a more or less similar sensitivity towards shock initiation.

Indentation volumes of the PBXs RU185, RU186 and RU187 and corresponding shock initiation pressures for PBXN109 type of formulations containing K1, K6 and K7.

PBX	RDX	Shock initiation pressure [kbar]	Volume Floret test [ml]
RU185	K7	53.3	2.54 ± 0.28
RU186	K6	38.6	2.78 ± 0.24
RU187	K1	50.6	2.53 ± 0.26

The preliminary results of the Floret tests show that a PBX containing K6 reacts more violently than the PBXs containing K1 and K7 (which show a more or less similar reaction); this is in line with the order in shock initiation pressure in the PBXN109-testing. Although the indentations of the RDX powder tests still need to be analyzed in more detail, the Floret test might be considered as a small scale characterization test to discriminate between different product qualities of a granular high explosive. However, further confirmation of this statement is required by analyzing the indentation volumes of the RDX batches K1, K6 and K7.

Our intention is to publish also these additional results to the DTRA program in a scientific paper [7].

Y4T4: Experimental determination of deformation initiation threshold with the Ballistic Impact Chamber set-up using unreacted samples taken from Y1T6 that were subjected to homogeneous deformation below their initiation threshold in order to assess whether the initiation threshold has changed.
A comparison has been made between the time-to-reaction (as determined by BIC tests) of the “as-cast” PBX samples and the PBX samples that have been homogeneously deformed below their initiation threshold by means of either a 4 mm or 5 mm thick layer of Semtex. These data are shown in the table below. As an example, typical BIC-curves of PBX RU185 (containing RDX-K7) are shown. Recovered PBXs from the explosion driven deformation test respond either equally fast or slower (higher time-to-reaction) in the BIC test. Based on the experimental results, the shear rate threshold as a single parameter describing mechanical sensitivity is challenged, and preference is given to the development of an ignition criterion based on inter-granular sliding friction under the action of a normal pressure.

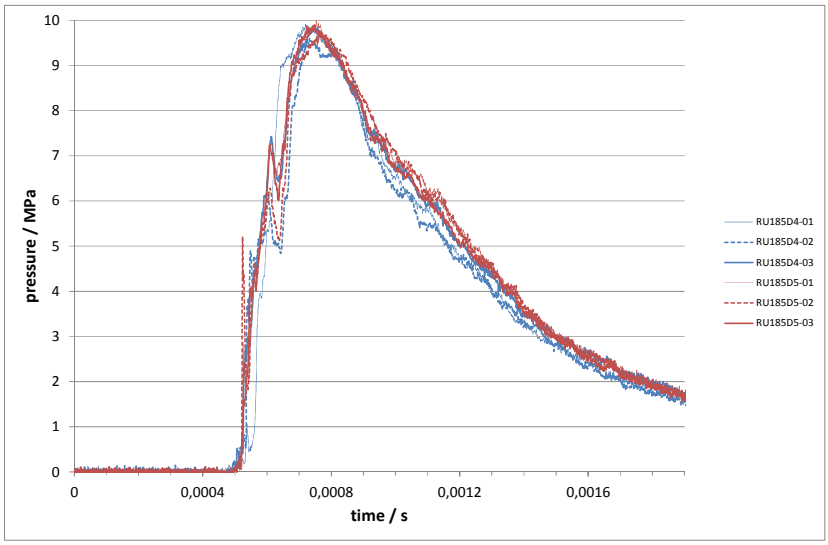

Mechanical response of 3.5 mm ∅ X 2.5 mm RU185 samples (containing RDX-K7) in BIC tests in triplicate experiments. Samples were taken from the explosion driven deformation tests with a 4 mm (RU185D4-xx) or 5 mm (RU185D5-xx) plastic explosive layer. Time scales are relative to the start of deformation measured for each individual experiment.

Time-to-reaction of the three PBX's containing either K1, K6 or K7; as-cast samples and samples after deformation (below initiation threshold) with a 4 mm or 5 mm thick Semtex layer.

PBX sample (RDX batch)	**Diameter × height [mm]**	**Time-to-reaction [ms]**		
		As-cast	After deformation with 4 mm Semtex	After deformation with 5 mm Semtex
RU185 (K7)	3.5 × 2.5	0.32 - 0.35	0.41 - 0.43	0.43 - 0.45
RU186 (K6)	3.5 × 2.5	0.35 - 0.43	0.40 - 0.42	0.38 - 0.45
RU187 (K1)	3.5 × 2.5	0.39 - 0.41	0.37 - 0.39	0.39 - 0.42
RU185 (K7)	5.0 × 2.4	0.31 - 0.35	0.40 - 0.44	0.40 - 0.43
RU186 (K6)	5.0 × 2.4	0.27 - 0.40	0.38 - 0.40	0.43 - 0.45
RU187 (K1)	5.0 × 2.4	0.41 - 0.43	0.37 - 0.39	0.40 - 0.42

A draft paper entitled "*The effect of RDX crystal defect structure on mechanical response of polymer bonded explosive"* has been prepared based on the results of these BIC-data (including data from Task Y5T4). This paper has been submitted to the *European Journal of the Mechanics of Solids/A* [5].

Y5T3: CSLM on crystal/PBX level using deformed unreacted samples from the BIC characterization (see Y2T4) and samples shocked below their deformation initiation threshold (see Y1T6)

Samples PBX-K1_5mm, PBX-K6_5mm and PBX-K7_5mm have been checked with optical microscopy to verify the correct polishing procedure of these samples. These observations showed similar results of the PBX samples that were deformed using a 4mm thick sheet explosive.

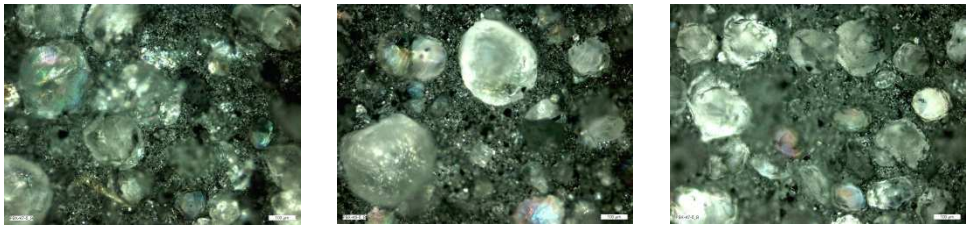

From left to right: optical microscopic image of polished PBX-K1_5mm, PBX-K6_5mm and PBX-K7_5mm surfaces (images: PBX-K1-5_B.jpg, PBX-K6-5_B.jpg and PBX-K7-5_B.jpg).

These samples, together with PBX-K1_4mm, PBX-K6_4mm and PBX-K7_4mm, have been subjected to CSLM imaging. In addition to the preliminary comparison of the CSLM images of the PBX-K1_4mm sample and the original RDX-K1 crystals, a further comparison including the above PBX-embedded and shock-loaded crystals, confirmed the presence of more blurry spots and even more extended areas of scattered light in all of the shock-loaded PBX samples (in addition to the bright, sharply edged spots/inclusions), though more prominently in the shock-loaded K1 crystals (5mm). These blurry spots as well as the more extended areas, point at regions with a (slightly) different or gradually changing refractive index compared to the remaining part of the crystals, leading to the scattering of light in the CSLM imaging. It is unclear whether the blurry spots originate from inclusions that were already present in the crystals but obtained a blurry appearance due to the shock loading, or that these were newly generated as a result of the shock loading. The fact that the blurry spots are most abundant in the periphery of the crystal surface, similar to the inclusions in the original RDX crystals, might indicate that already existing inclusions become more intensely “stressed” due to the shock loading. If the blurry spots were newly generated, one would expect that these would also have been formed in the bulk and not primarily in the periphery of the crystals.

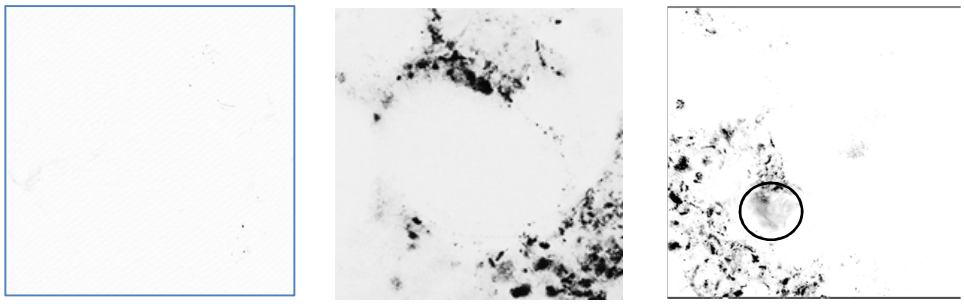

Typical CSLM image of a K1 crystal (left, RDX K1_01_Series002_z000_ch00inverted.tif), a K1 crystal embedded in the PBX-K1_4mm sample (middle, PBX K1 4mm_Series020_z000_ch00.tif) and in the PBX-K1_5mm sample (right, PBX K1 5mm_1_Series012_z038_ch00inverted.tif). All three images cover a surface area of 375×375 μm^2. In the image on the right, the circle indicates an extended area of ca. 70x70 μm^2 (xy-direction) that could be indicative of an area where mechanical stress has been induced by the shock loading of the PBX sample. The dimension of this particular area in the z-direction is ca. 17 μm.

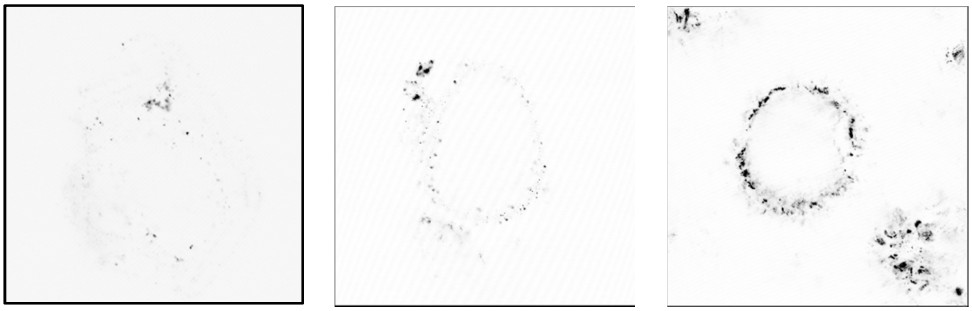

Typical CSLM image of K6 crystal (left, RDX K6_01_Series012_z000_ch00inverted.tif), a K6 crystal embedded in the PBX-K6_4mm sample (middle, PBX K6 4mm_1_Series011_z132_ch00inverted.tif) and in the PBX-K6_5mm sample (right, PBX K6 5mm_1_Series016_z110_ch00inverted.tif). All three images cover a surface area of 375×375 μm^2.

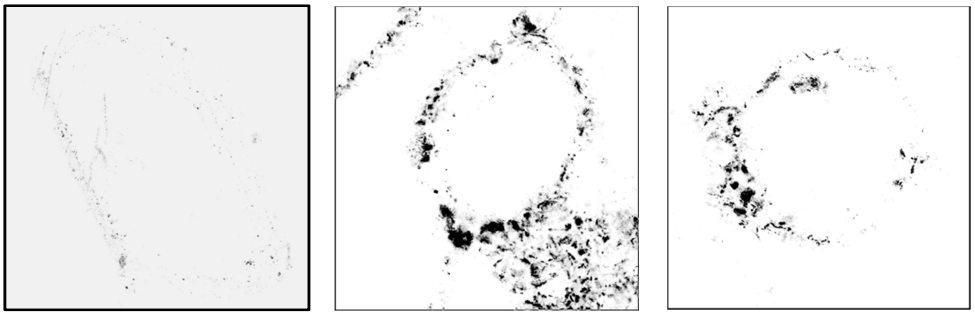

Typical CSLM image of K7 crystal (left, RDX K7_Series009_z000_ch00inverted.tif) and a K7 crystal embedded in the PBX-K7_4mm sample (middle, PBX K7 4mm_1_Series007_z111_ch00inverted.tif) in the PBX-K7_5mm sample (right, PBX K7 5mm_1_Series004_z120_ch00inverted.tif). All three images cover a surface area of 375×375 μm^2.

A likely explanation is that the shock loading of the different PBX samples leads to areas with a higher level of mechanical stress in the crystals, which (locally) changes the density of the material and in this way also the refractive index. This is shown in the CSLM pictures below (N.B.: the images have been digitally converted from bright spots against a dark background (original image), to dark spots against a bright background (inverted image)). The slices of 0.5 µm thickness that have been recorded with CSLM, have been converted to avi-movies, which very nicely show the defect structures within the RDX crystals while moving several tens of microns downwards into the crystals. The area within the circle indicated in the CSLM image of the PBX-K1_5mm sample has a dimension (*xyz*) of ca. 70x70x17 μm^3.

The reporting of the CSLM results of the deformed/unreacted PBX-samples in a paper entitled *"Confocal scanning laser microscopic study of deformed polymer bonded explosives"* has been submitted to *Journal of Applied Physics* [6].

Y5T4: Experimental determination of deformation initiation threshold with the Ballistic Impact Chamber set-up using unreacted samples from Y2T4 that were subjected to deformation below their initiation threshold in order to assess whether the initiation threshold has changed

The samples tested in the BIC and subjected to deformation below the initiation threshold, have been flattened to such an extent that it is not possible to prepare samples for a re-test with the BIC. Therefore, new samples have been prepared which were first by deforming cylindrically shaped samples by impacting these samples with a 10 kg drop weight. These deformed sample have been used as starting material for Y5T4 testing (see picture below).

Collected samples of three different PBXs after deformation.

Due to the samples being very flexible/elastic, it was rather difficult to cut samples from both the middle part and peripheral part of the deformed samples. Instead, small cylindrical samples with two different diameters (three samples each) were cut from these deformed samples at an approximately constant distance from the centre of the deformed sample (see picture below); these samples were used in the BIC testing.

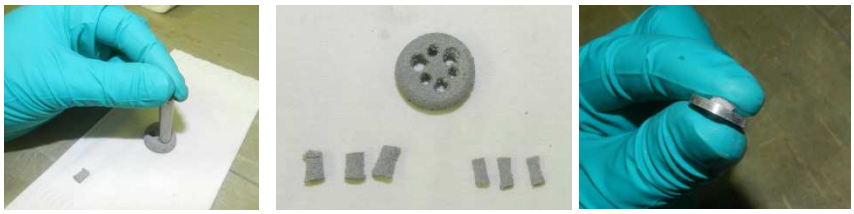

Pictures showing cutting of a deformed PBX-sample (left) and the two types of samples for BIC testing after cutting (middle). Sample after mounting it in the sample holder for the BIC set-up (right).

The results of the BIC tests on the different deformed/unreacted PBX-samples is given in the table below, giving the range in time-to-reaction (in ms) after impact of the drop weight during the BIC. The two diameters (Ø3.5 and Ø5.0 mm) were tested in duplicate. For all measurements, the pressure transducer was positioned in the barrel. The measured times-to-reaction show that the deformed PBX samples react ~0.1 ms later than the “as-cast” PBX samples (see times-to-reaction for the “as-cast” PBXs in the table under Y4T4).

Test	Dimensions [mm]	Mass [mg]	Time-to-reaction [ms]
PBX-K1			
RU187M-01	Ø3.5 x H2.5	40	0.48
RU187M-02	Ø3.5 x H2.5	45	0.42 – 0.45
RU187M-03	Ø5.0 x H2.4	76	0.42 – 0.51
RU187M-04	Ø5.0 x H2.4	73	0.41 – 0.42
PBX-K6			
RU186M-01	Ø3.5 x H2.5	42	0.48 – 0.48
RU186M-02	Ø3.5 x H2.5	44	0.48 – 0.50

RU186M-03	Ø5.0 x H2.4	76	0.45 – 0.47
RU186M-04	Ø5.0 x H2.4	80	0.45 – 0.48
PBX-K7			
RU185M-01	Ø3.5 x H2.5	45	0.44 – 0.46
RU185M-02	Ø3.5 x H2.5	42	0.46 – 0.48
RU185M-03	Ø5.0 x H2.4	72	0.44 – 0.45
RU185M-04	Ø5.0 x H2.4	72	0.48 – 0.49

Presentations / publications during project

[1] R.H.B. Bouma, presentations at NATO AC/326 SG/A meetings in 2011 and 2013

[2] R.H.B. Bouma, A.E.D.M. van der Heijden, T.D. Sewell and D.L. Thompson, *Simulations of Deformation Processes in Energetic Materials*, in: Numerical Simulations of Physical and Engineering Processes, Intech, ISBN: 978-953-307-620-1, 2011

[3] R.H.B. Bouma, A.E.D.M. van der Heijden, *Analytical model development related to mechanical deformation and initiation of PBXs*, 9th New Models and Hydrocodes for Shock Wave Processes, April 23-27, 2012, London, United Kingdom

[4] R.H.B. Bouma, W. Duvalois and A.E.D.M. van der Heijden, *Characterization of defect structure in RDX crystals*, Journal of Microscopy **252** (2013) 263 – 274

[5] R.H.B. Bouma and A.E.D.M. van der Heijden, *The effect of RDX crystal defect structure on mechanical response of polymer bonded explosive*, submitted to European Journal of the Mechanics of Solids/A (2013)

[6] A.E.D.M. van der Heijden and R.H.B. Bouma, *Confocal scanning laser microscopic study of the RDX defect structure in deformed polymer bonded explosives*, submitted to Journal of Applied Physics (2013)

[7] A.E.D.M. van der Heijden and R.H.B. Bouma, (provisional title) *On the use of Floret tests for characterization of granular and polymer-embedded RDX*, in preparation (outside DTRA project award; journal still to be decided)

Personnel supported

Name	Role
Richard Bouma, PhD	Principal investigator
Antoine van der Heijden, PhD	Co-principal investigator
Willem Duvalois, BSc	Microscopist
Arien Boluijt, BSc	Explosives engineer (testing)
John Makkus	Explosives engineer (testing)
Rudie Krämer, BSc	Explosives engineer (PBX formulations)


TNO innovation for life

Investigations of Fundamental Processes and Crystal-Level Defect Structures in Metal-Loaded High-Explosive Materials under Dynamic Thermo-Mechanical Loads and their Relationships to Impact Survivability of Munitions


TNO innovation for life

Tasks year 3

- CSLM on crystal/PBX level using deformed unreacted samples from the BIC characterization and samples shocked below their deformation initiation threshold (continued from Year 2)

- Experimental determination of deformation initiation threshold with the Ballistic Impact Chamber set-up using unreacted samples that were subjected to deformation below their initiation threshold in order to assess whether the initiation threshold has changed ➔ *Additional Floret tests have been carried out to investigate whether differences in the product quality of the RDX grades cause differences in the growth of the reaction of the non-deformed PBXs*

Characterization on crystal/PBX level by CSLM

Deformed (using either a 4 or 5 mm thick Semtex layer), unreacted PBX, embedded in epoxy and cut/polished for microscopic examination

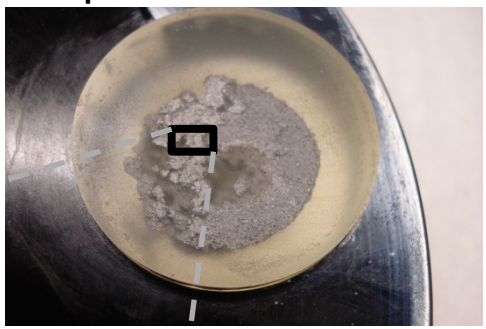

Hole, previously containing AP particle (washed out due to polishing)

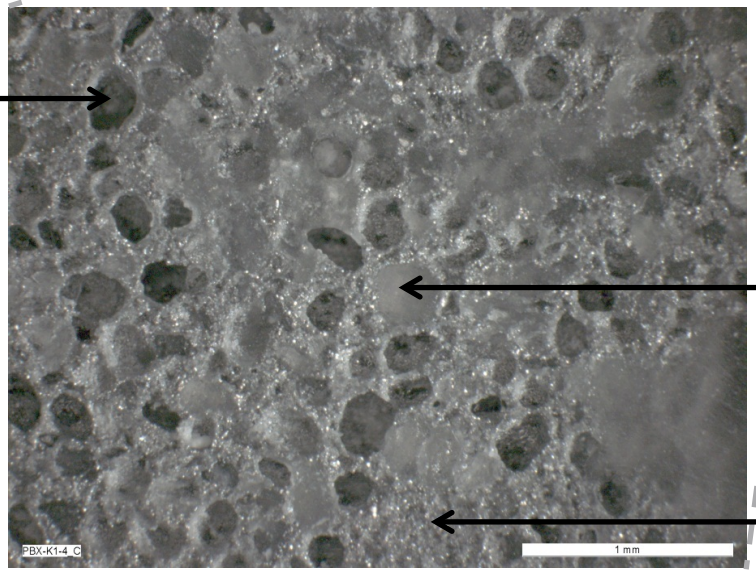

RDX particle

Binder matrix, containing Al

Characterization on crystal/PBX level by CSLM

RDX K1 (5 mm)

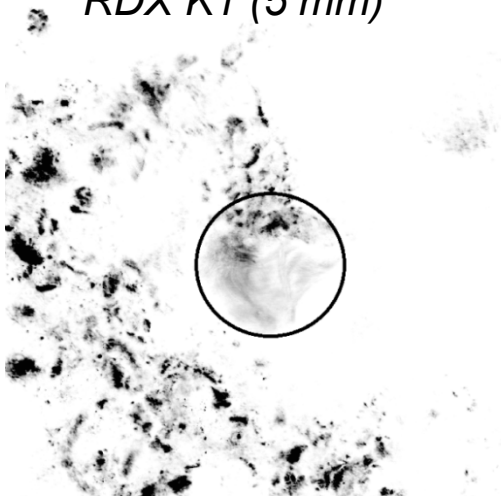

RDX K6 (4 mm)

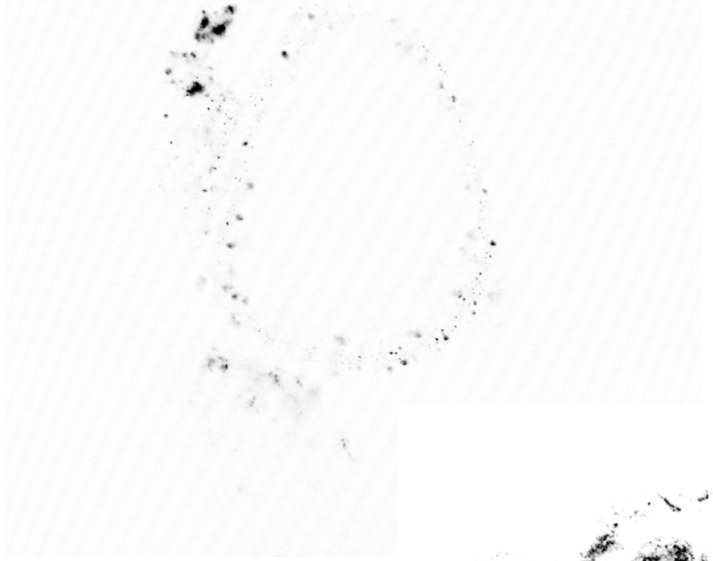

Characteristic features:

- **'Cloudy' regions**, formed in practically inclusion-free areas of the original RDX
- **'Blurred' speckles**, rather than sharply-edged spots (like those observed in original RDX)

Features point at **shock-induced, mechanically stressed locations or areas** in RDX

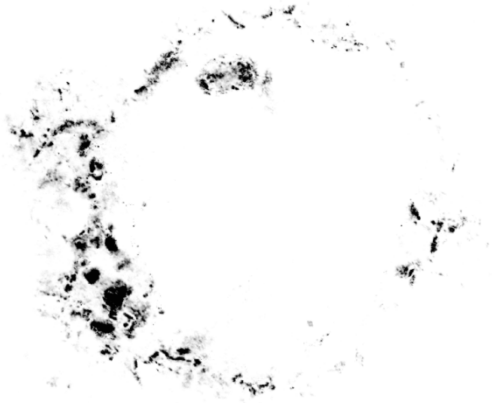

RDX K7 (5 mm)

Comparison with molecular dynamics simulations

Void collapse under impact with a piston in various, oriented single crystals of RDX have been studied in MD simulations by Cawkwell and Sewell. Results indicate considerable structural complexity in the shock response, i.e. regions of intense plastic deformation and stacking faults, qualitatively in line with the experimental CSLM observations.

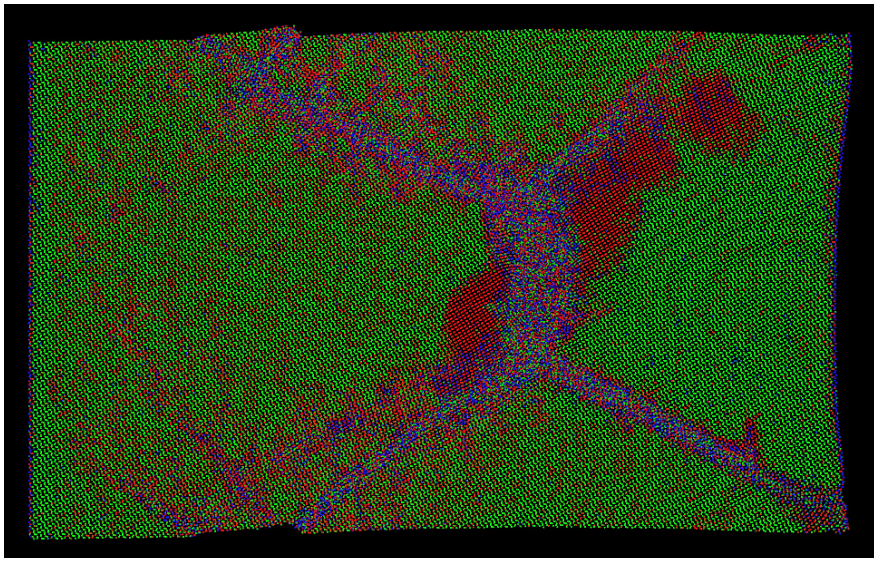

Snapshot of a molecular dynamics simulation showing void collapse of a 20 nm void in an RDX crystal in a shock on (210) planes (courtesy: Marc Cawkwell & Tommy Sewell).

Floret tests

No correlation between shock sensitivity and sensitivity towards mechanical deformation has been found from the BIC and explosion-driven deformation tests. In addition, the 3 non-deformed PBXs have been examined in a Floret test. In the Floret test a sufficiently strong shock is imposed to deliberately cause a Shock-to-Detonation transition in the central part of the sample. The purpose of these tests is to investigate the lateral growth of the reaction, which is considered to be a combination of the sensitivity towards mechanical deformation and the speed of the SDT transition in the central part of the sample.

Disassembled (left) and assembled (right) Floret test set-up

Floret tests

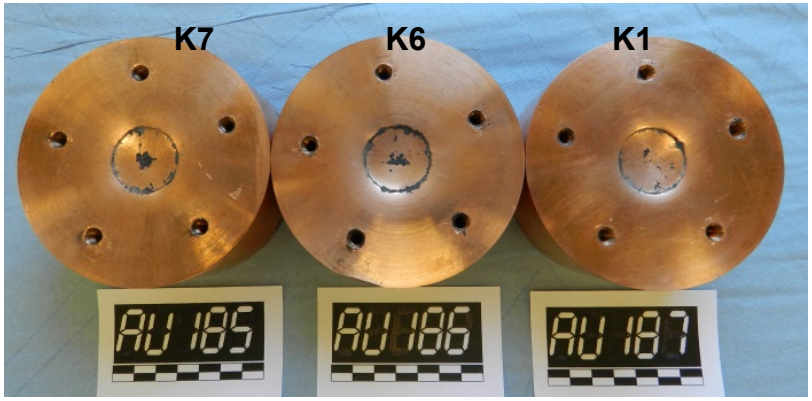

Indentations in copper, from left to right: RU185 (K7), RU186 (K6) and RU187 (K1)

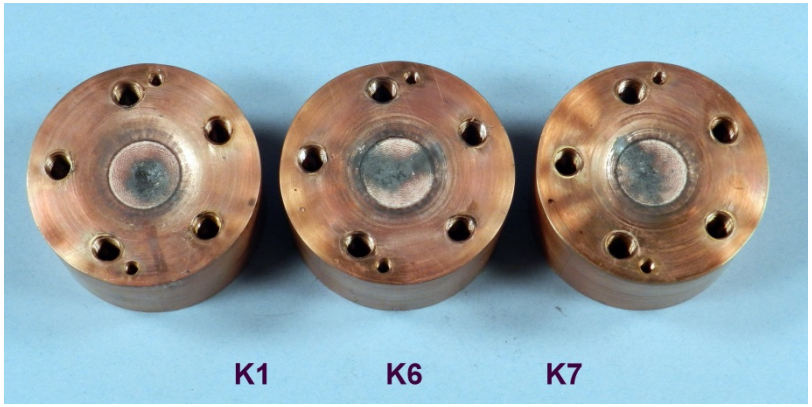

Indentations in copper, from left to right: K1, K6 and K7

Sequence reaction Floret test: RU186 (K6) > RU187 (K1) ≈ RU185 (K7)*

Initiation pressure (PBXN109): 38.6 kbar (K6) < 50.6 kbar (K1) ≈ 53.3 kbar (K7)

** Based on the diameter of the indentation in the copper block*


TNO innovation for life

Conclusions

- For the first time experimental confirmation has been obtained that **mechanically stressed areas are formed around inclusions** as a result of explosion-driven deformation of PBXs containing different grades of RDX
- In addition, also **homogeneously nucleated, shock-induced deformations** have been observed in RDX crystals by CSLM
- Preliminary Floret tests show that a **PBX containing K6 reacts more violently than the PBXs containing K1 and K7** (which show a more or less similar reaction); this is in line with the order in shock initiation pressure in the PBXN109-testing
- Floret test might be considered as a **small scale characterization test to discriminate between different product qualities of a granular high explosive**

Theoretical Work: U. of Missouri

Prof. D. L. Thompson

- Dr. Luis Rivera-Rivera: Shock waves in (100)-nitromethane
- Mr. Reilly Eason: Shock-induced pore collapse in (100)-RDX
- Dr. Lan He: Shock waves in coarse-grained PBD
- Dr. Markus Fröhlich: Shock waves in atomic HTPB

Reilly Eason

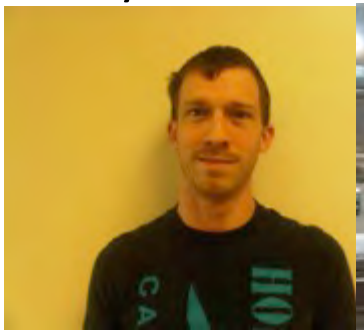

Lan He

Max Fröhlich

Luis Rivera

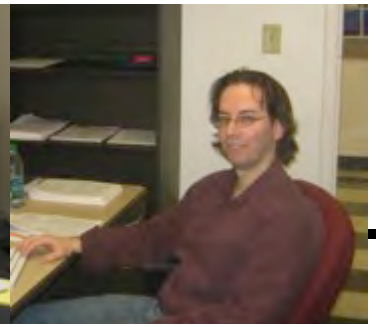

Void Collapse in (100)-RDX

Mr. Reilly M. Eason

Shock-induced pore collapse in (100)-α-RDX

Mr. Reilly M. Eason

Eason and Sewell, to be submitted to *Modelling and Simulation in Materials Science and Engineering (MSMSE)*

Pore collapse in RDX: System setup

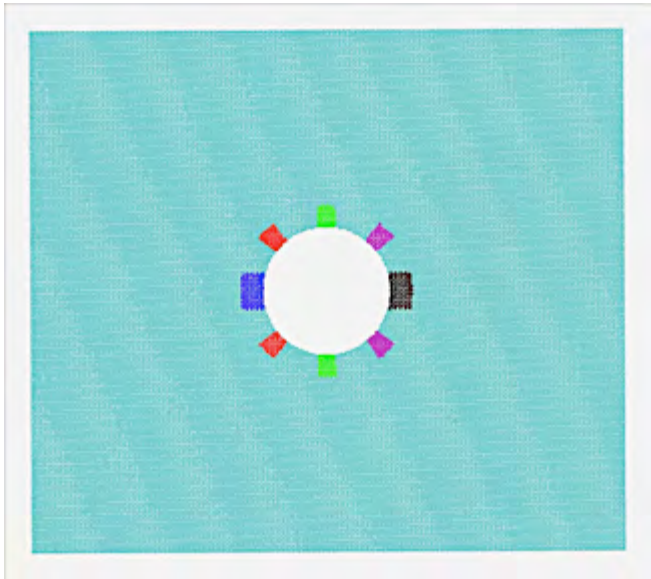

- Quasi-2D: ~150 nm × ~150 nm × ~3.5 nm
- Shock on (100) planes
- Cylindrical void, initial diameter 35 nm
- Three impact speeds: 1.0, 2.0, and 3.0 km/s
- Yes, non-reactive force field (S-B)

- A couple of different views of the collapse
- Snapshots of ro-vibrational temperatures

- Not shown:
  - Velocity fields
  - Rotational diffusion
  - Orientational correlation
  - Potential energy components

Collapse varies considerably with shock strength

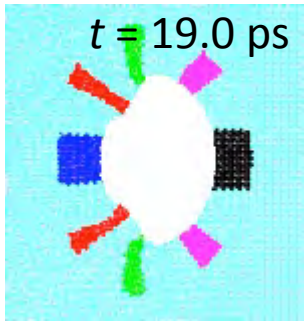

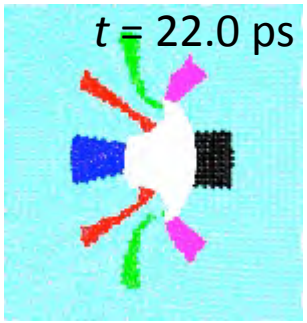

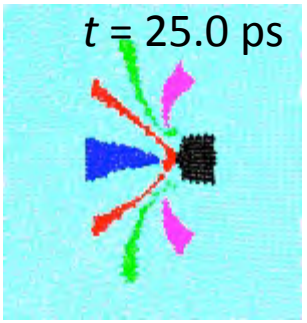

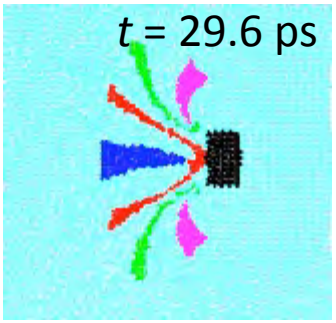

1.0 km/s

Penetration:
1.6 nm

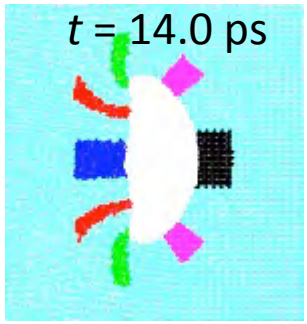

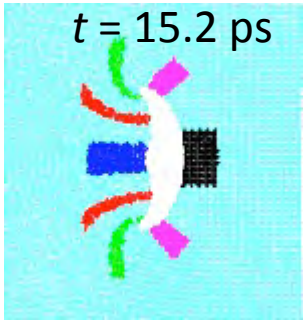

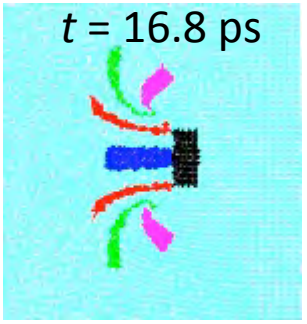

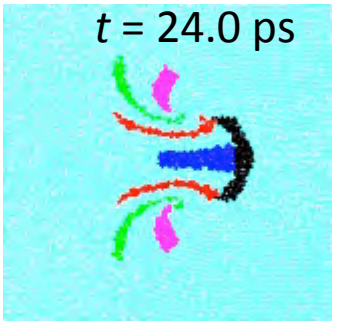

2.0 km/s

Penetration:
7.3 nm

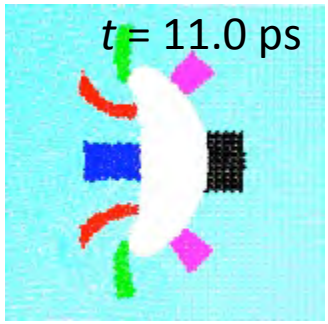

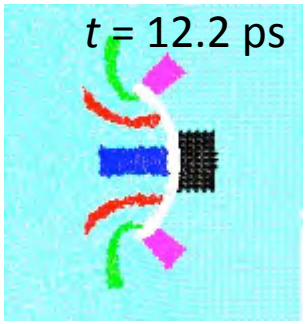

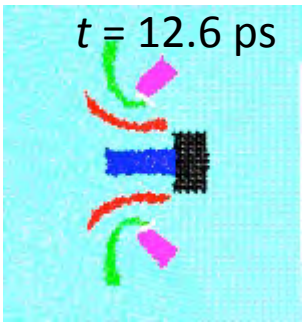

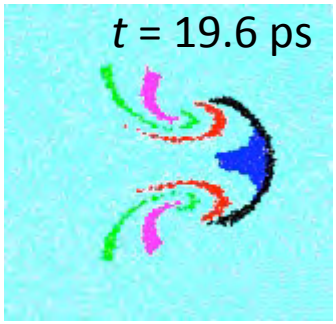

3.0 km/s

Penetration:
10.3 nm

Snapshots of centers of mass for concentric semi-annular regions provides additional information

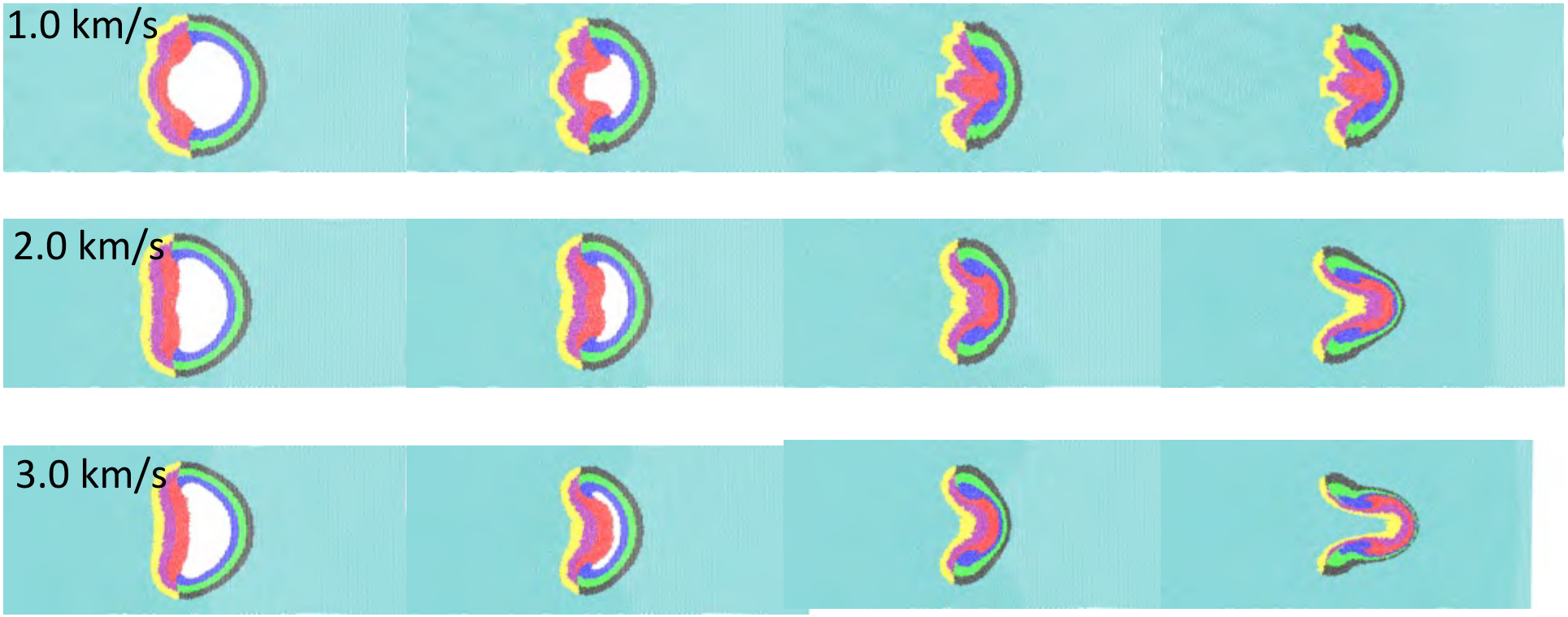

Pore collapse in RDX: Snapshots of ro-vibrational temperature

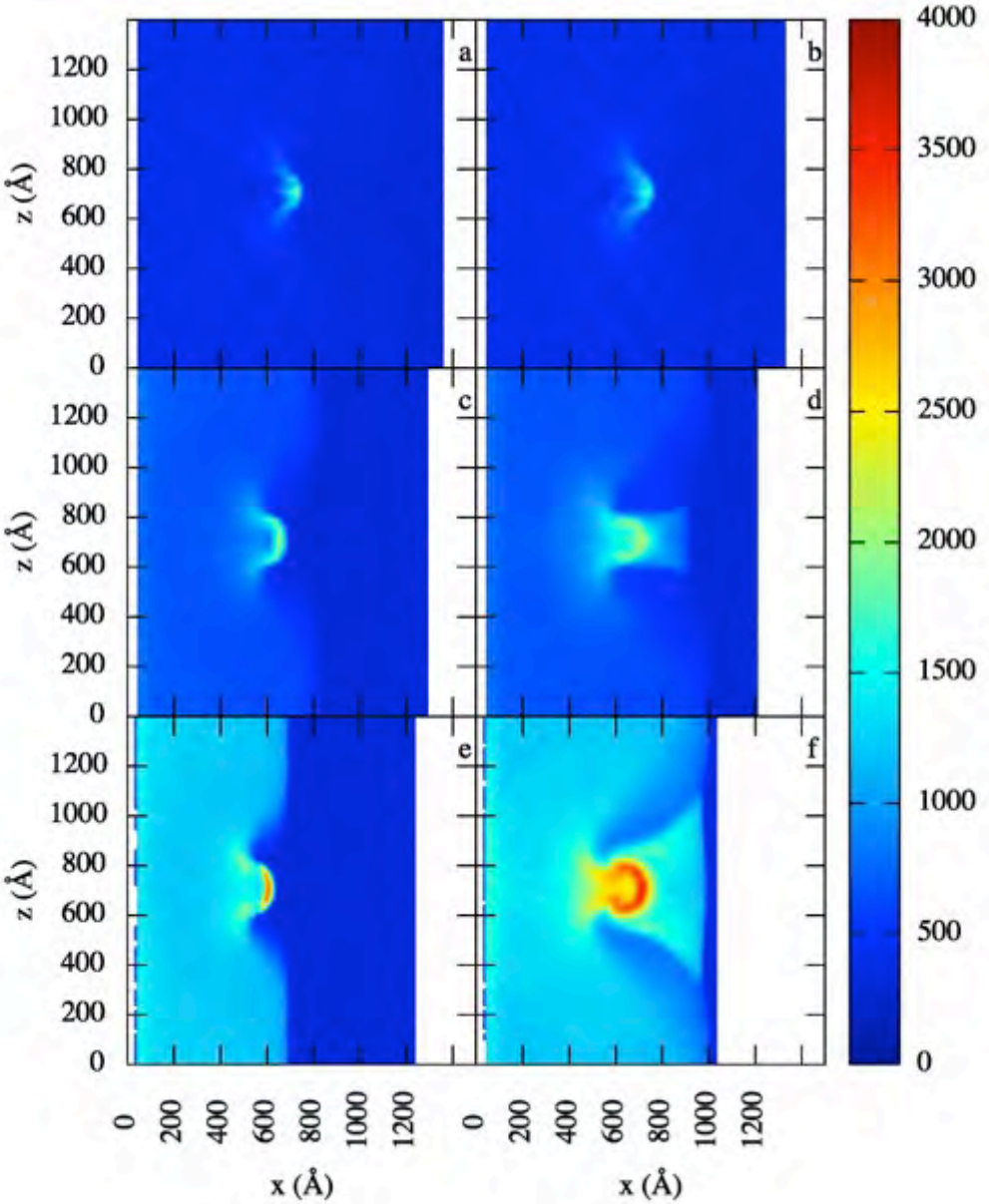

t-x plots of average shear stress for the different regions and shock strengths exhibit complicated behaviors

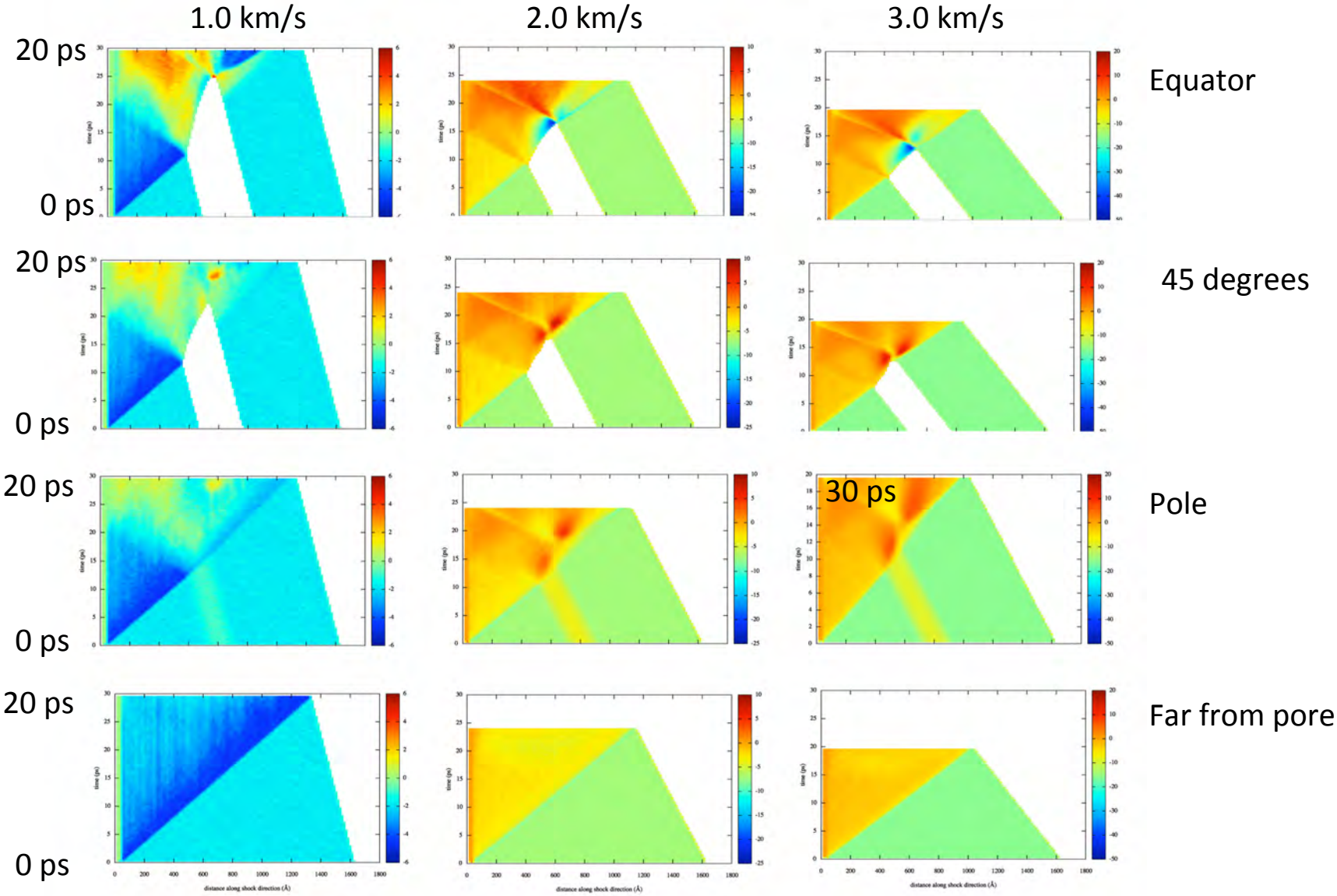

Re-establishment of thermal equilibrium in shocked (100)-nitromethane

Dr. Luis A. Rivera-Rivera

Rivera-Rivera, Sewell, and Thompson, J. Chem. Phys. **138**, 084512 (2013)

How much time is required to re-establish thermal equilibrium in shocked (100)-nitromethane?

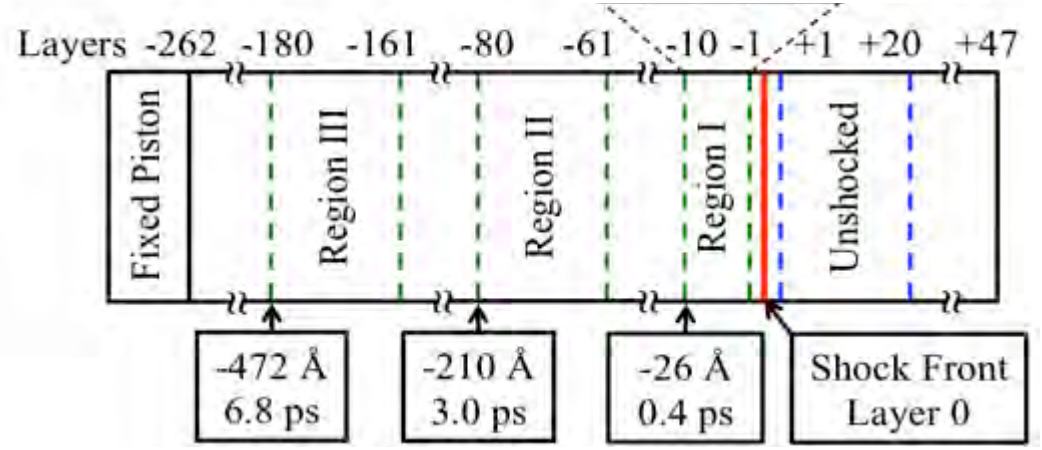

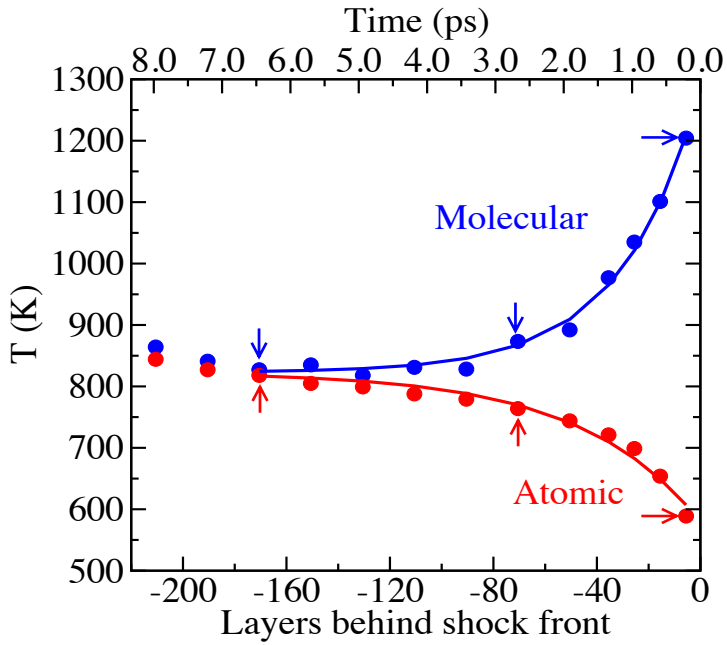

Kinetic Temperature

$$T = \frac{2\langle E_k \rangle}{3N\kappa}$$

Maxwell-Boltzmann *T*

$$P(E_k) = 2\sqrt{\frac{E_k}{\pi(\kappa T)^3}}e^{-E_k/\kappa T}$$

Temperatures in 'atomic' and 'molecular' degrees of freedom were determined as functions of distance/time behind the shock front by fitting kinetic energies to the Maxwell-Boltzmann distribution.

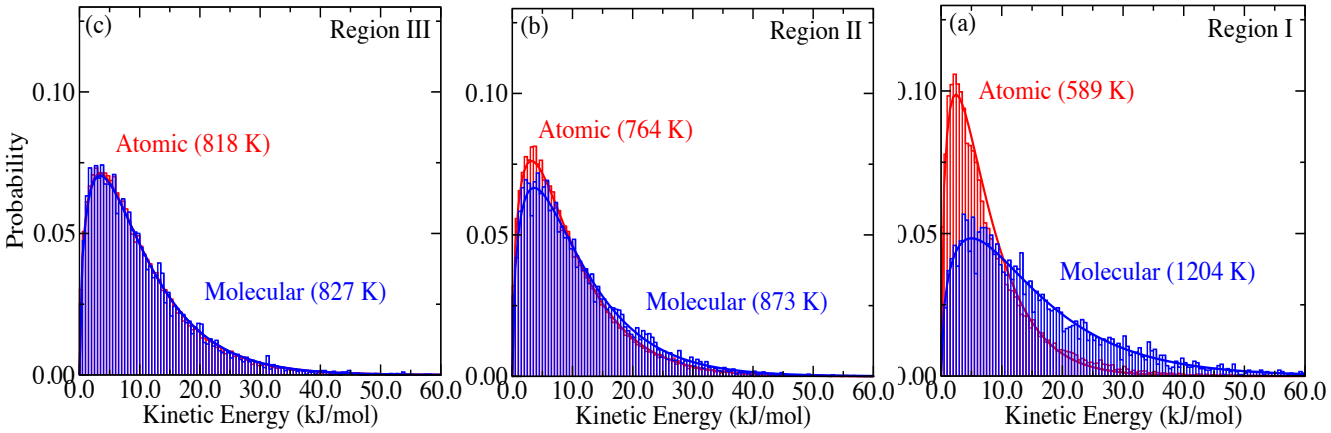

In contrast to (100)-PETN (lower right), in (100)-nitromethane atomic and molecular degrees of freedom are (separately) thermal even at very short post-shock times.

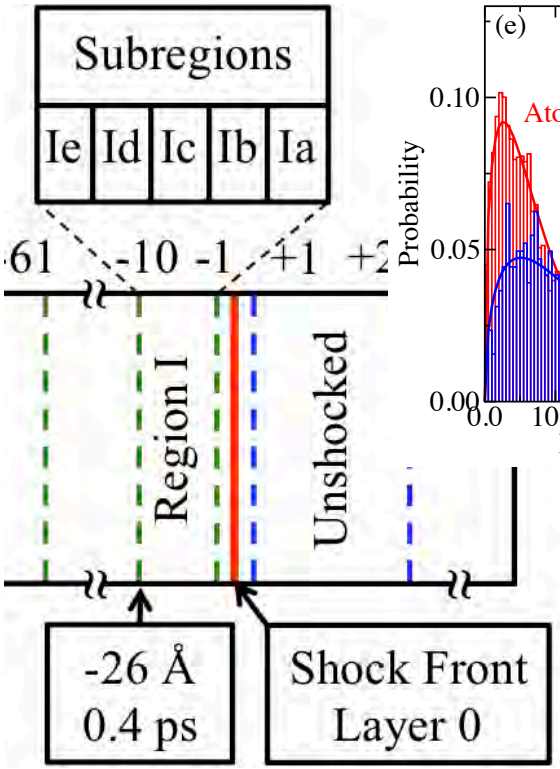

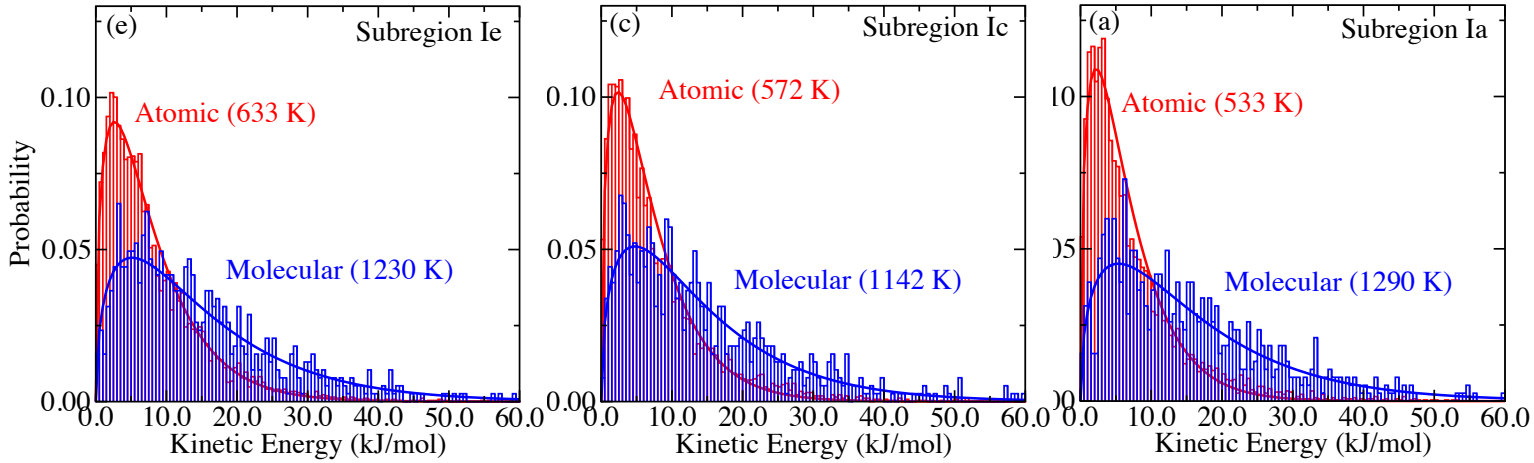

1 layer post-shock

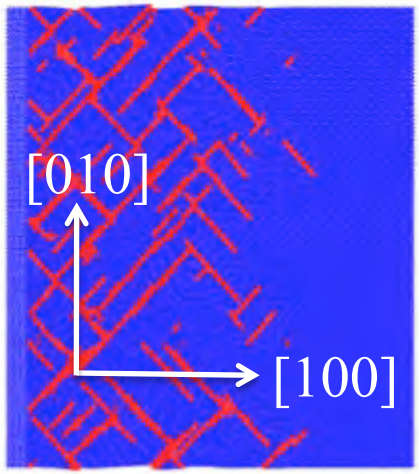

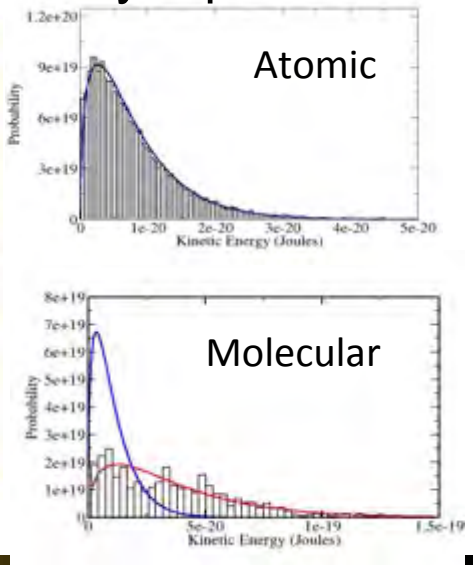

Eason & Sewell, J. Phys. Chem. C **116**, 2226 (2012)

Bond length distributions remain Gaussian

(→ 'effective harmonic bonds' even though the FF uses Morse bonds)

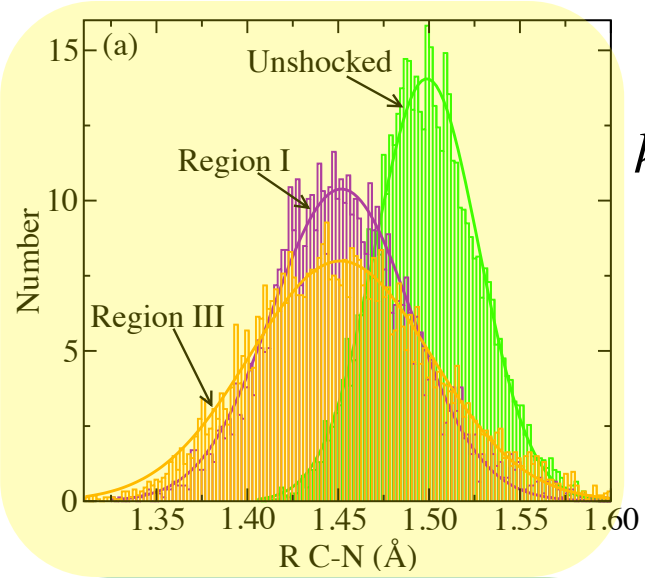

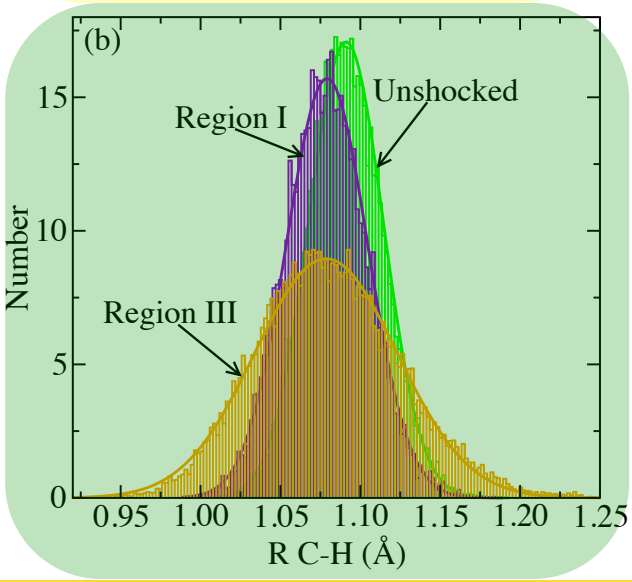

$$k_F^{eff} = k_B T \Big/ \left(\frac{FWHM}{2\sqrt{2\ln 2}} \right)^2$$

C-N	R_0 (Å)	FWHM (Å)	k_F (kJ·mol^{-1}Å^{-2})
SRT[a]	1.49957	--	2019
Unshocked	1.49876	0.06684	2074
Region I	1.45178	0.09044	3320
Region III	1.45125	0.11755	2729

C-H	R_0 (Å)	FWHM (Å)	k_F (kJ·mol^{-1}Å^{-2})
SRT[a]	1.09000	--	3057
Unshocked	1.09102	0.05501	3062
Region I	1.07914	0.05982	7589
Region III	1.07847	0.10491	3427

Shock waves in amorphous *cis*-1-4-polybutadiene: Coarse-grain vs. all-atom models

Drs. Lan He and Markus Fröhlich

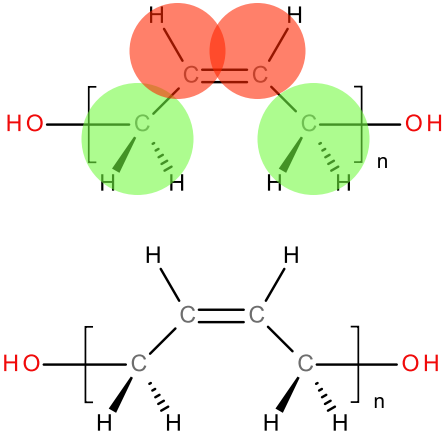

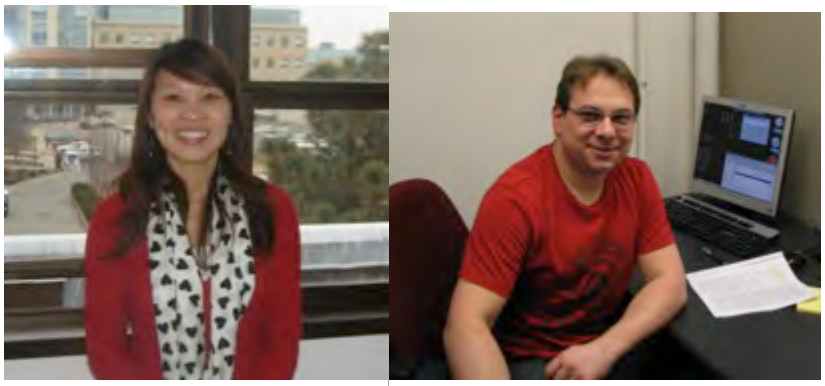

United-Atom:

He, Sewell, and Thompson, submitted to J. Appl. Phys. (July 2013)

All-Atom:

Sewell and Fröhlich, Macromolecular Theory and Simulation (in press, 7/13)

Fröhlich, Sewell, and Thompson (in preparation)

United-atom simulation setup & system generation

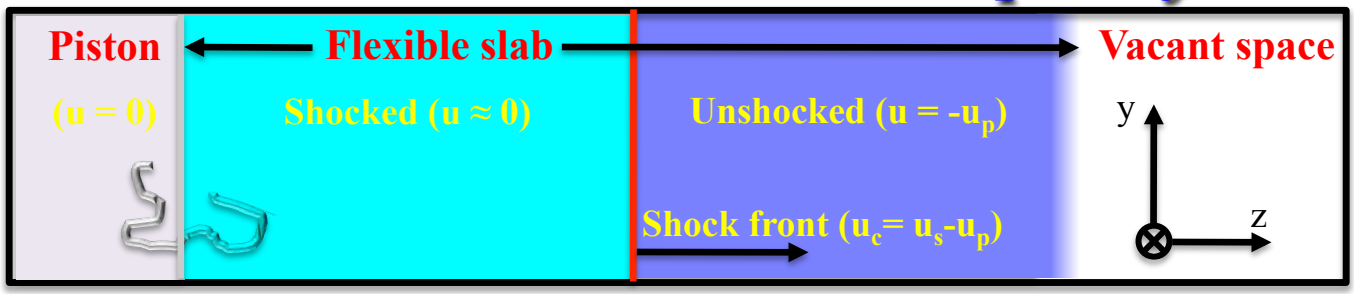

C_{32}, C_{64}, and C_{128} systems
Initial dimensions:
50 Å × 50 Å × 3000 Å (C_{32}, C_{64})
74 Å × 74 Å × 3000 Å (C_{128})
Impact speed: 2.0 km/s
P_{shock} ~ 7.25-8.25 GPa

System generation: (1) Individual chains grown in bond-by-bond fashion using the equivalent Markov process for the PBD family developed by Flory[1]; (2) random packing into 3-D simulation cell; (3) NPT/NVT molecular dynamics to equilibrate

Force field: Smith-Paul[2] United Atom Force Field; Lennard-Jones 12-6 during chain generation, both 12-6 and Buckingham exp-6 for shock simulations

Bulk properties
1 atm and 413 K

C_{32}: 8202 chains
C_{64}: 4303 chains

Comparisons to Tsolou *et al.*[3] for 12-6 systems

Comparisons between 12-6 and exp-6 systems

	C_{32} 12-6	C_{32} exp-6	C_{64} 12-6	C_{64} exp-6
$\langle\rho\rangle$ (g·cm^3)	0.7854±0.0002 [0.789][b]	0.7953±0.0002 (+1.3%)[c]	0.826±0.002 [0.827]	0.838±0.001 (+1.5%)
$\langle R^2\rangle$ (Å^2)	283±1 [270±10]	274±1 (-3.2%)	618±6 [600±15]	603±7 (-2.4%)
$\langle R_g^2\rangle$ (Å^2)	41.5±1 [45±5]	40.4±1 (-2.7%)	96±1 [95±10]	94±1 (-2.1%)
D (10^{-7} cm^2·s^{-1})	381.9	315.18 (-17.5%)	193.83	224.23 (+15.7%)

1. Macromolecules **4**, 219 (1971) 2. J. Phys. Chem. A **102**, 1200 (1998) 3. Macromolecules **38**, 1478 (2005)

The supported shocks are essentially steady and the behavior is systematic with respect to non-bonded potential and chain length

Instantaneous temperature vs. distance from shock

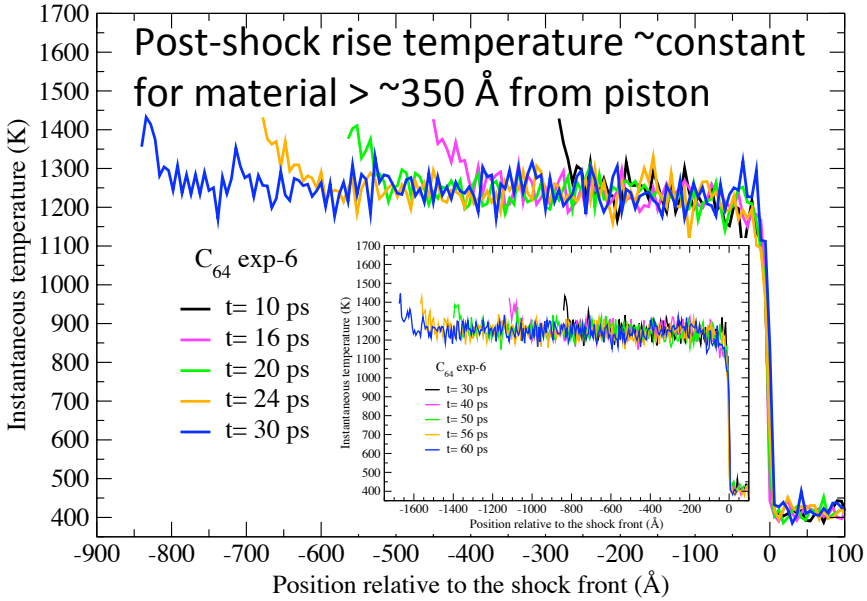

Mass density vs. distance from shock

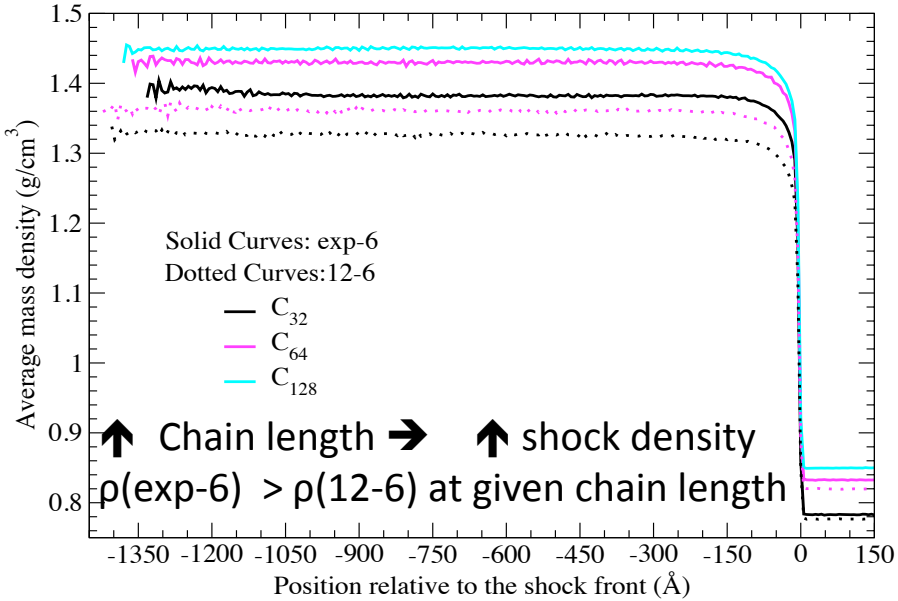

Princip. stress vs. dist. from shock

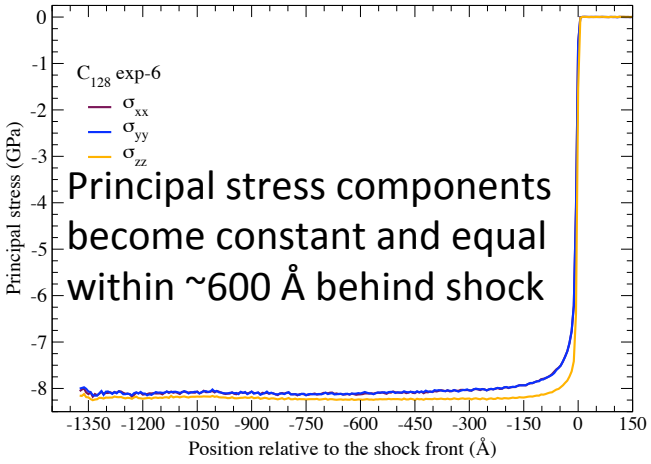

Longitud. stress vs. dist. from shock

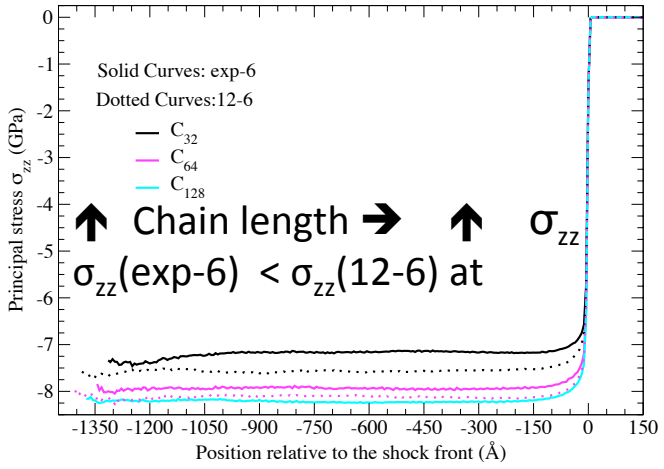

Shear stress vs. dist. from shock

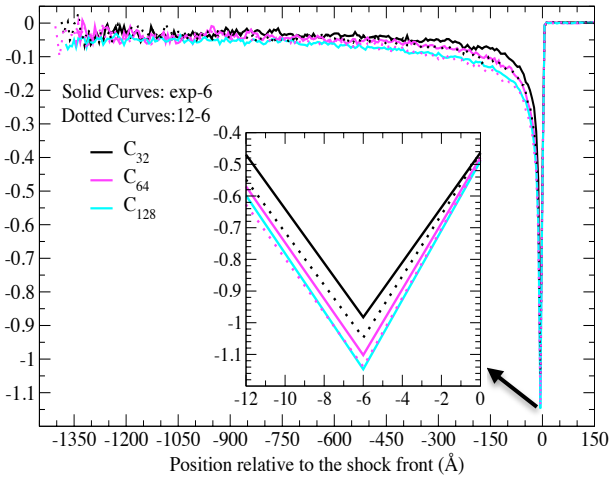

Post-shock reorientation of covalent bonds (in the lab frame) and dihedral angles occurs within several ps behind the shock; chain shape and orientation relaxation requires much longer

Distributions of angles formed by covalent bonds and the x direction at various times

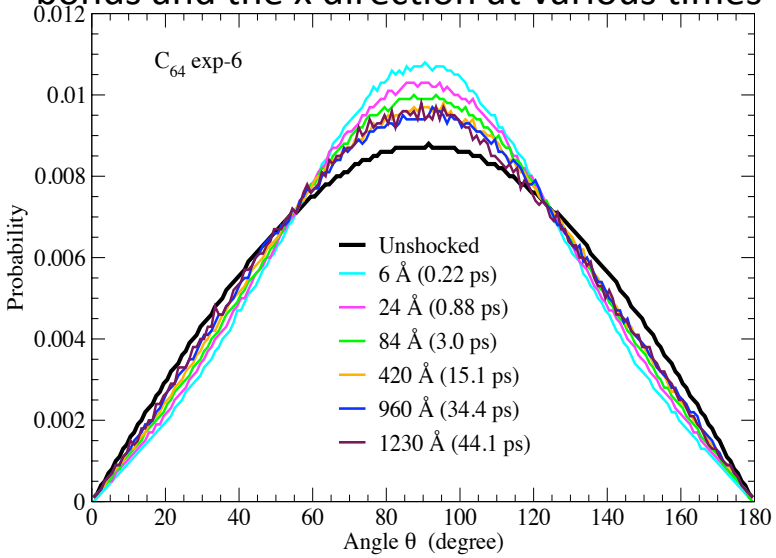

Distributions of CH_2-CH_2 dihedral angles at various times

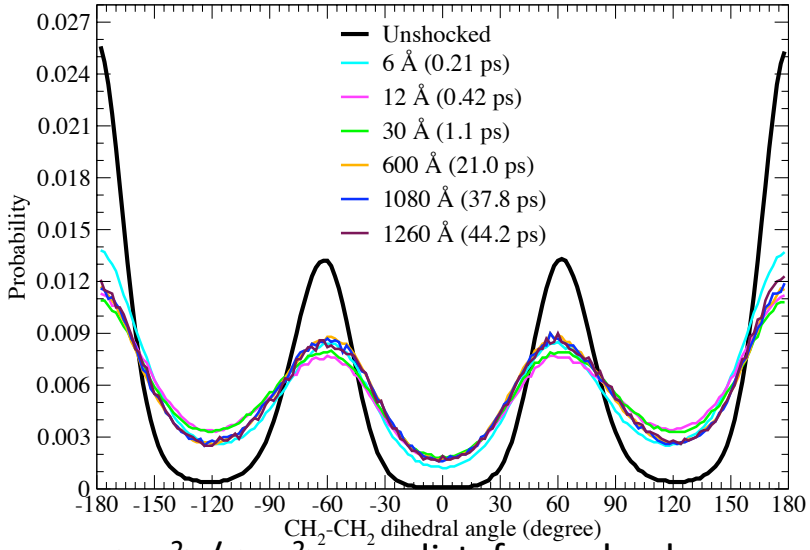

2^{nd}-Legendre order parameter vs. dist. from shock

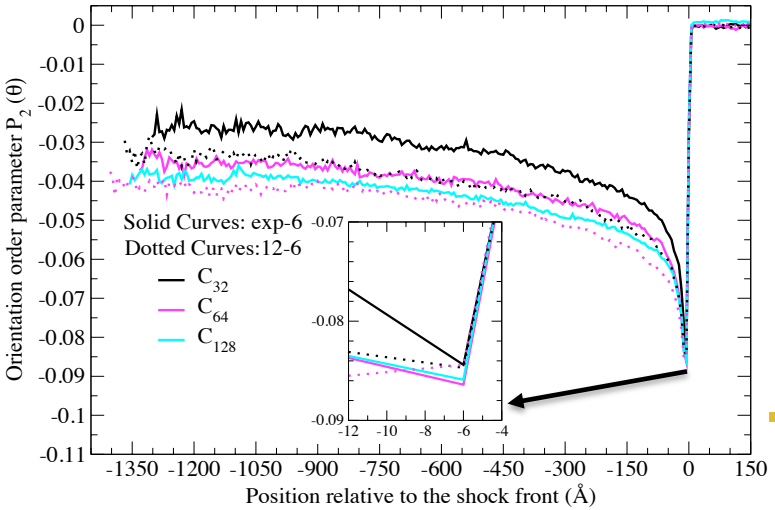

$\langle s_{g,z}^2 \rangle / \langle s_{g,z}^2 \rangle_0$ vs. dist. from shock

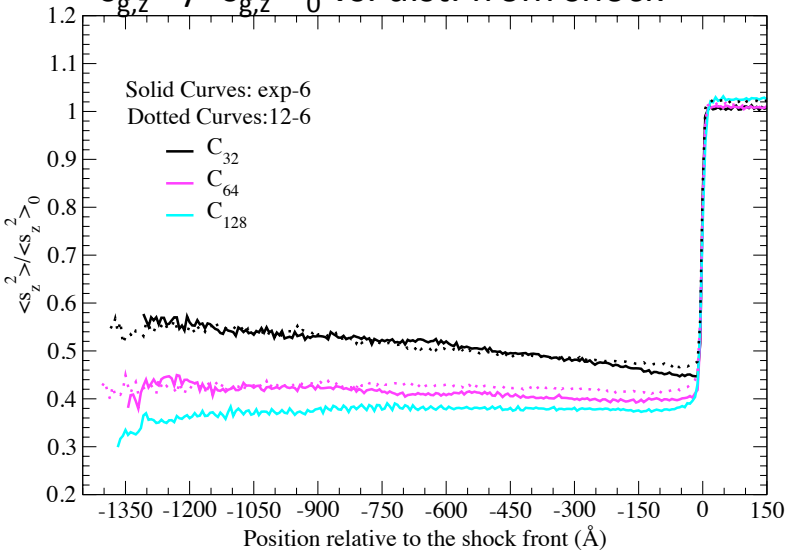

All-atom simulation setup & system generation

Box: 300 nm x 8 nm x 8 nm; ≈ 2.000.000 atoms

Chain generation: Metropolis-Rosenbluth Monte Carlo technique Equilibration: Monte Carlo + NPT/NVT molecular dynamics
Force field: OPLS-AA; 12-6 Lennard-Jones during chain generation, exp-6 Buckingham for shock simulations

Generated chains thoroughly assessed and compared to other simulations and experimental studies!

n_C	ensemble size	$\langle r^2 \rangle$ [nm²]	$\langle s^2 \rangle$ [nm²]	$\langle r^2 \rangle / \langle s^2 \rangle$ –	s_m [nm]
32	48650	2.78±0.02	0.425±0.001	6.56±0.01	0.562
48	49860	4.38±0.03	0.692±0.002	6.34±0.01	0.719
64	50488	5.94±0.04	0.958±0.003	6.20±0.01	0.842
96	51132	9.11±0.06	1.500±0.006	6.07±0.01	1.044
128	51464	12.34±0.08	2.043±0.008	6.04±0.01	1.214
256	51968	25.13±0.17	4.216±0.017	5.96±0.01	1.734

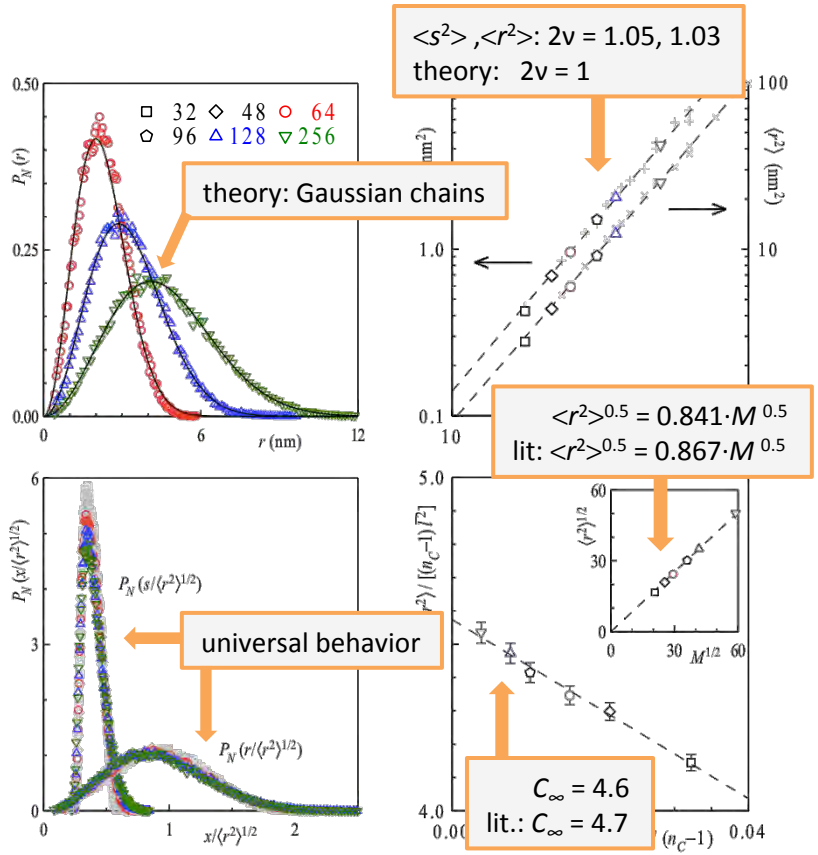

M.G. Fröhlich, T.D. Sewell, *Macromol. Theory Simul.* 2013, in press.

Analysis overview

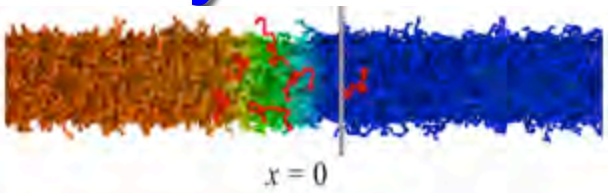

$n_C = 128,\ u_P = 2.0$ km/s

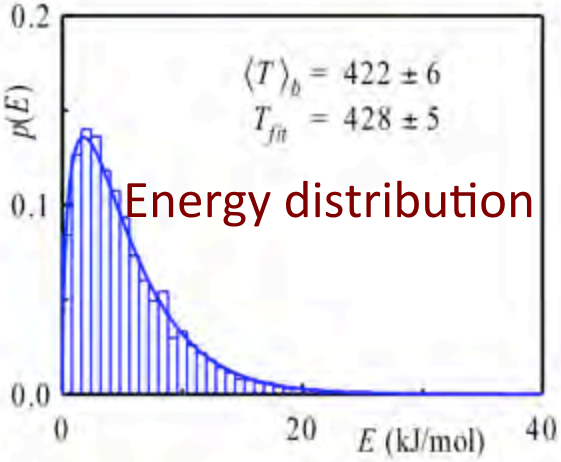

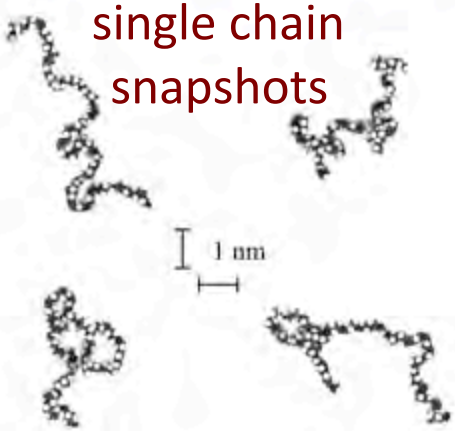

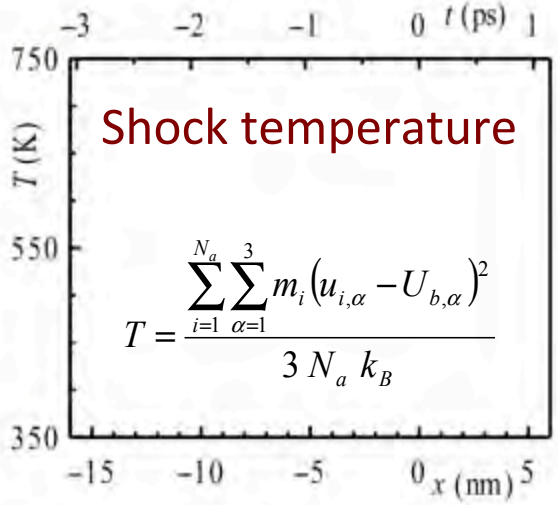

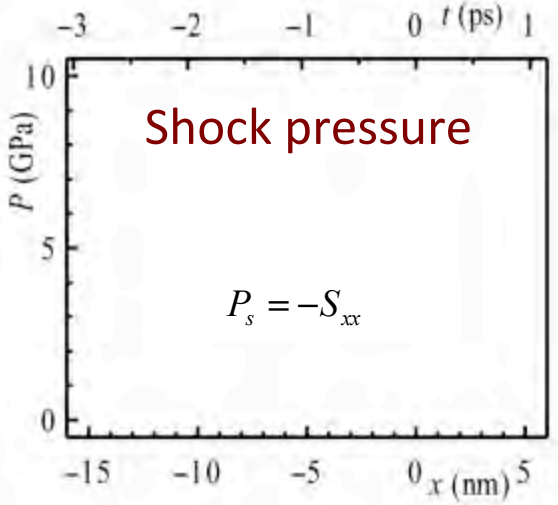

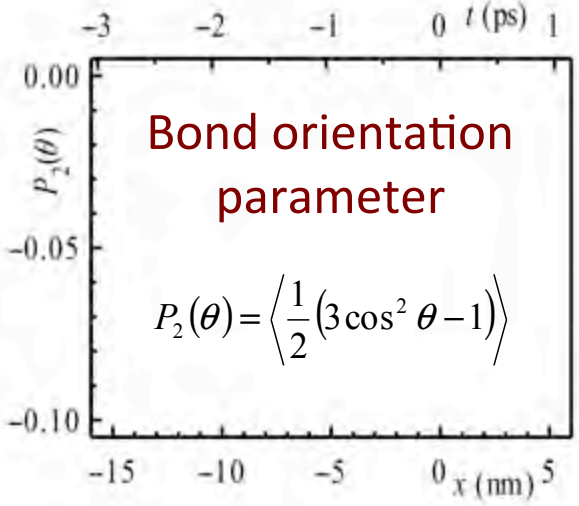

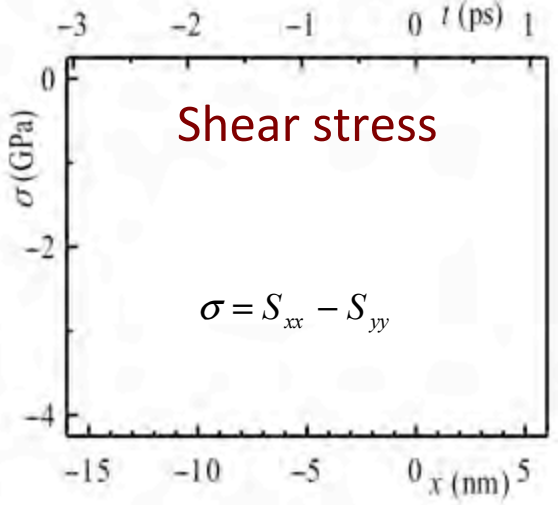

General shock response

(a) Temperature, (b) density

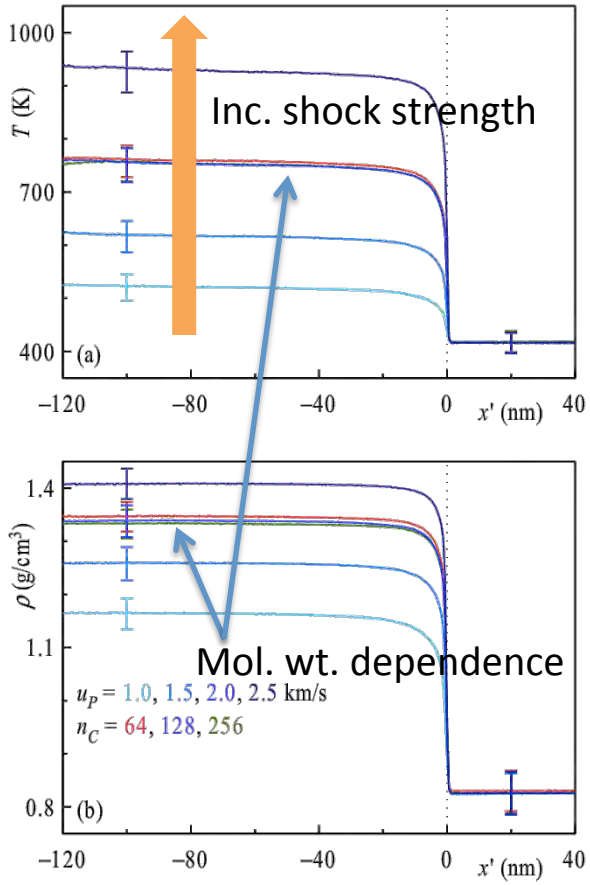

(all error bars for 3 standard deviations of the distribution)

Hugoniot locus: (a) $u_S - u_P$ plane, (b) $P - V/V_0$ plane

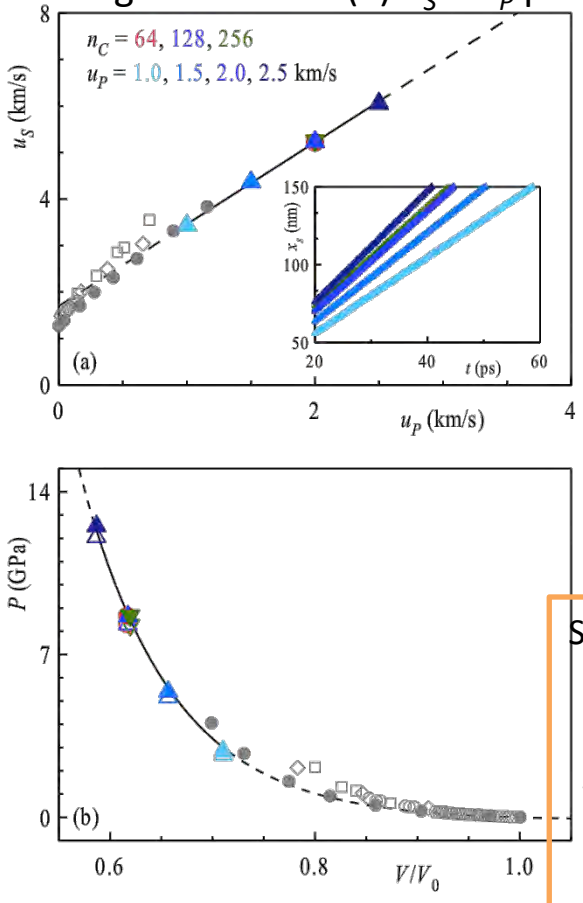

J.B. Hooper, D. Bedrov, G.D. Smith, B. Hanson, O. Borodin, *J. Phys. Chem.* **130**, 144904 (2009)

J.C.F. Millet, N.K. Bourne, J. Akhavan, *J. Appl. Phys.* **95**, 4722 (2004)

$$u_s = \left[\frac{P-P_0}{\rho_0}\frac{1}{1-V/V_0}\right]^{1/2}$$

$$u_p = u_s\left[1-V/V_0\right]$$

Solid line: fit to Tait equation of state

$$\frac{V(P)}{V_0} = 1 - C\cdot\ln\left(1+\frac{P}{B}\right)$$

w/ C = 0.08936 (universal for polymers)

B = 0.122246 ± 0.001024 (fit)

allows estimation of bulk sound-speed

$c_0 = \sqrt{\kappa_0/\rho_0}$ ≈ 1300 m/s

Experimental (Millet et al.) ≈ 1450 m/s

UA sim. (Hooper et al.) ≈ 1250 m/s

Mechanical & structural response

(a) Shock pressure, (b) shear stress

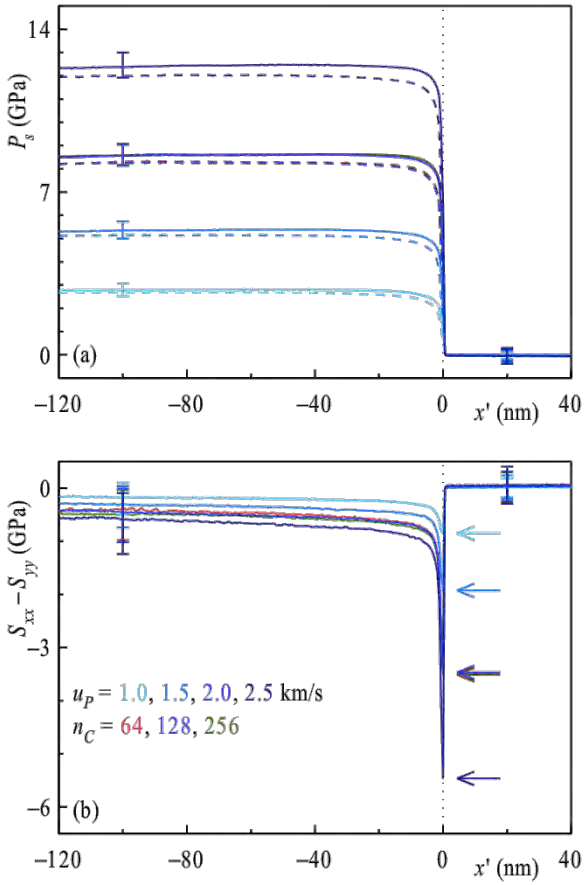

(a)Relative squared radius of gyration, (b) relative asphericity, (c) bond orientation, and (d) molecular orientation

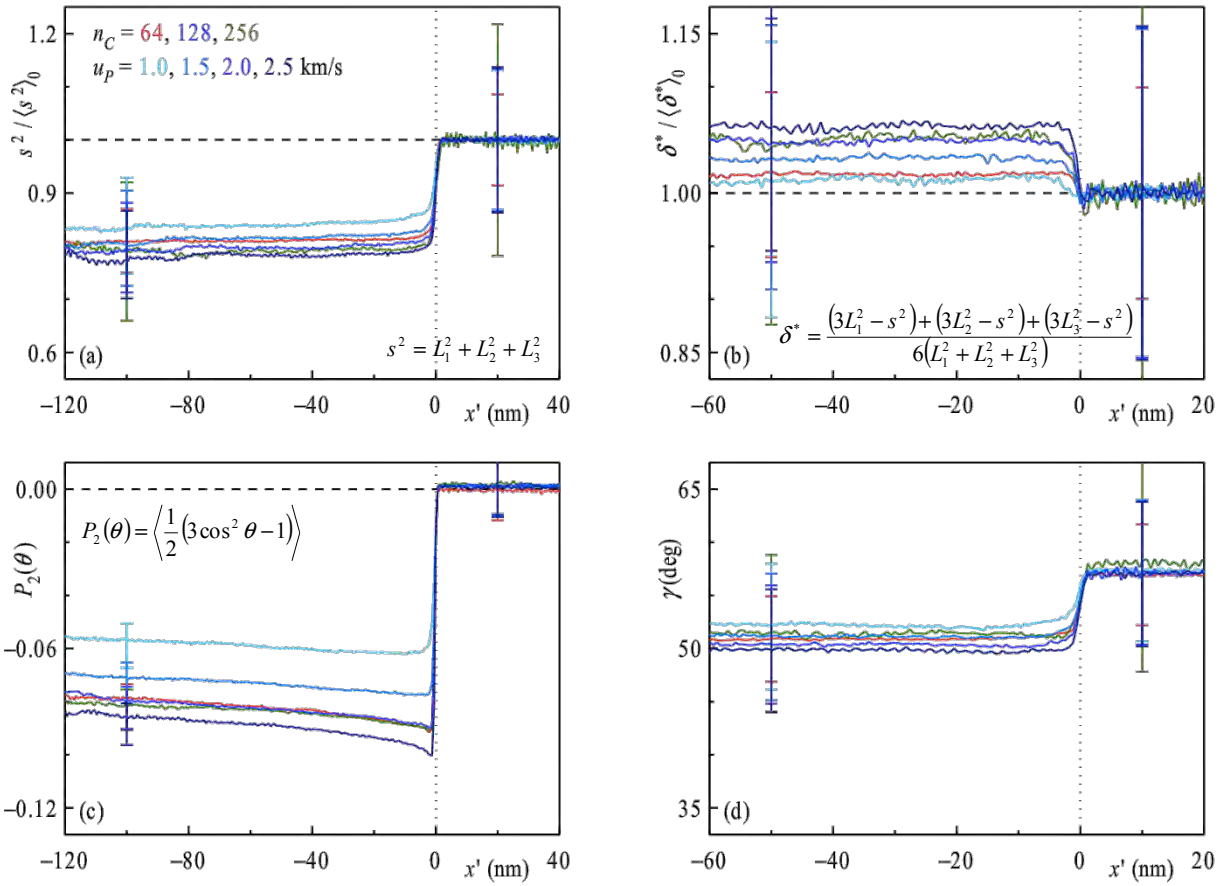

Comparison: all-atom (AA) *vs.* united-atom (UA) simulations

left AA, right UA: same qualitative but different quantitative behavior (a) shear stress, (b) bond orientation

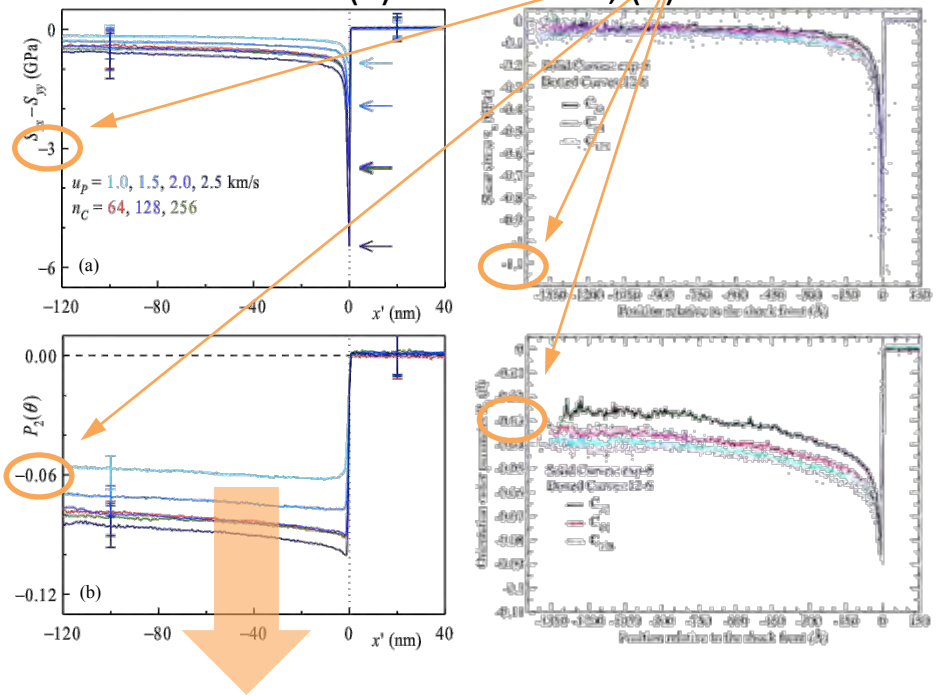

(a)Temperature, (b) density, (c) shock rise AA *vs*. UA

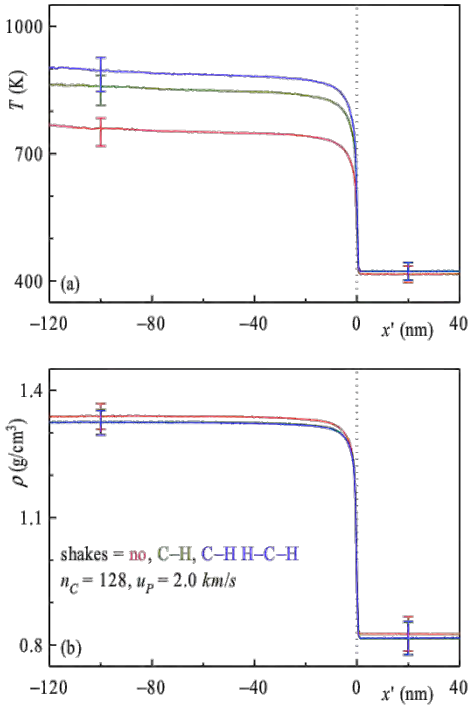

Influence of heat capacity: approach UA model by constraining bonds and angles, *i.e.*, decreasing the number of vibrational degrees of freedom

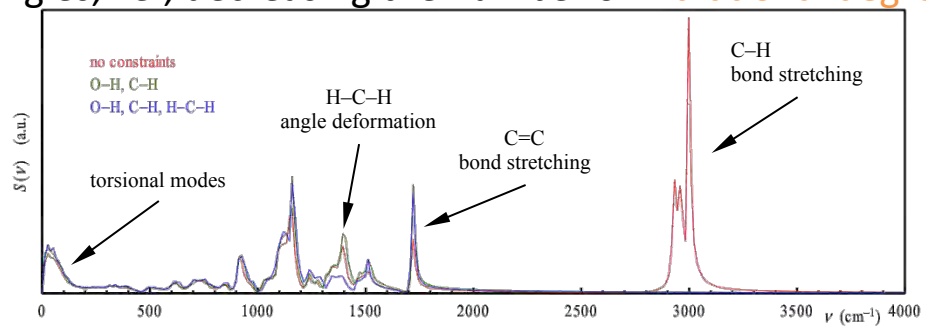

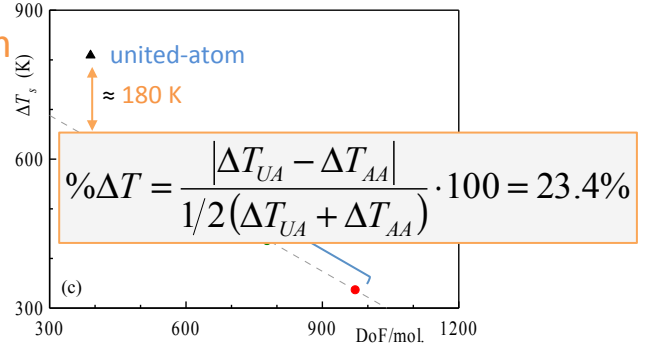

Spectroscopic response

Mass weighted normalized velocity autocorrelation function $C(\tau)$ ➔ vibrational density of states $S(\nu)$

$$C(\tau)=\sum_{i=1}^{n}\sum_{\alpha=1}^{3} m_i \cdot \frac{\langle v_{i\alpha}(0)\cdot v_{i\alpha}(\tau)\rangle}{\langle v_{i\alpha}(0)\cdot v_{i\alpha}(0)\rangle} \quad \rightarrow \quad S(\nu)\propto \int_{-\infty}^{\infty} C(\tau)\exp[-i2\pi\nu\tau]d\tau$$

allows for the analysis of the excitation of vibrational modes as *f(t)* in the vicinity of the shock rise:

weak shock: u_P = 1.0 km/s, P_s ≈ 2.8 GPa

strong shock: u_P = 2.5 km/s, P_s ≈ 12.5 GPa

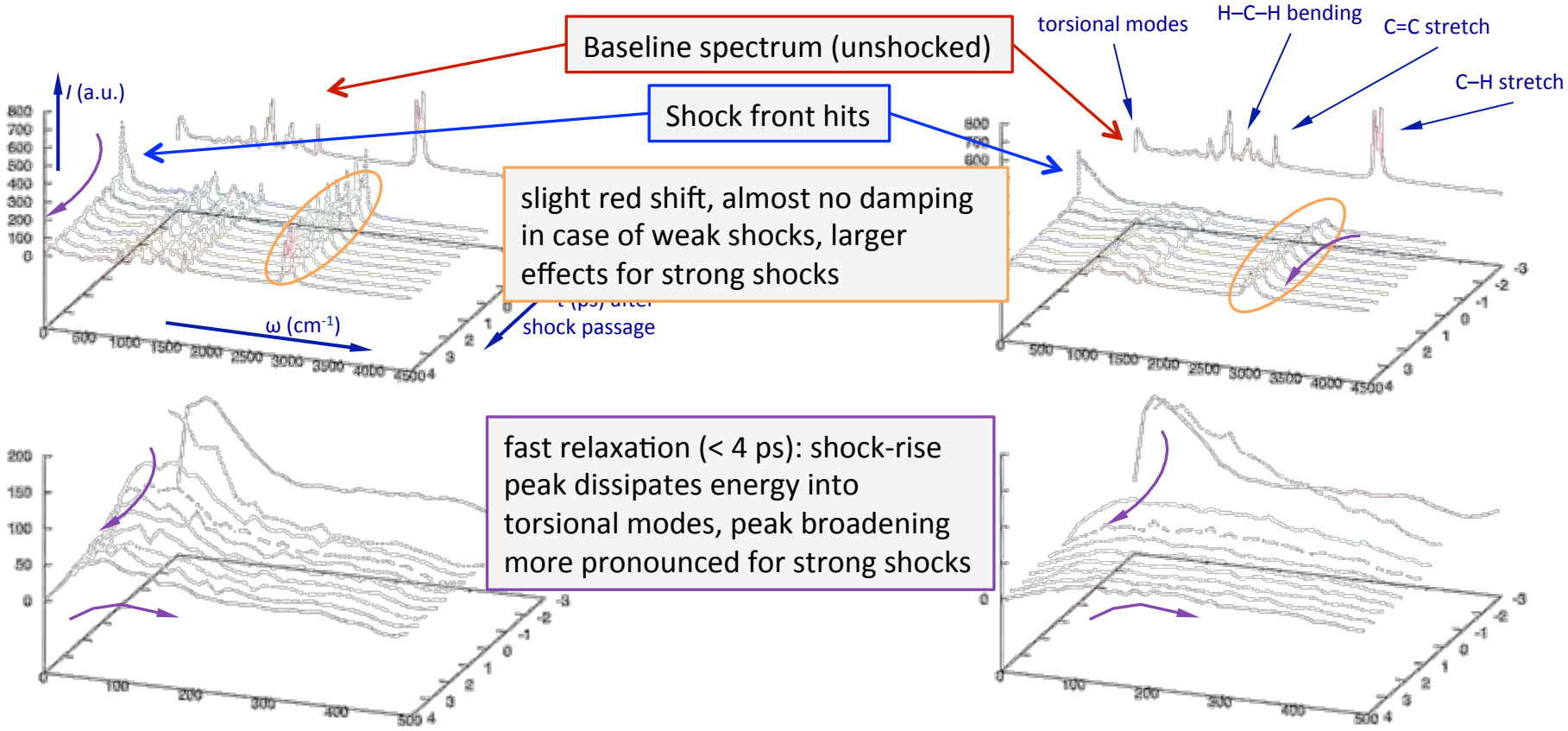

Relaxation of an Excited Molecule in Crystalline NM

Dr. Luis A. Rivera-Rivera

A single molecule in crystal at 200 K and 1 atm was "vertically" excited by energy E^* using momentum scaling

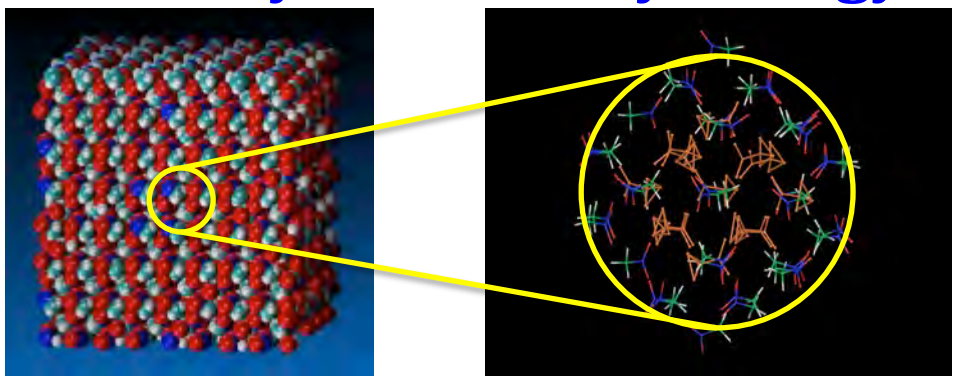

$$p_{ij} = \sqrt{\frac{E^* + E^0_{\text{kin}}}{E^0_{\text{kin}}}}\, p^0_{ij}$$

Seven E^* between 25.0 and 125.0 kcal/mol
Ensembles of 200 trajectories for each E^*

The kinetic energy in the excited molecule was monitored as a function of time

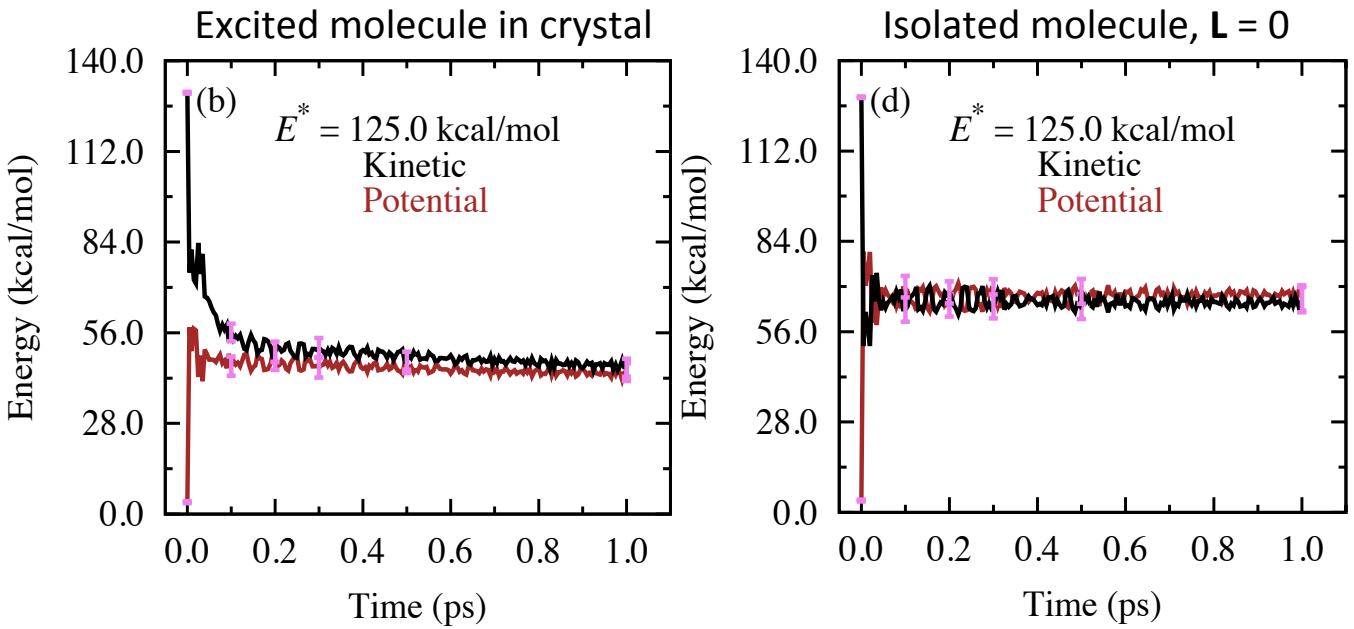

Intramolecular kinetic and potential energy exchange occurs on a sub-ps time scale

- Similar results for molecule in crystal and isolated molecule
- Identical phase space points except $\mathbf{v}_{cm}$ and **L** removed from isolated molecule at $t = 0$

For $t > \sim 0.2$ ps the decay is approximately exponential

The ensemble-average kinetic energy time history was fitted to the exponential function: $E_k(t) = E_\infty(E^*) + Ae^{-t/\tau}$

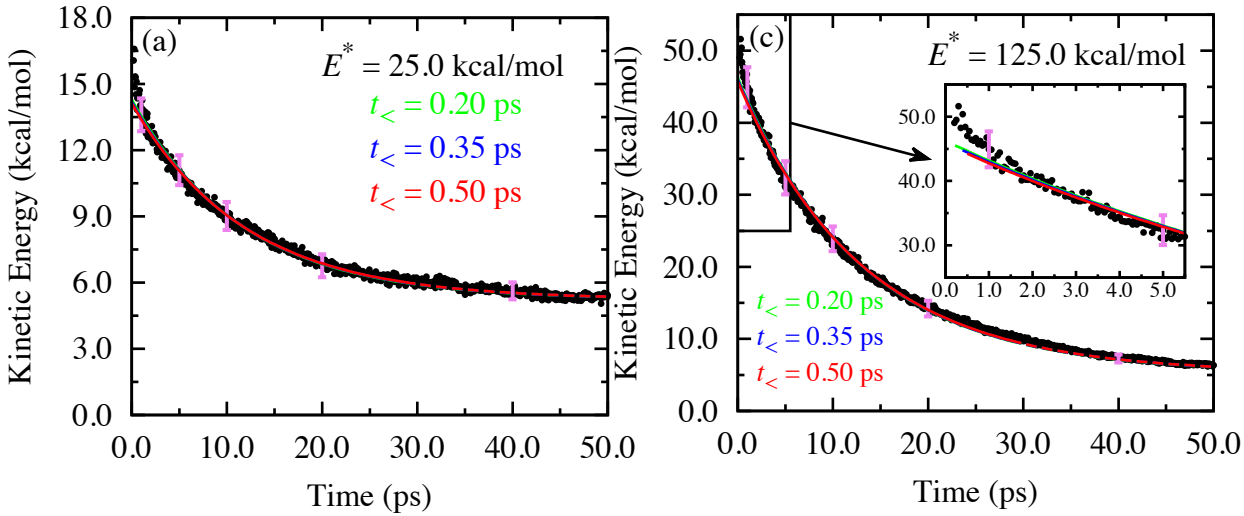

A and τ are fitting parameters

$E_\infty(E^*)$ is determined using the equiparitition theorem

Fits were performed for $t_< \le t \le 30.0$ ps, with $t_<$ = 0.20, 0.35, and 0.50 ps

E^* (kcal/mol)	$E_\infty(E^*)$	E_{bath} (50.0 ps)	A	τ	A	τ	A	τ
			0.20 ps $\le t \le$ 30.0 ps[a]		0.35 ps $\le t \le$ 30.0 ps[a]		0.50 ps $\le t \le$ 30.0 ps[a]	
25.0	5.23	5.23	9.07(4)[b]	11.58(7)[b]	8.96(3)[b]	11.73(6)[b]	8.89(3)[b]	11.83(6)[b]
30.0	5.23	5.23	10.52(3)	12.44(6)	10.43(3)	12.55(5)	10.36(3)	12.65(5)
37.5	5.23	5.23	13.62(4)	13.31(7)	13.51(4)	13.43(6)	13.42(3)	13.54(5)
50.0	5.24	5.24	16.59(5)	13.57(6)	16.48(5)	13.68(6)	16.36(4)	13.79(5)
75.0	5.25	5.25	25.02(7)	13.56(6)	24.88(7)	13.65(6)	24.73(6)	13.75(5)
100.0	5.26	5.26	34.5(1)	13.46(5)	34.28(9)	13.56(6)	34.14(9)	13.62(5)
125.0	5.27	5.27	41.0(1)	12.90(6)	40.7(1)	12.99(5)	40.5(1)	13.07(5)

The results show that $A(E^*)$ increases monotonically and linearly, while $\tau(E^*)$ exhibits a maximum

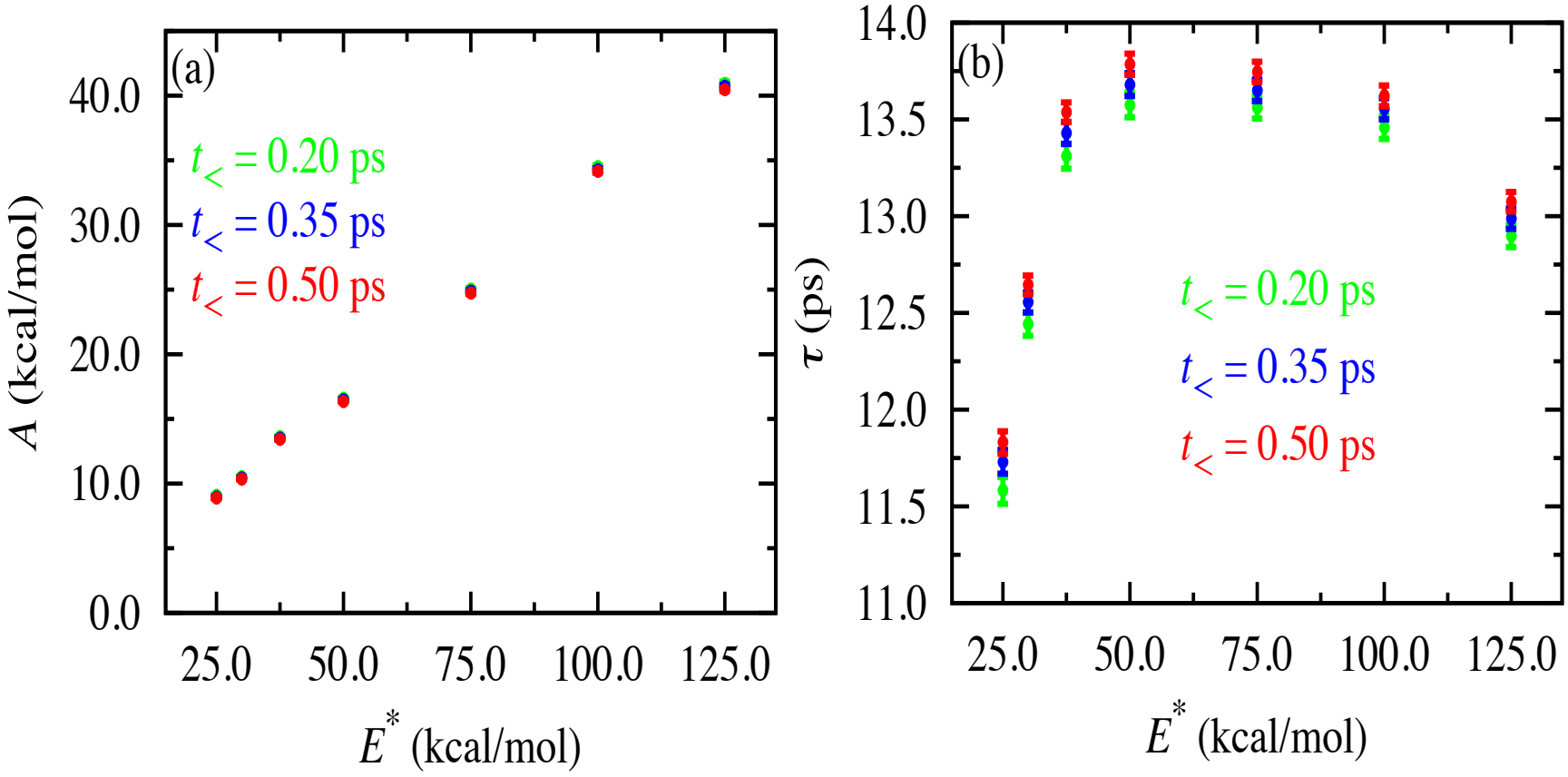

- The results are qualitatively insensitive to $t_<$
- The dependence of A on E^* is easily understood
- We think we understand the variation of τ with E^*, but lack mathematical proof

Simulations of Spall in Nitromethane and PBD

Dr. Lan He

Tension wave shock simulations of crystal nitromethane

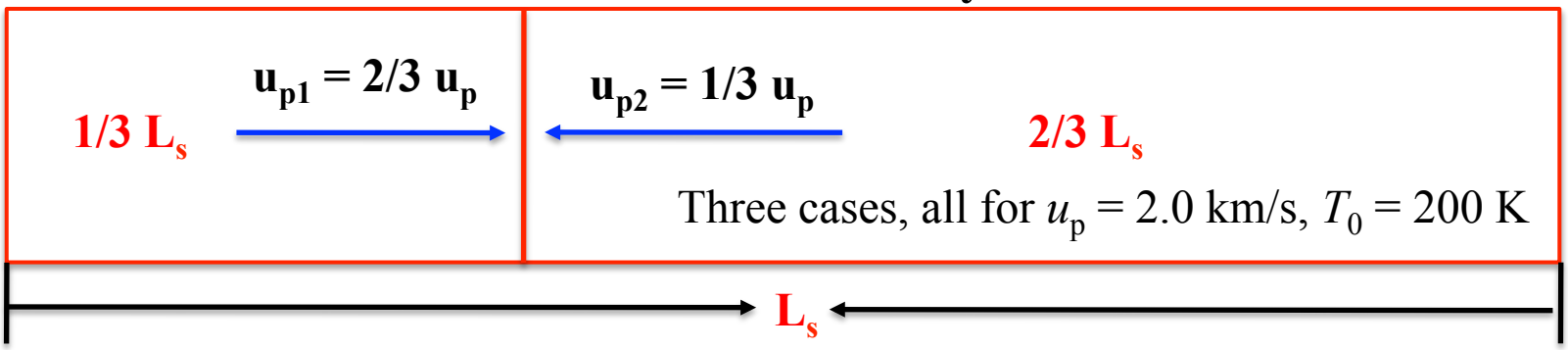

[100]: 80a×16 ×12c; t = 14.8 ps [010]: 20a×65b×12c; t = 15 ps [001]: 20a×16b×48c; t = 14.8 ps

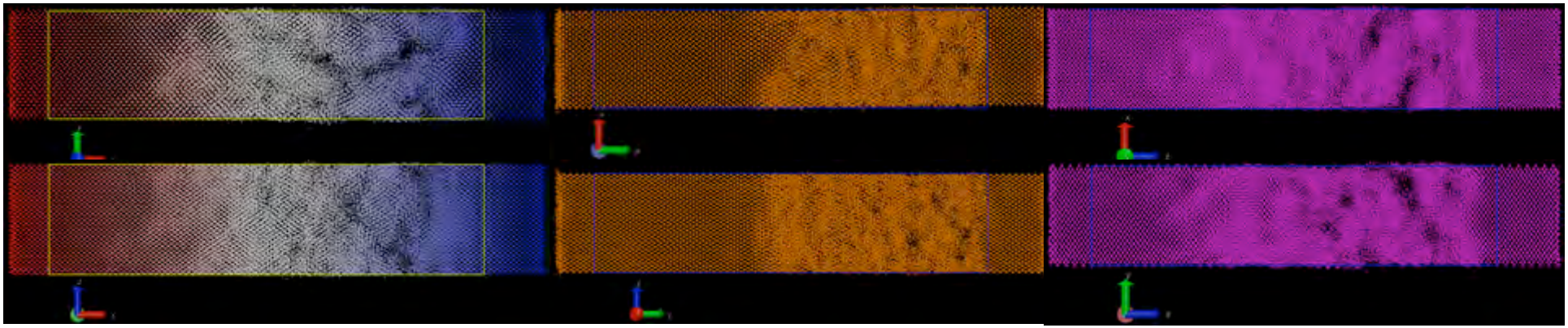

The next three slides contain results for evolution of:

- Number density and temperature
- Stress
- Void growth

[100] Nitromethane

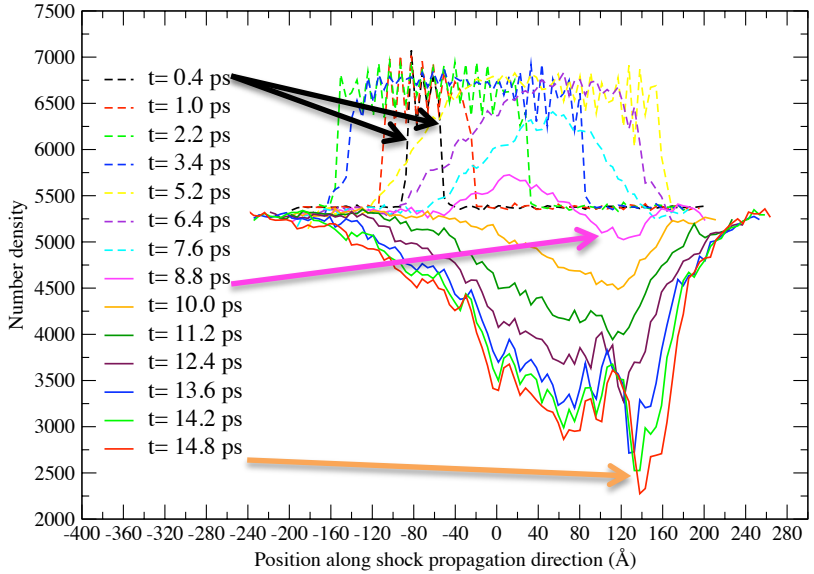

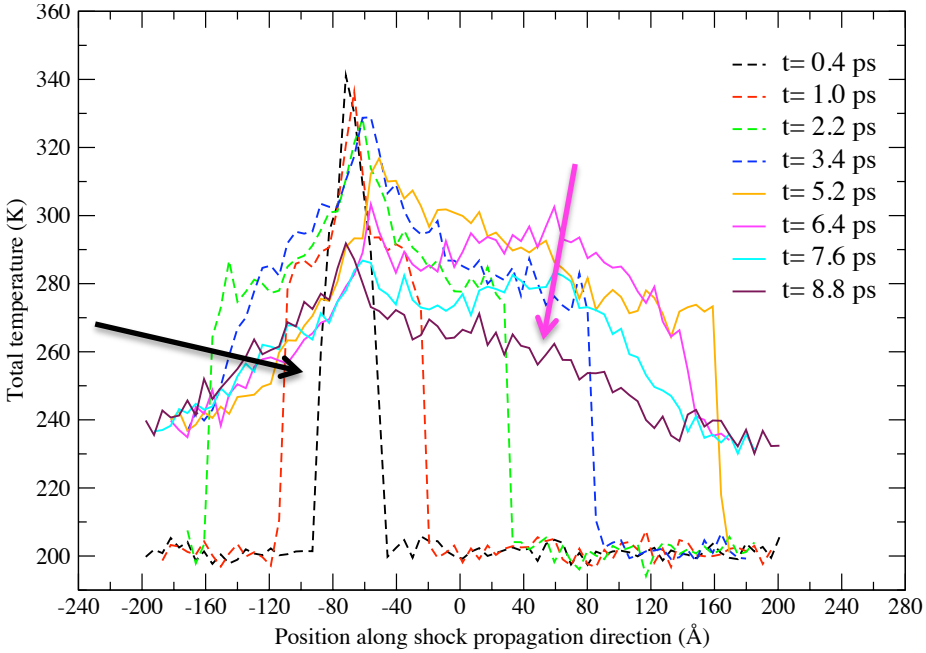

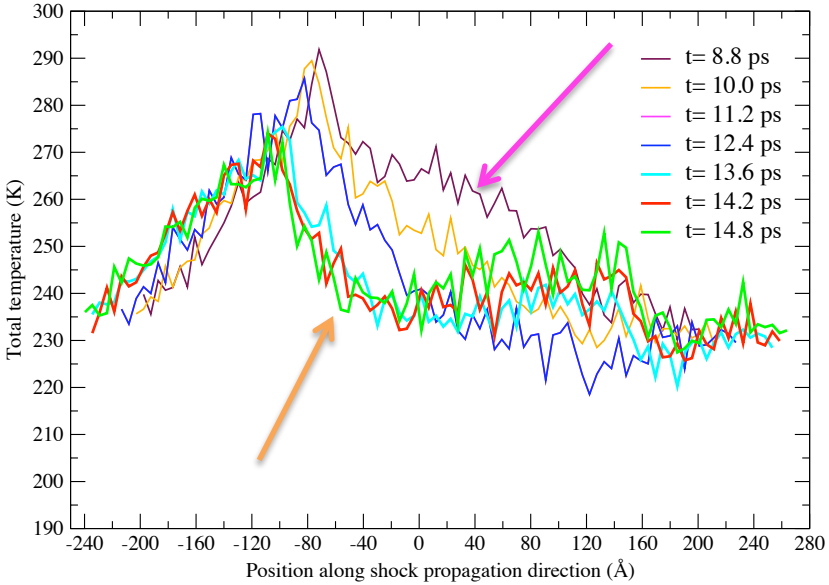

Longitudinal stress profile for [100] case prior to spall

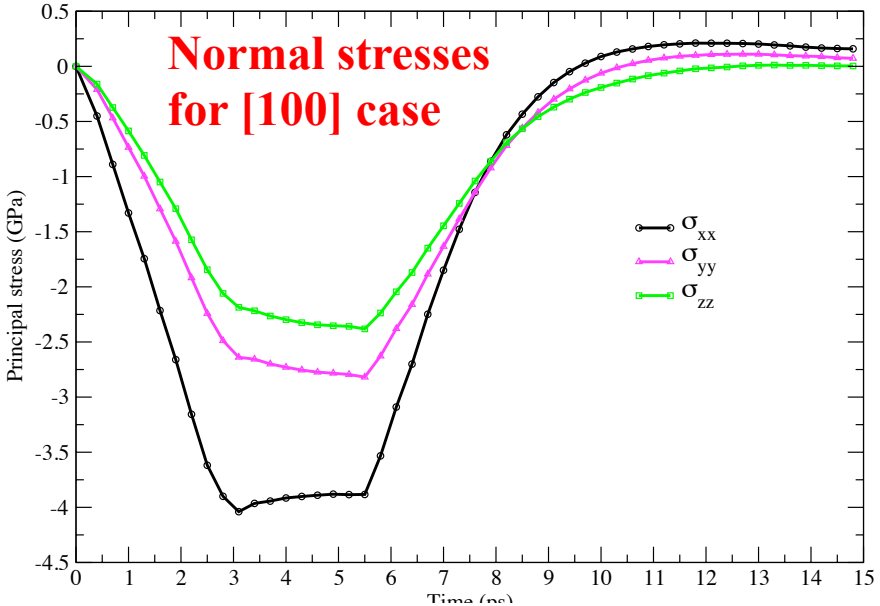

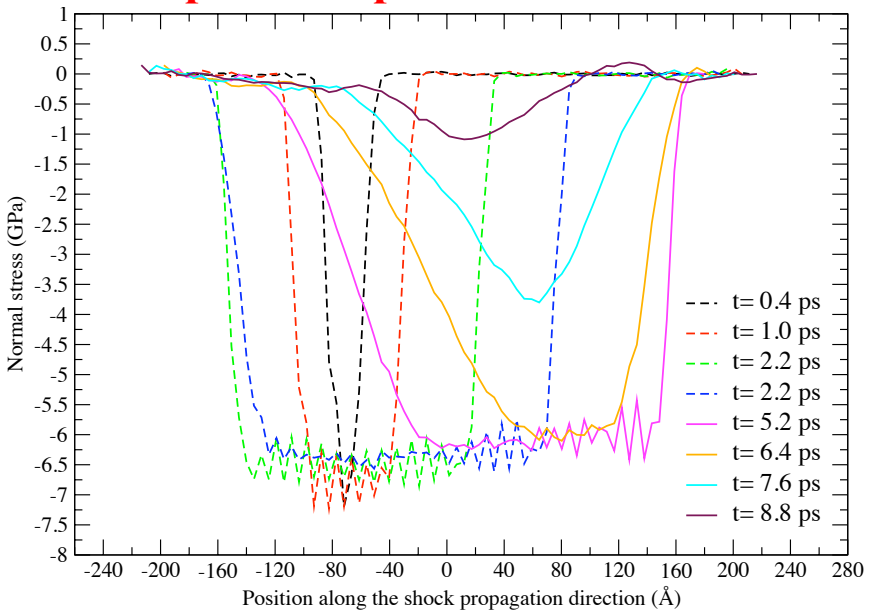

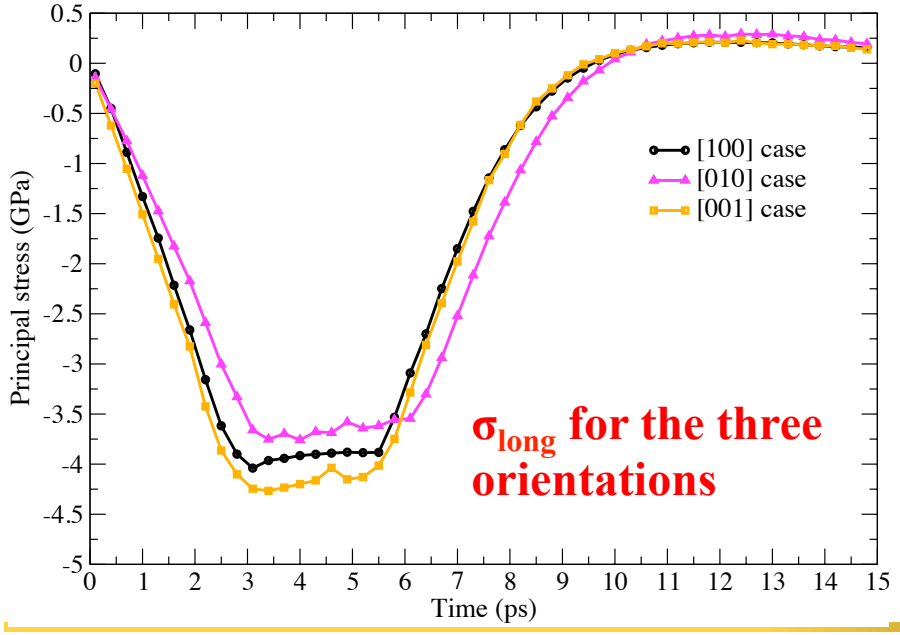

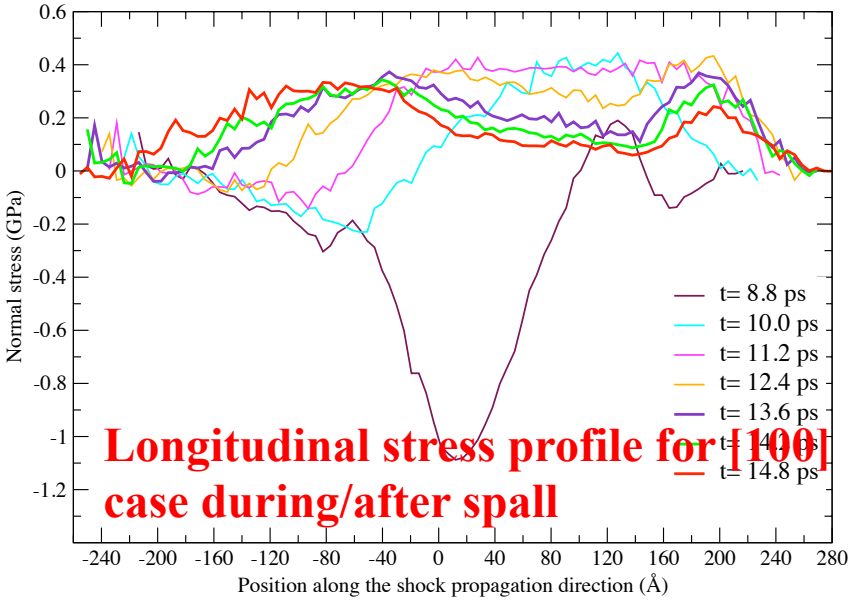

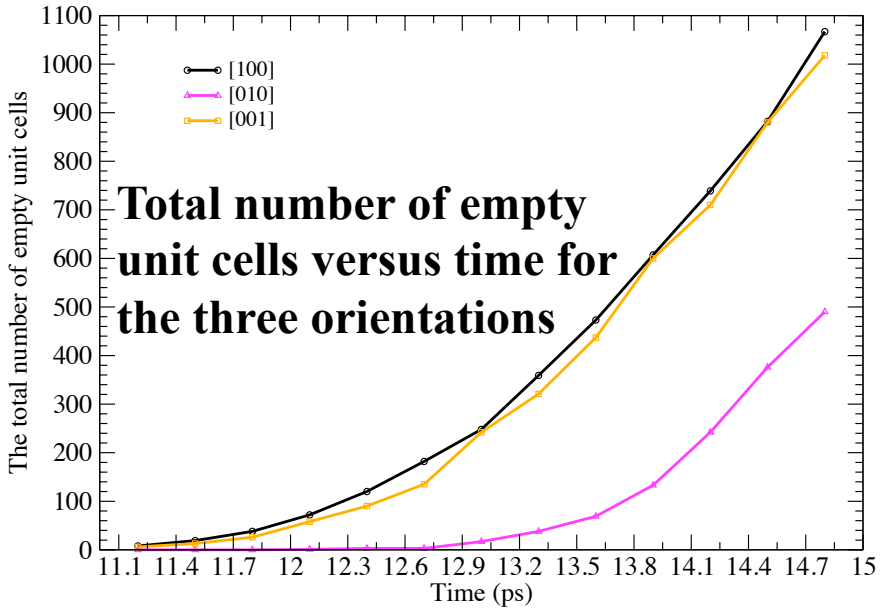
[100]
[010]
[001]
The total number of empty unit cells
Time (ps)
Total number of empty unit cells versus time for the three orientations

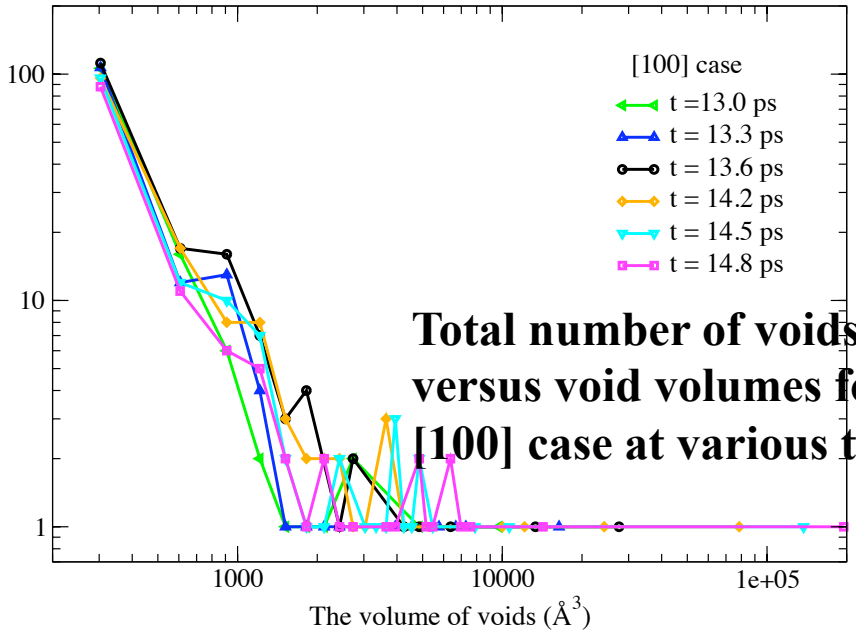
[100] case
t =13.0 ps
t = 13.3 ps
t = 13.6 ps
t = 14.2 ps
t = 14.5 ps
t = 14.8 ps
The volume of voids (Å3)
Total number of voids versus void volumes for [100] case at various times

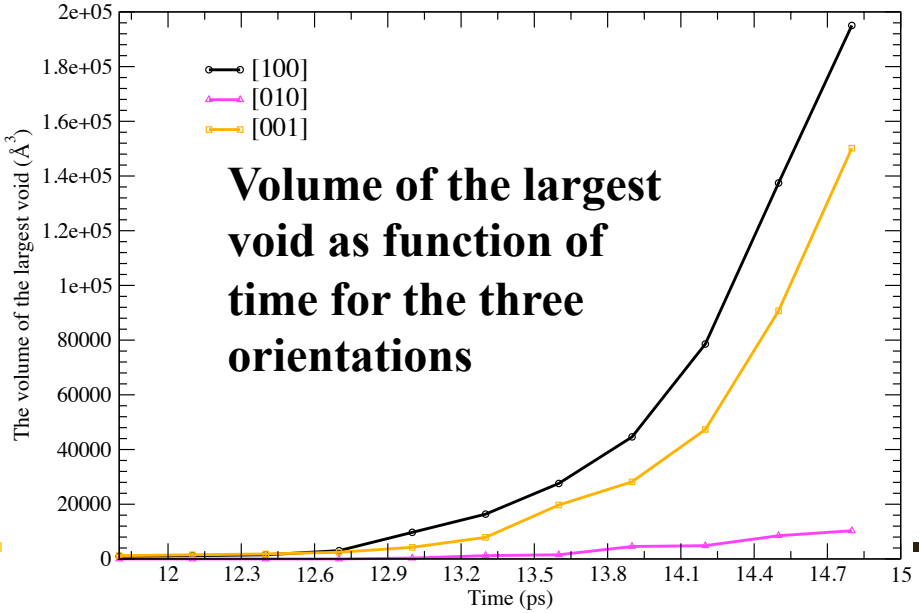
[100]
[010]
[001]
The volume of the largest void (Å3)
Time (ps)
Volume of the largest void as function of time for the three orientations

Metrics (since beginning of project)

- Personnel
  - TNO:
    - Bouma, van der Heijden, senior technicians
  - MU:
    - Faculty: Thompson, Sewell
    - Postdoctoral Researchers: Lan He, Markus Froehlich, Ali Siavosh-Haghighi, Luis Rivera-Rivera
    - Students: Reilly Eason (Ph.D. student, expected graduation Dec. 2013), Matt Kroonblawd
- Publications (MU)
  - Bouma, van der Heijden, Sewell, and Thompson, *Simulations of deformation processes in energetic materials,* in "Numerical Simulations of Physical and Engineering Processes", J. Awrejcewicz Ed. (InTech Open Access, Rijeka, Croatia, 2011). pp. 17-58.
  - Eason and Sewell, *Shock-Induced Inelastic Deformation in Oriented Crystalline Pentaerythritol Tetranitrate (PETN)*, J. Phys. Chem. C **116**, 2226 (2012)
  - He, Sewell, and Thompson, *Molecular dynamics simulations of shock waves in oriented nitromethane single crystals*, Journal of Chemical Physics **134**, 124506 (2011).
  - *He, Sewell, and Thompson, Molecular dynamics simulations of shock waves in oriented nitromethane single crystals: Plane-specific effects*, Journal of Chemical Physics **136**, 034501 (2012).
  - Rivera-Rivera, Sewell, and Thompson*, Post-shock relaxation in crystalline nitromethane*, J. Chem. Phys. **138**, 084512 (2013)
  - Frohlich and Sewell, *Pivot Algorithm and Push-off Method for Efficient System Generation of All-Atom Polymer Melts: Application to Hydroxyl-Terminated Polybutadiene*, Macromolecular Theory and Simulation (in press 7/13); DOI: 10.1002/mats.201300103
  - He, Sewell, and Thompson, *Molecular Dynamics Simulations of Shock Waves in Cis-1,4-Polybutadiene Melts*, submitted to J. Appl. Phys. (July 2013)
  - Rivera-Rivera, Sewell, and Thompson, *A Molecular Dynamics Study of the Relaxation of an Excited Molecule in Crystalline Nitromethane* (in preparation)
  - Frohlich, Sewell, and Thompson, *Molecular dynamics simulations of shock waves in hydroxyl-terminated polybutadiene melts: Mechanical and structural response* (in preparation)
  - Eason and Sewell, Impact Strength Dependent Void Collapse in (100)-oriented RDX (in preparation)
  - He, Sewell, and Thompson, *Molecular Dynamics Simulation Study of Shock-Induced Spall in Crystalline Nitromethane* (in preparation)

- Presentations
  - Invited talk by Sewell at Pacifichem 2010 (Honolulu, December 2010)
  - Keynote presentation by Sewell at Plasticity '11 (Puerto Vallarta, January 2011)
  - Contributed presentation by Dr. Lan He at the 2011 APS Shock Conference (Chicago, June 2011)
  - Contributed presentation by Mr. Reilly Eason at the 2011 APS Shock Conference (Chicago, June 2011)
  - Contributed presentation by Mr. Reilly Eason at the 2011 LAMMPS Users Workshop (Albuquerque, August 2011)
  - Departmental poster presentation by Mr. Matthew Kroonblawd (University of Missouri, July 29, 2011)
  - Poster presentation by Dr. Lan He, Chemistry in Dynamic Extremes Workshop (Santa Fe, January 2012)
  - Presentation by Bouma at NATO AC/326 SG1 on Energetic Materials, NATO HQ (Brussels, 26-27/10/2011)
  - Presentation by Bouma at TNO colloquium (8/11/2011)
  - Invited presentation by Sewell at APS March Meeting, Focus Session: Simulation of Matter at Extreme Conditions - Energetic Materials (Boston, February 2012)
  - Invited lecture by Sewell at Institute of Shock Physics (Imperial College London) – Symposium on Energetic Materials (London, February 2012)
  - Presentation by Bouma at New Models and Hydrocodes (London, April 2012)
  - Invited presentation by Sewell at New Models and Hydrocodes (London, April 2012)
  - Invited presentation by Sewell at International Center for Applied Computational Mechanics (ICACM), ICACM-2012, Structured Materials: The role of structure on emerging material properties (New York City, June 2012)
  - Invited talk by Thompson at 2012 GRC on Energetic Materials (Snow Mountain, VT, June 2012)
  - Invited Colloquium by Sewell at Naval Postgraduate School (to be given August 2012)
  - Invited talk by Sewell at 2013 APS Shock Conference (Seattle, WA, July 2013)
  - Contributed talk by Sewell at 12th U.S. National Congress on Computational Mechanics (Raleigh, NC, July 2013) [mini symposium coorganizer: *Multiscale Thermo-Mechanical Response of Molecular Solids: Theory, Simulation, Modeling, and Experiments*]
  - Invited talk by Sewell at APS National Meeting (Indianapolis, IN, September 2013)
  - Keynote presentation by Sewell at Plasticity '14 (Bahamas, January 2014)

Overview of papers / presentations (TNO)

- R.H.B. Bouma, presentations at NATO AC/326 SG/A meetings in 2011 and 2013
- R.H.B. Bouma, A.E.D.M. van der Heijden, T.D. Sewell and D.L. Thompson, *Simulations of Deformation Processes in Energetic Materials*, in: Numerical Simulations of Physical and Engineering Processes, Intech, ISBN: 978-953-307-620-1, 2011
- R.H.B. Bouma, A.E.D.M. van der Heijden, *Analytical model development related to mechanical deformation and initiation of PBXs*, 9th New Models and Hydrocodes for Shock Wave Processes, April 23-27, 2012, London, United Kingdom
- R.H.B. Bouma, W. Duvalois and A.E.D.M. van der Heijden, *Characterization of defect structure in RDX crystals*, submitted to Journal of Microscopy (2013)
- R.H.B. Bouma and A.E.D.M. van der Heijden, *The effect of RDX crystal defect structure on mechanical response of polymer bonded explosive*, to be submitted to Journal of the Mechanics and Physics of Solids (2013)
- A.E.D.M. van der Heijden and R.H.B. Bouma, *Confocal scanning laser microscopic study of the RDX defect structure in deformed polymer bonded explosives*, to be submitted to Journal of Applied Physics

DEPARTMENT OF DEFENSE

DEFENSE THREAT REDUCTION
AGENCY
8725 JOHN J. KINGMAN ROAD
STOP 6201
FORT BELVOIR, VA 22060
ATTN: S. PEIRIS

DEFENSE TECHNICAL
INFORMATION CENTER
8725 JOHN J. KINGMAN ROAD,
SUITE 0944
FT. BELVOIR, VA 22060-6201
ATTN: DTIC/OCA

DEPARTMENT OF DEFENSE CONTRACTORS

EXELIS, INC.
1680 TEXAS STREET, SE
KIRTLAND AFB, NM 87117-5669
ATTN: DTRIAC

UNIVERSITY OF MISSOURI
316 UNIVERSITY HALL
COLUMBIA, MO 65211-3020
ATTN: D. THOMPSON

UNIVERSITY OF MISSOURI
316 UNIVERSITY HALL
COLUMBIA, MO 65211-3020
ATTN: T. SEWELL